Annica de Barros Rosa

Graduated in Cellular and Molecular Biology

Multifunctional Organometallic Compounds for Auger Therapy

Dissertation to obtain Master's Degree in Biochemistry

Supervisor: Dr. António Manuel Rocha Paulo, C^2TN-IST

Jury:

President: Prof. Dr. Pedro António de Brito Tavares
Examiner: Prof. Dr. Paula Dolores Galhofas Raposinho
Supervisor: Prof. Dr. António Manuel Rocha Paulo

FACULDADE DE CIÊNCIAS E TECNOLOGIA
UNIVERSIDADE NOVA DE LISBOA

October 2014

Multifunctional Organometallic Compounds for Auger Therapy

Acknowledgments

To my mentor, Dr. António Paulo, I thank you for the mentoring, transmitted knowledge and incentives. For the availability and accessibility demonstrated.

To Dr. Isabel Rego dos Santos for the opportunity and acceptance in the group Ciências Radiofarmacêuticas of C^2TN.

To Letícia Alves do Quental for all the support with the laboratory practices, teaching, availability and all the extra help.

To Dr. Paula Raposinho, Dr. Sofia Gama and Dr. Célia Fernandes for the studies provided, availability and for all the help. To Dr. Goreti Morais and Dr. Elisa Palma for the teaching and friendship.

To Susana, Sofia M., Elisabete R., Inês, Filipe, Maria, Vera, Mariana and Maurício for the NMR spectra, friendship and company. To the rest of the group, I am equally grateful for the welcoming and friendship.

To you my parents, I thank you. For the financial support, but essentially, for the emotional support, and for calling me religiously every Friday night during these 5 years I have been away from home. And thank you dad for coming visit me during my writing.

To my favorite person in this world, my big brother Yannick. To my grandmothers and to all my relatives, for the calls, and for supporting me from the distance.

To my BFF Maira, for the friendship and endless random talking. Thank you to all my other fellow compatriots for bringing a piece of home to this foreign country. In special my relatives, high school buddies and housemates.

To all the Portuguese and other PALOP friends I've made, my colleagues, teachers, co-workers and in special my housemates Tânia and Maria.

Abstract

Auger emitters gained significant interest in the past years due to the favorable suitability for target therapy at cellular level. Among Auger emitters, ^{99m}Tc seems like the most appealing candidate for this task due to its great advantages regarding low cost, high availability and almost ideal radiochemical properties. The short range of Auger electrons demands that the radionuclide must be as close as possible to the target, usually the nuclear DNA, in order to cause significant therapeutic effects. Thus, the search for efficient delivery systems is the major challenge for Auger therapeutic applications. Radioactive complexes capable of entering the cell and target the nucleus showing affinity for the DNA molecule have been reported in the literature. Such compounds comprise efficient multifunctional chelators with the ability to stabilize the *fac*-$[^{99m}Tc(CO)_3]^+$ core, as well as DNA-intercalating agents that ensure close proximity to the target. Herein we aimed to synthesize ^{99m}Tc complexes (**Tc1-4**) stabilized by multifunctional chelators of the pyrazole-diamine type, containing anthracene (**L1** and **L2**) or acridine orange (**L3** and **L4**) as DNA-binding groups with longer (**L2** and **L3**) or shorter (**L1** and **L4**) spacer between the latter and the chelating agent. The corresponding Re complexes (**Re1-4**) were also foreseen for full chemical characterization. Due to the demanding synthesis processes and available time, only **Tc1** and **Tc2** could be synthesized, characterized and biologically evaluated. The Re congeners showed ability to interact with the CT-DNA molecule trough spectroscopic studies. **Tc1** and **Tc2** also showed great ability to target the nucleus, once diffused into the cells of B16-F1 murine melanoma and PC3 human prostate cells, but no radio-cytotoxic effect in these cell lines. Although efficient delivery system at subcellular level could be provided in this work, the relevance of the complexes for the design of Auger emitting ^{99m}Tc radiopharmaceuticals could not be demonstrated.

Keywords

Nuclear Medicine

Radiotherapy

Radiometal

Auger electrons

Technetium-99m

DNA-interaction

Resumo

A terapia com emissores Auger tem despertado interesse nos últimos anos devido à possibilidade de explorar terapia direccionadas, a nível celular. Entre os emissores Auger conhecidos, o ^{99m}Tc oferece diferentes vantagens: baixo custo, elevada disponibilidade e propriedades radioquímicas favoráveis. O curto alcance dos electrões Auger constitui um factor limitante para a sua eficácia biológica exigindo que o radionucídeo se encontre o mais próximo possível do seu alvo, usualmente o DNA nuclear, de modo a exercer os seus efeitos terapêuticos. Assim, o maior desafio para o uso deste tipo de radionuclídeos em procedimentos terapêuticos é o desenho de vectores de entrega eficientes a nível subcelular. Já se encontra descrito um reduzido número de complexos radioactivos com capacidade de se localizar no núcleo das células e com afinidade para o DNA. Para esse efeito, tais compostos possuem em geral um agente quelante multifuncional com capacidade de estabilizar a unidade *fac*-$[^{99m}Tc(CO)_3]^+$ e, simultaneamente, um agente intercalador do DNA que assegura a proximidade e afinidade para o alvo. Neste trabalho propôs-se a síntese de complexos de tecnécio (**Tc1-4**) estabilizados por agentes quelantes do tipo pirazolo-diamina contendo os agentes intercaladores antraceno (**L1** e **L2**) ou alaranjado de acridina (**L3** e **L4**), com um espaçador metilénico maior (**L2** and **L3**) ou menor (**L1** and **L4**) entre o agente quelante e intercalador. Perspectivou-se ainda a síntese dos respectivos complexos de rénio (**Re1-4**) para uma completa caracterização dos compostos. Devido à elevada exigência da síntese dos ligandos e ao tempo disponível, apenas os complexos **Tc1** e **Tc2** foram sintetizados e caracterizados. Estudos espectroscópicos com os congéneres de Re mostraram que os complexos interagem com o DNA. **Tc1** e **Tc2** demonstraram elevada capacidade de se localizar no núcleo celular em estudos com células B16-F1 de melanoma de ratinho e células PC3 de cancro de próstata humana. No entanto, não exerceram qualquer efeito radio-citotóxico. Apesar de os complexos apresentarem uma elevada capacidade para atingir o núcleo de células tumorais, não foi possível demonstrar o seu interesse para o desenho de radiofármacos de ^{99m}Tc para terapia Auger.

Palavras-chave

Medicina Nuclear

Radioterapia

Radiometal

Electrões Auger

Tecnécio-99m

Interacção com DNA

Index

Acknowledgments ... **iii**
Abstract ... **v**
Keywords ... v
Resumo ... **vii**
Palavras-chave ... vii
List of Figures ... **xiii**
List of Schemes ... **xv**
List of tables ... **xvii**
List of symbols and abbreviations ... **xix**

1 Introduction ... **1**
1.1 General aspects about Nuclear Medicine ... 1
1.1.1 Diagnosis in Nuclear Medicine ... 2
1.1.2 Therapy in Nuclear Medicine ... 4
1.1.2.1 Biological effects of ionizing radiation ... 4
1.1.2.2 Systemic cancer therapy in Nuclear Medicine ... 5
1.2 Auger electrons and cancer therapy ... 7
1.2.1 Auger electrons ... 7
1.2.2 Prospective Auger emitters for cancer therapy ... 8
1.3 Design of metal-based radiopharmaceuticals ... 10
1.4 Technetium ... 11
1.4.1 Basic chemical and radiochemical aspects ... 11
1.4.2 ^{99m}Tc and cancer theranostics ... 15
1.5 Background and aim of the thesis ... 20
1.6 Rationale for the design and evaluation of the proposed complexes ... 22
1.6.1 Pyrazole-diamine BFCs ... 22
1.6.2 DNA-binding groups and DNA interaction ... 23
1.6.2.1 DNA binders and DNA-binding modes ... 24
1.6.2.2 Acridine orange and anthracene ... 25
1.6.2.3 Evaluation of DNA-binding ... 26
1.6.3 Functionalization with a bioactive peptide and a nuclear localization sequence: a perspective ... 27
1.6.3.1 Bioactive peptide ... 27
1.6.3.2 Nuclear localization sequence ... 28

2 Results and discussion: synthesis and characterization of the ligands and complexes ... **31**
2.1 Synthesis and characterization of the ligands ... 31
2.2 Synthesis and characterization of the Re(I) and ^{99m}Tc(I) tricarbonyl complexes ... 40

3 Results and discussion: *in vitro* and biological studies 47

3.1 Spectroscopic studies of the interaction of the ligands and corresponding Re(I) complexes with the DNA molecule 47

3.2 Lipophilicity of the ^{99m}Tc complexes 49

3.3 *In vitro* stability and protein binding of the ^{99m}Tc complexes 50

3.4 Cellular uptake and subcellular distribution of the ^{99m}Tc complexes 51

3.4.1 Cell uptake and cell internalization 52

3.4.2 Nuclear and mitochondrial uptake 54

3.5 Cytotoxicity of the tricarbonyl complexes and respective ligands 56

3.5.1 Cytotoxicity of the ligands and Re complexes 57

3.5.2 Radio-cytotoxicity of the ^{99m}Tc complexes 59

4 Conclusions and future prospects 61

5 Experimental section 63

5.1 General aspects 63

5.2 Materials and methods 63

5.2.1 Solvents and reagents 63

5.2.2 Techniques for purification and/or characterization 64

5.3 Synthesis and characterization of the ligands 67

5.3.1 Synthesis and characterization of the pyrazol units 67

5.3.2 Synthesis and characterization of the DNA-binding units 76

5.3.3 Synthesis and characterization of Ant-CH_2-pzNN (L1) 80

5.3.4 Synthesis and characterization of Ant-$(CH_2)_3$-pzNN (L2) 82

5.3.5 Synthesis and characterization of AO-$(CH_2)_3$-pzNN (L3) 83

5.4 Synthesis and characterization of the Re complexes 85

5.4.1 *fac*-[$Re(CO)_3$(Ant-CH_2-pzNN)]Br (Re1) 85

5.4.2 *fac*-[$Re(CO)_3$(Ant-$(CH_2)_3$-pzNN)]Br (Re2) 85

5.5 Synthesis and characterization of the ^{99m}Tc complexes 86

5.5.1 Precursor *fac*-[$^{99m}Tc(H_2O)_3(CO)_3]^+$ 86

5.5.2 *fac*-[$^{99m}Tc(CO)_3$(Ant-CH_2-pzNN)]$^+$ (Tc1) 87

5.5.3 *fac*-[$^{99m}Tc(CO)_3$(Ant-$(CH_2)_3$-pzNN)]$^+$ (Tc2) 87

5.6 Spectroscopic studies of the interaction of the ligands and Re complexes with the DNA molecule 88

5.7 *In vitro* studies of the ^{99m}Tc-Ant-$(CH_2)_3$-pzNN (Tc2) 89

5.7.1 Lipophilicity 89

5.7.2 *In vitro* stability 89

5.7.2.1 Stability in the presence of histidine 89

5.7.2.2 Stability in Human serum and determination of protein binding 89

5.8 Cell studies 90
5.8.1 Cell lines and cultures 90
5.8.2 Cell internalization of the ^{99m}Tc complexes 90
5.8.3 Cellular and nuclear uptake of the ^{99m}Tc complexes 91
5.8.4 Mitochondrial and nuclear uptake of the ^{99m}Tc complexes 92
5.8.5 Radio-Cytotoxicity of the ^{99m}Tc complexes 92
5.8.6 Cytotoxicity of the ligands and Re complexes 93

6 References 95

List of Figures

Figure 1.1 Representation of a target-specific or 2nd generation radiopharmaceutical and its target[4] 2

Figure 1.2 Direct *vs* indirect effects of ionizing radiation on DNA molecule[7] 5

Figure 1.3 Representation of the path lengh of the α-, β- and Auger radiation at cellular and subcellular levels. The Auger emitter requires close proximity to the target in order to have high biological effectiveness 7

Figure 1.4 Left: schematic representation of internal conversion (IC) process. The de-excitation of the radionuclide may occur by γ-ray or IC electron emission. The gap created can be filled by an electron of a higher electronic shell, with energy release.[1] Right: schematic representation of Auger electron emission. A gap in eletronic shell originated by IC or by electron capture is filled by an electron of a higher shell. The energy is transfrerred to another electron of the higher shell which is emitted. 8

Figure 1.5 Schematic representation of the bifunctional chelator (BFC) approach 10

Figure 1.6 Schematic representation of SPECT imaging with the brain perfusion agent ^{99m}Tc-ethyl cysteinate dimer (ECD, or Bicisate) in patient. Right: molecular structure of ECD; Center: schematic representation of a gamma camera image acquisition; Left: SPECT image obtained 12 hours after ECD administration in a patient with a cerebral embolism (adapted)[27–29] 12

Figure 1.7 Obtention of ^{99m}Tc from a ^{99}Mo/^{99m}Tc generator followed by ^{99m}Tc radiopharmaceutical preparation and administration in patient (adapted) [30] 12

Figure 1.8 Molecular scrutures of some of the currently approved perfusion ^{99m}Tc-radiopharmaceuticals[29] 13

Figure 1.9 Section of the Periodic Table with the group 7 elements Tc and Re 15

Figure 1.10 ^{99m}Tc-tricarbonyl complexes containing pyrene (left) or anthraquinone (right) DNA-binding groups[12] 17

Figure 1.11 Re-tricarbonyl complexes containing acridine orange as DNA-binding group (left) functionalized with bombesin (BBN) bioactive peptide (right) introduced by Alberto and coworkers[43] 18

Figure 1.12 ^{99m}Tc-tricarbonyl complexes containing anthracene DNA-binding group at terminal amine of the pyrazole-diamine chelator (left) or at 4-position of the pyrazolyl ring (right) introduced by Vitor *et al*[48] 19

Figure 1.13 Left: Molecular structure of Re-tricarbonyl complexes containing acridine orange DNA-binding group at 4-position of the pyrazolyl ring and functionalized with bombesin analogues. Right: Single-cell fluorescence distribution of the Re-complexes in PC-3 cells, visualized by time-lapse cofocal microscopy imaging at time points of 5, 15, 30 and 60 min.[47] 20

Figure 1.14 Molecular structures of the Re and ^{99m}Tc complexes proposed in this thesis 21

Figure 1.15 Schematic representation of ^{99m}Tc radiopharmaceuticals intended with this thesis 21

Figure 1.16 Schematic representation of different possibilities for functionalization of pyrazole-diamine BFCs with biomolecules and/or DNA-binding groups. The N donor atoms for stabilization of *fac*-$[M(CO)_3]^+$ are also featured. 22

Figure 1.17 The three main binding modes of small molecules with the DNA with biomedical interest for drugs containing DNA-binding units (A-intercalation; B-minor groove binding; C-major groove binding) 24

Figure 1.18 Molecular structure of some DNA-binding molecules[56,57] 25

Figure 1.19 Molecular structures of acridine orange and antracene 26

Figure 2.1 ^{1}H-NMR spectrum of ethyl 1-(2-bromoethyl)-1H-pyrazole-4-carboxylate (22) 38

Figure 2.2 ^{13}C-NMR spectrum of ethyl 1-(2-bromoethyl)-1H-pyrazole-4-carboxylate (22) 38

Figure 2.3 ^{1}H-NMR spectrum of ethyl 1-(2-(tert-butoxycarbonyl(2-(tert-butoxycarbonylamino)ethyl)amino)ethyl)-1H-pyrazole-4-carboxylate (25) 39

Figure 2.4 ^{1}H-NMR spectrum of 1-(2-(tert-butoxycarbonyl(2-(tert-butoxycarbonylamino)ethyl)amino)ethyl)-1H-pyrazol-4- hydroxymethyl (26) 39

Figure 2.5 ESI-MS spectrum of Re-Ant-$(CH_2)_3$-pzNN (Re2) 42

Figure 2.6 [^{1}H, ^{1}H] COSY spectra of Re2 in CD_3OD (ampliation of the aliphatic region) 42

Figure 2.7 ^{1}H-NMR spectra of Re2 in CD_3OD 43

Figure 2.8 [^{1}H, ^{13}C] HSQC spectra of Re2 in CD_3OD (ampliation of the aliphatic region) 43

Figure 2.9 ^{13}C-NMR spectra of Re2 in CD_3OD 43

Figure 2.10 HPLC trace of the precursor $[^{99m}Tc(H_2O)_3(CO)_3]^+$ 44

Figure 2.11 HPLC chromatograms of Tc1 and Re1 obtained by γ- and UV-detection, respectively 45

Figure 2.12 HPLC chromatograms of Tc2 and Re2 obtained by γ- and UV-detection, respectively 45

Figure 3.1 Absorption spectra of solutions containing 50 µM of L2 (left) or 100 µM of Re2 (right) in PBS (10 mM, pH = 7.2) with different equivalent amounts of CT-DNA. 47

Figure 3.2 Fluorescence spectra of solutions containing 8 µM of L2 (left) or Re2 (right) in PBS (10 mM, pH = 7.2) with different equivalent amounts of CT-DNA 48

Figure 3.3 Stability of Tc2 in presence of histidine in PBS (pH = 7) after 2 hours of incubation at 37°C 50

Figure 3.4 Stability of Tc2 in presence human serum after 6 hours of incubation at 37°C 51

Figure 3.5 Cell internalization of Tc1 in function of time, after 4 hours incubation at 37°C, in B16-F1 cells (left) and PC-3 cells (right) 53

Figure 3.6 Cell internalization of Tc2 in function of time, after 4 hours incubation at 37°C, in B16-F1 cells (left) and PC-3 cells (right) 53

Figure 3.7 Cell uptake of Tc1 and Tc2 as a function of time, after 4 hours incubation at 37°C, in B16-F1 and PC-3 cells 54

Figure 3.8 Cellular, nuclear and mitochondrial uptakes of Tc1 and Tc2 by B16-F1 and PC-3 cells per million cells after 2 hours incubation at 37°C 56

Figure 3.9 Cytotoxicity of L1 and Re1 at different concentrations, after 40 hours incubation at 37°C, in B16-F1 cells (left) and PC-3 cells (right) 58

Figure 3.10 Cytotoxicity of L2 and Re2 at different concentrations, after 40 hours incubation at 37°C, in B16-F1 cells (left) and PC-3 cells (right) 58

Figure 3.11 Radio-cytotoxicity of Tc1 at different activities, after 40 hours incubation at 37°C, in B16-F1 cells (left) and PC-3 cells (right) 60

Figure 3.12 Radio-cytotoxicity of Tc2 at different activities, after 40 hours incubation at 37°C, in B16-F1 cells (left) and PC-3 cells (right) 60

List of Schemes

Scheme 1.1 Simplified scheme of $^{99}Mo/^{99m}Tc$ generator nuclear decays (adapted)[31] 13

Scheme 1.2 Aqueous-based *kit* preperation of *fac*-$[^{99m}Tc(H_2O)_3(CO)_3]^+$ precursor by Alberto *et al*, 2001[36] 14

Scheme 2.1 Synthesis of Ant-CH_2-pzNN (L1) 31

Scheme 2.2 Synthesis of the N-hydroxysuccinimine (NHS) activated ester pyrazole-diamine derivative (13) 33

Scheme 2.3 Synthesis of 3-(anthracen-9-yl)propan-1-amine (14) 34

Scheme 2.4 Syntheis 10-(3-aminopropyl)-3,6-bis(dimethylamino)acridinium (18) 34

Scheme 2.5 Synthesis of Ant-$(CH_2)_3$-pzNN (L2) and AO-$(CH_2)_3$-pzNN (L3) 35

Scheme 2.6 First strategy for the synthesis of AO-CH_2-pzNN (L4) 36

Scheme 2.7 Second strategy for the synthesis of AO-CH_2-pzNN (L4) 36

Scheme 2.8 Synthesis of tert-butyl 2-(2-(4-(hydroxymethyl)-1H-pyrazol-1-yl)ethylamino)ethylcarbamate (24) and 1-(2-(tert-butoxycarbonyl(2-(tert-butoxycarbonylamino)ethyl)amino)ethyl)-1H-pyrazol-4- hydroxymethyl (26) 37

Scheme 2.9 Synthesis of 4-(bromomethyl)-1-trityl-1H-pyrazole (28) 40

Scheme 2.10 Synthesis of Re-Ant-CH_2-pzNN (Re1) by reaction of L1 with the precursor $[Re(CO)_5]Br$ 41

Scheme 2.11 Synthesis of Re-Ant-$(CH_2)_3$-pzNN (Re2) by reaction of L2 with the precursor $[Re(H_2O)_3(CO)_3]Br$ 41

Scheme 2.12 Synthesis of Tc1 and Tc2 with the precursor *fac*-$[^{99m}Tc(H_2O)_3(CO)_3]^+$ 44

List of tables

Table 1.1 Commonly used β^+ emitters for PET imaging[6] 3

Table 1.2 Commonly used γ-ray emitters for SPECT imaging[6] 4

Table 1.3 Examples of α- and β-emitters radionuclides for therapeutic applications[3] 6

Table 1.4 Examples of Auger electron emitters with potential interest for radiotherapy[10] 9

Table 1.5 Bombesin receptor subtypes and the respective native peptide sequences[77] 28

Table 1.6 Exemples of nuclear localization sequences of the different classes[80,81] 29

Table 3.1 Intrinsic binding constants (*k*) of L1, Re1, L2 and Re2 48

Table 3.2 Stern-Volmer constant (K_{sv}) of L2 and Re2 49

Table 3.3 Partition coefficient (log $P_{o/w}$) values of Tc1 and Tc2 49

Table 3.4 Cellular, nuclear and mitochondrial uptakes of Tc1 in B16-F1 and PC-3 cells after 2 hours incubation at 37°C 55

Table 3.5 Cellular, nuclear and mitochondrial uptakes of Tc2 by B16-F1 and PC-3 cells after 2 hours incubation at 37°C 55

Table 3.6 50% inhibitory concentration (IC_{50}) of L1, Re1, L2 and Re2 in B16-F1 and PC-3 cells 58

List of symbols and abbreviations

ACN - Acetonitrile

Ant - Anthracene

AO - Acridine orange

aq - Aqueous

BBN - Bombesin

BFC - Bifunctional chelator

BM - Biomolecule (s)

BOC - *tert*-Butyloxycarbonyl

Boc_2O - Di-*tert*-butyl dicarbonate

br - Broad

C^2TN - Centro de Ciências e Tecnologias Nucleares

CD_3OD - Deuterated methanol

$CDCl_3$ - Deuterated chloroform

Ci - Curie

cpm - Counts *per* minute

CR group - Ciências Radiofarmacêuticas group

CT-DNA - Calf Thymus DNA

d - Doublet

DCM - Dichloromethane

DIPEA - *N*,*N*-Diisopropylethylamine

DMF - Dimethylformamide

DMSO - Dimethyl Sulfoxide

DNA - Deoxyribonucleic acid

DSB - Double strand break

EDC - 1-Ethyl-3-(3-dimethylaminopropyl)-carbodiimide

ESI/MS - Electrospray ionization Mass spectrometry

Et - Ethyl

Et_2O - Diethyl ether

EtOH - Ethanol

***fac* -** facial

h - Hour (s)

HPLC - High-performance liquid chromatography

IC - Internal conversion

IST - Instituto Superior Técnico

IT - Isomeric transition

K - Intrinsic binding constant

LET - Linear energy transfer

Log P - Partition coefficient

m - Multiplet

MeOH - Methanol

Met - Methyl

min - Minute (s)

MTT - 3-(4,5-dimethylthiazol-2-yl)-2,5-diphenyltetrazolium bromide

NHS - *N*-Hydroxysuccinimide

NLS - Nuclear Localization Sequence

NMR - Nuclear Magnetic Resonance

O-PPh3 - Triphenylphosphine oxide

PBS - Phosphate Buffered Saline

PET - Positron emission tomography

PPh3 - Triphenylphosphine

ppm - Parts per million

pz - Pyrazole

pzNN - Pyrazole-diamine

q - Quartet

r.t. - Room temperature

R_f - Retardation factor

ROS - Reactive oxygen species

rpm - Rotation per minute

s - Singlet

SPECT - Single photon emission computed tomography

SSB - Single strand break

t - Triplet

$t_{1/2}$ - Half life time

TFA - Trifluoroacetic acid

THF - Tetrahydrofuran

TLC - Thin layer chromatography

t_R - Retention time

Tr - Trityl

UV - Ultraviolet

UV-Vis - Ultraviolet Visible

α - Alfa

β - Beta

γ - Gamma

δ - Chemical shift

ε - Molar absorptivity

1 Introduction

1.1 General aspects about Nuclear Medicine

Nuclear Medicine is a specialized medical area for development and application of pharmacological agents (carrier) carrying radioactive atoms (radioisotopes) that emit penetrating and/or non-penetrating radiation. Both components, the carrier and the radioisotope, constitute the radiopharmaceutical agent and are determinant for its effectiveness. The characteristics of the carrier should provide tissue/organ specificity and good clearance from the organism, while the radionuclide should provide adequate amount and type of energy for the intended procedure. The different characteristics of the radiation emitted by the radioisotopes define if they can be applied for diagnostic or therapeutic purposes. However, a given radionuclides can be used to obtain therapeutic and diagnostic radiopharmaceuticals, and can also provide *in vivo* monitoring of therapeutic procedures. Its half-life ($t_{1/2}$) is also very important for the data acquisition in diagnosis and for the dose-limiting in therapy.[1–3] Theranostics is another, very attractive, modality for the use of the radiopharmaceutical agents, as many radionuclides or matched/pairs of radionuclides have physical properties suitable both for imaging and therapeutic applications.

Depending on the mode of their biodistribution, the radiopharmaceutical agents can be classified as **perfusion** or **1st generation radiopharmaceuticals** and **target-specific** or **2nd generation radiopharmaceuticals**. The biodistribution of the former depends primarily on its physical-chemical properties such as charge, size and lipophilicity; while the latter are conjugated with a bioactive molecule (BM) that specifically recognizes and binds to its molecular target. Most of the available radiopharmaceuticals are perfusion agents but target-specific radiopharmaceuticals are gaining more interest with the advances in molecular biology, and are more appealing for targeted procedures.

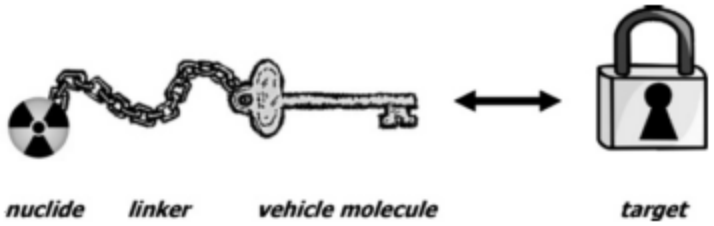

Figure 1.1 Representation of a target-specific or 2nd generation radiopharmaceutical and its target[4]

The targets for the target-specific radiopharmaceuticals are usually receptors but they can also be other biological entities. The BMs are referred as vehicle molecules and they can be enzyme substrates, agonists or antagonists for receptors and transporters or metabolites. A linker is usually used to minimize eventual structural-related changes in the properties and specificity of the BM with the introduction of the radionuclide. It can also be used as pharmacokinetics modulator of the final radiopharmaceutical.

The final radiopharmaceutical should have good physical-chemical properties and pharmacokinetics, preferably with high metabolic stability; short but effective biological half-life, which represents the time needed for half of the radiopharmaceutical disappear from the biologic system; high specificity for the target and minimal accumulation in non-target tissue (ensured by the carrier); and should be easily produced with ready and cheap availability in clinical facilities (highly dependent on the $t_{1/2}$ and availability of the radionuclide). If it is a radiotherapeutic agent it should also present emission of ionizing particles that can cause damage to the target biological system.[1,4,5]

The use of radiopharmaceuticals for cancer diagnosis and/or therapy is of great interest. Early detection and targeted therapy can be provided (and possibly monitored simultaneously); however, as we will see throughout this thesis, it is a very demanding and complex process involving multiple areas such as molecular biology, organic and inorganic chemistry, biomedicine, etc.

1.1.1 **Diagnosis in Nuclear Medicine**

The big majority (> 90%) of the existing radiopharmaceuticals are for diagnostic applications, through molecular imaging procedures. This procedure is non-invasive and allows *in vivo* visualization of chemical and biological processes at cellular and molecular levels without interfering with its mechanisms. The trace quantity of the radiopharmaceutical used is not toxic for the living organism and allows image acquisition with good special resolution thanks to the available techniques. Unlike other imaging techniques as X-ray or ultrasound, where the images

are obtained through externally applied radiation, in Nuclear Medicine, the images are obtained by equipments that detect the tissue-penetrating radiation of the administrated (usually intravenously) radiopharmaceutical from the inside the body. Two imaging modalities, single photon emission computed tomography (SPECT) and positron emission tomography (PET) are the basis of Nuclear Medicine. These techniques are often coupled to computed tomography (CT) or to magnetic resonance imaging (MRI) to give hybrid imaging systems such as PET/CT, SPECT/CT or PET/MRI. This is because the SPECT and PET techniques have poor anatomic special resolution, contrary to the CT and MRI. The hybrid techniques provide acquisition of both anatomical and molecular/functional information with high resolution.[1–3,6]

The radionuclides for PET imaging decay by emission of positron. This positively charged particle is annihilated by an electron in the matter originating two 511 keV γ-ray at opposite directions which are then detected simultaneously.

Table 1.1 Commonly used β^+ emitters for PET imaging[6]

Nuclide	Half-life/min	Max. energy/MeV
^{11}C	20.3	0.97
^{13}N	10	1.20
^{15}O	2	1.74
^{18}F	110	0.64
^{64}Cu	762	0.66
^{68}Ga	68.1	1.90
^{76}Br	972	4.00
^{124}I	60 192	2.14

Two remarkable characteristics of the radionuclides used for PET imaging play important roles in radiopharmaceutical design. The first is the nature of the majority of these elements (see Table 1.1). In particular, the ^{11}C, ^{13}N and ^{15}O isotopes are highly abundant in the biological systems and compose the majority of the molecules in the organism. This is a great advantage as these radionuclides can directly be incorporated in natural biomolecules without interfering with its biological properties. On the other hand, the second characteristic, which is the short half-lives of most of these radionuclides, is limiting for the efficacy and feasibility of the respective radiopharmaceuticals. The majority of these radionuclides are produced in cyclotrons, and along with the short half-lives, it is mandatory the presence of such equipments in or near to the clinical facilities, making PET imaging a very expensive procedure. Still, the ^{11}C and ^{18}F present reasonable properties and are widely used, and the exploitation of the more convenient metallic radionuclides such as ^{64}Cu and ^{68}Ga is gaining particular interest in PET.[1,2,4,6]

Table 1.2 Commonly used γ-ray emitters for SPECT imaging[6]

Nuclide	Half-life/h	Principal photon emission energies/MeV
^{123}I	13.2	0.16
^{99m}Tc	6	0.14
^{111}In	67.9	0.17/0.25
^{67}Ga	78.3	0.09/0.19/0.30
^{201}Tl	73.1	0.17

The radionuclides for SPECT imaging are γ-photon emitters with an energy range about 30-300 keV (minimal and maximum energies detectable using the commonly available collimators) with an optimal range around 150 keV. The collimator is positioned in front of the gamma camera and it defines the angle of incidence of the emitted γ-rays. In SPECT, the detection system is less sensitive and less efficient than in PET, thus presenting images with lower resolution. The major advantage for the use of SPECT over PET is the higher availability of suitable radionuclides, with longer half-lives at low cost. However, the SPECT radionuclides are mostly metallic elements (Table 1.2) requiring different and more difficult approaches for the synthesis of efficient radiopharmaceuticals compared to PET (see Section 1.3).[1,6]

1.1.2 **Therapy in Nuclear Medicine**

1.1.2.1 **Biological effects of ionizing radiation**

Ionizing radiations lead to different ionizing events, when in contact with matter, which can cause damage to the cell molecules. The nuclear DNA is the most radiation-sensitive molecule of the cell, and the fact that it is determinant for the cell survival makes it its most valuable target. The DNA damage through ionizing radiation can occur by two processes: direct and indirect (Figure 1.2).

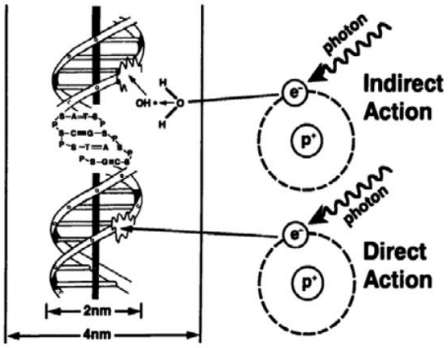

Figure 1.2 Direct *vs* indirect effects of ionizing radiation on DNA molecule[7]

In **direct effect** the energy is directly transferred to the target molecule while in **indirect effect** an intermediate molecule is ionized leading to generation of highly reactive species which react with the target. The most important intermediate molecule for indirect effect is the extremely abundant H_2O (about 80% of the cell mass) which produces reactive oxygen species (ROS), especially the hydroxyl radical ($OH^{\bullet}$), by radiolysis. It is estimated that the indirect effect occurs twice as much as the direct effect of radiation.[7,8]

The main DNA lesions introduced by ionizing radiation are bases and sugar damage, single strand breaks (SSB) and double strand breaks (DSB). The damages can lead to cell death by necrotic or apoptotic activation pathways. The presence of scavengers or DNA-repair mechanisms may reduce significantly the potential of radiation damage. But they are not very effective for high radiation deposition which is associated with the direct effect and DSB lesions and present reduced rate of cell survival.[7]

1.1.2.2 **Systemic cancer therapy in Nuclear Medicine**

Cancer is one of the most common and challenging diseases of today's society. The search for highly specific and efficient therapeutic agents is incessant with two major modalities: chemotherapy and radiotherapy. The reduced blood supply and biological transformation usually observed in cancer cells are limiting for systemic targeted therapy.[9] Systemic radiotherapeutic procedures in Nuclear Medicine are still less developed, and the majority of the available radiopharmaceutical agents are yet at pre-clinical stage. This field is more challenging due to the poor availability of suitable therapeutic radionuclides and the need of developing highly specific delivery systems. The lack of specificity makes the determination of the administration dose a very difficult task.[5,10,11]

Again, ideal radionuclides for therapeutic purposes must be highly available, with adequate $t_{1/2}$ and with abundance of particle/electron emission. The amount of the eventual accompanying penetrating radiation (such as γ-ray) must be minimal. There are three classes of suitable

radionuclides for therapeutic use: the α-emitters, β-emitters and Auger emitters. The overwhelming majority of the current radiotherapeutic agents in clinical use are β-emitters. Until recently, only α- and β-emitters radionuclides have been explored for therapeutic application (Table 1.3) but nowadays the potential of Auger electrons is gaining more attention.[3,10,12]

Table 1.3 Examples of α- and β-emitters radionuclides for therapeutic applications[3]

Radionuclide	Emission type	Half-life	Emax (keV)	Range in tissue
^{186}Re	β, γ (9.4%)	89.2 h	(β): 1069	Maximum (5 mm)
^{166}Ho	β, γ (6.7%)	26.9 h	(β): 1853	Maximum (10.2 mm)
^{188}Re	β, γ (15.1%)	17.0 h	(β): 2120	Maximum (11 mm)
^{89}Sr	β	52.7 days	1463	Maximum (3 mm)
^{32}P	β	14.3 days	1710	Maximum (8.7 mm)
^{90}Y	β	64.1 h	2280	Maximum (12 mm)
^{225}Ac	α	10 days	5830, 5792, 5790, 5732	40–80 μm
^{211}At	α	7.2 h	5870	60–80 μm
^{213}Bi	α	45.7 min	5869	50–80 μm

Besides the type of energy, the three classes of therapeutic radionuclides differ in the magnitude of the **linear energy transfer** (LET) and therefore in radiation range/penetration and biological effects. LET corresponds to the average energy deposition per unit distance along the path of the radiation and it is expressed as keV/ μm. The density of the energy deposition in biological tissue or cell determines the biological effectiveness of the radiation.[7]

β-particles have low LET and long path length in order of millimeters, compared to the 20 μm diameter of the average cell. The biological effects are due to indirect effects. The LET of these particles is so low that the targeted therapy towards a specific macromolecule is not viable, because the energy deposition is not high enough to cause significant damage. The long range of β^- particles can be advantageous for the treatment of big metastases even if there is a non-uniform drug distribution. The big disadvantageous is that there is an enhanced irradiation of the surrounding healthy cells.

On the other hand, α-particles have high LET and very short range, in order of micrometers (30-80 μm). It is suitable for treatment of metastatic cells with adequate blood supply at single-cell to a few cell-cluster levels. The major limitation for the application in therapy is the low availability of α-emitting radionuclides with adequate half-lives.[3,10,12]

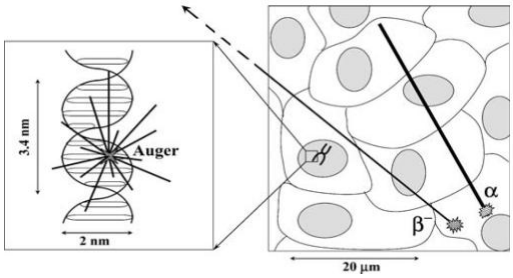

Figure 1.3 Representation of the path lengh of the α-, β- and Auger radiation at cellular and subcellular levels. The Auger emitter requires close proximity to the target in order to have high biological effectiveness

Similarly to the α-particles, Auger electrons present high LET but lower range, in order of nanometers (<100 nm), and very short penetration in biological systems. It is also suitable for the treatment of small metastases at single-cell level, preferentially by direct energy deposition on a cell target-component such as the DNA (Figure 1.3). Contrary to the case of β^- emitters, the high LET of α- and Auger emitters allow higher biological effectiveness by causing significant DSB through direct effect on the DNA molecule. The short range would provide a more efficient target therapy for the radiopharmaceuticals with minimal burden for the healthy tissue.[10,12]

1.2 Auger electrons and cancer therapy

1.2.1 Auger electrons

Daughter nuclides in excited states may be generated after radioactive decay by the parent radionuclides. The de-excitation by isomeric transition (IT) to the ground state may occur by γ-ray emission or by direct transfer of photons to an orbiting electron leading to its ejection in a process called internal conversion (IC) (Figure 1.4, left). This process creates a vacancy in the internal atomic shell. Another process that also generates this gap is the electron capture process in which an electron is transferred from the internal atomic shell into the nucleus.[1,7,10,13]

In both cases the vacancy can be filled, followed by a cascade of electron transitions, by an electron of a higher electron shell. The energy difference between the two shells is released as photons by a radiative transition or as low-energy electrons (Auger electrons) by non-radiative processes (Figure 1.4, right). These electrons, named after the physicist Pierre Auger, are classified as Auger, Coster-Kroning or Super-Coster-Kroning if the filling and the ejected electrons come from a higher shell of the vacancy, if the ejected electron comes from a higher

shell but the filling electron comes from the same shell of the vacancy or if both the filling and ejected electrons came from the same shell of the vacancy, respectively. All these low-energy electrons are generally referred as Auger electrons.[10,13]

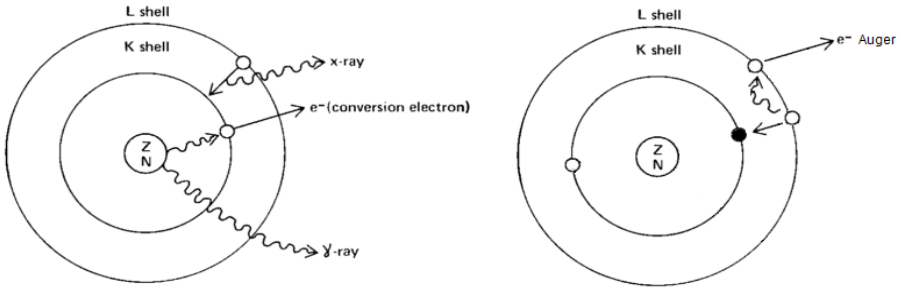

Figure 1.4 **Left**: schematic representation of internal conversion (IC) process. The de-excitation of the radionuclide may occur by γ-ray or IC electron emission. The gap created can be filled by an electron of a higher electronic shell, with energy release.[1] **Right**: schematic representation of Auger electron emission. A gap in eletronic shell originated by IC or by electron capture is filled by an electron of a higher shell. The energy is transfrerred to another electron of the higher shell which is emitted.

1.2.2 **Prospective Auger emitters for cancer therapy**

The recent interest for Auger electron emitters in nuclear medicine is because α and β^- emitters failed as therapeutic agents for the treatment of small metastases due to the lack of ideal nuclides, low specificity or high potential for causing unwanted side effects. The therapeutic potential of Auger electrons was once neglected because of its short range, low penetration and low energy yield per decay. But since Carlson and White[14] in 1963 demonstrated that the Auger-emitter ^{125}I could cause molecular fragmentation, and with the advances in molecular biology, targeted therapy at subcellular level gained much interest and potentiated the exploitation of Auger emitting radiopharmaceuticals. The use of Auger electrons emitters for targeted therapy presents great advantages. The short range and high LET (4-26 keV/μm) provide high effectiveness in the irradiation of the target with low toxicity for the non-target molecules/cells.[10,13,15]

The DNA is the main target for targeted therapy at subcellular level and most of the cancer therapeutic agents prevent or reduce tumor grow by interfering with the DNA integrity directly or through inhibition of DNA enzymes. The radiotoxicity of Auger electrons by indirect effect towards DNA molecule has been reported and it's the most common effect caused by this type of particles.[15] But the search for specific therapy via direct effect through DNA targeting is more appealing as the damage can be greater and difficult to repair. The biggest challenge relies on the development of efficient radioactive compounds able to ensure close proximity of the

nuclide to the molecule target and with high specificity and clearance from the body in order to reduce the dose limiting toxicity. This would provide administration of adequate doses without accumulation in non-target tissue and efficient tumor-cell killing as the absorbed doses tend to be non-uniform. In other words, this type of radiopharmaceuticals require uptake by all the cells of the tumor in order to exert its therapeutic functions.[13,16]

Table 1.4 Examples of Auger electron emitters with potential interest for radiotherapy[10]

Isotope	Auger electrons/ decay	IC electrons/ decay	Auger energy/decay (keV)	IC energy/decay (keV)	Total energy/ decay (keV)	Auger energy in % of total energy/decay	IC energy in % of total energy/decay	$T_{1/2}$
^{55}Fe	5.1	0	4.2	0	5.8	71.9	0	2.7 yr
^{67}Ga	4.7	0.3	6.3	28.1	201.6	3.1	13.9	78 h
^{99m}Tc	4.0	1.1	0.9	15.4	142.6	0.6	10.8	6 h
^{111}In	14.7	0.2	6.8	25.9	419.2	1.6	6.2	67 h
^{123}I	14.9	0.2	7.4	20.2	200.4	3.7	10.1	13 h
^{125}I	24.9	0.9	12.2	7.2	61.4	19.9	11.8	59.4 d
^{201}Tl	36.9	1.1	15.3	30.2	138.5	11.0	21.8	73 h

Data from American Association of Physicists in Medicine (AAPM). The total energy per decay also includes γ and X-ray contributions.

The efficiency of Auger emitter-based radiopharmaceuticals is also dependent on the characteristics of the radionuclide. As seen in Table 1.4, there are different Auger emitters of different chemical nature (halogens and metals) with different energy range and Auger electrons yield per decay. The IC electrons energies are presented separately because, despite being higher than those of most Auger electrons, IC electrons present low LET and high penetration (in μm range), thus presenting different biological effectiveness. Herein we only consider the Auger electrons for therapy at single-cell level. Other characteristics like half-lives, availability or suitability for functionalization are also critical for the use of such radionuclides. For example, ^{55}Fe present one of the highest Auger electrons yield per decay but its $t_{1/2}$ makes it unsuitable for clinical use.[10]

The Auger emitters ^{111}In, ^{125}I, and ^{123}I are already considered as potential therapeutic radionuclides showing great results in *in vitro* cytotoxic studies by causing DSB or SSB in DNA. The toxicity at single-cell level is comparable to that of α and higher than that of β radionuclides as the low LET of the latter provide predominantly non-specific irradiation effects.[13,17–19] Still, the reduced availability (cyclotron produced radionuclides)[1] is limiting for the use of these radioisotopes.

It is known that the cytotoxicity induced by Auger electron emitters is significantly higher when the radionuclide is positioned as close as possible to the DNA. When located outside the cell nucleus, the cytotoxicity of the radionuclide is much reduced.[10] An important study by Balagurumoorthy and co-workers evaluated the effect of the distance between the decaying Auger-emitter, ^{125}I, and the DNA molecule on DSB yield.[20] In this study, the correlation between

the distance augmentation and the shift on the mechanism, as well as on the magnitude of DSB yield, was quite obvious. The evaluated compounds were derivatives of the DNA groove binder Hoechst 33258, which were labeled with the radionuclide ^{125}I. The compounds only differed on the spacer size between the DNA binder and the radionuclide, which positioned the latter at different distances from the DNA molecule as estimated by molecular modeling. They noticed that in absence of the *OH scavenger dimethyl sulfoxide (DMSO), all the compounds were able to cause DSB although the DSB yield was lower for those compounds that placed the ^{125}I at higher distances from the DNA. However, in the presence of DMSO, the DSB yield remained nearly unchanged for the compounds that ensured closer proximity of ^{125}I to the DNA while the ones with higher ^{125}I distances basically were not able to cause DSB. They concluded that for Auger emitters, the occurrence of direct effect requires a closer proximity at certain distance, even if the potential radiopharmaceutical is bound to the DNA target molecule.

1.3 **Design of metal-based radiopharmaceuticals**

As seen previously, there is available a large variety of metallic radionuclides with favorable features to be used in the development of diagnostic and/or therapeutic radiopharmaceuticals. For this reason, inorganic chemistry is an important area for the development of radiopharmaceuticals. In fact, most of the available radiopharmaceuticals are 1st or 2nd generation metal-based agents. The metallic radionuclides present great advantages because of its high availability at low cost, rich coordination chemistry and generally adequate characteristics such as half-lives, magnitude/type of the energy emitted or particle emission.[5,11,21]

The major limitation for the use of these radionuclides is its incorporation into the pharmacologic agents to obtain specific and efficient final radiopharmaceuticals. For design of target-specific compounds, usually a bifunctional chelator (BFC) is needed to provide the attachment of the radiometal to the BM (Figure 1.5).

Figure 1.5 Schematic representation of the bifunctional chelator (BFC) approach

The choice of the BFC is dictated by the oxidation state of the radiometal and its affinity for the donor atoms of the chelating agent. The BFC approach must ensure tight bounding of the

radiometal to the carrier to obtain kinetically inert and termodinamically stable complexes to avoid unbundling or transchelation by the natural chelators, which would lead to accumulation in non-target tissue. It also must retain the specificity of the BM for its target, which is usually ensured by linkers of appropriate length to move away the BM from the radioactive metal. The synthesis of the BFC usually includes the functionalization with the BM before coordination with the radiometal. Both steps must be feasible with reasonable cost and production time, but the latter is limiting, meaning rapid complexation kinetics and high purity of the final radio-conjugate is needed for viable application. Thus, the BFC should provide versatility for chemical conjugation with both radiometal and BM and high selectivity for the radiometal.[2,5,11,21–23]

1.4 Technetium

1.4.1 Basic chemical and radiochemical aspects

Technetium, from the Greek *technetos* (artificial), is the first artificially made chemical element by man before its discovery in nature. It was first predicted by Mendeleev in 1869 as a second row transition metal with the atomic number of 43 but only discovered in 1937 by Perrier and Segrè, from a molybdenum plate bombarded with deuterons accelerated in a cyclotron. This metallic element belongs to the group 7 of the Periodic Table, presenting eight different oxidation states (+7 to -1) and diverse coordination chemistry that allows coordination with several chelators or BFC ligand systems with different denticity.[24,25]

At least thirty-five isotopes of Tc (^{86}Tc-^{120}Tc) have been identified and none of them is stable.[26] The most relevant Tc radioisotope in Nuclear Medicine is the ^{99m}Tc, being applied in over 70% of all procedures in this field. This metastable radionuclide has almost ideal nuclear properties for medical imaging and till date it has only been applied for diagnosis. ^{99m}Tc emits a highly abundant 140 keV γ-ray (90%), very close to the optimal energy required for detection by the gamma cameras, hence providing images with high resolution (see Figure 1.6). This energy is ideal to penetrate biological tissue without overexposure of the patient to radiation. Also, the radiation from the daughter nuclide is not preoccupant as the β^- energy emission by the ^{99}Tc is very low. What also contributes to the minimal exposure to the radiation dose is the short 6 hours $t_{1/2}$ of ^{99m}Tc. However this $t_{1/2}$ is long enough to enable the synthesis of the ^{99m}Tc radiopharmaceutical, analytical control and purification, administration and imaging procedures in patients.

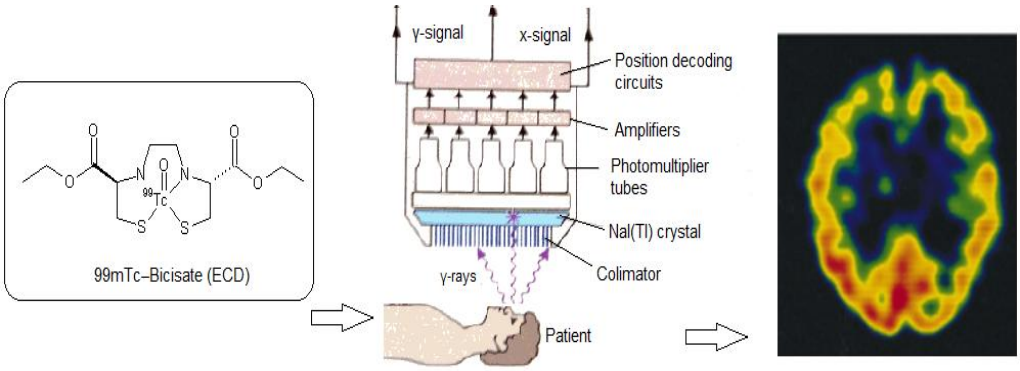

Figure 1.6 Schematic representation of SPECT imaging with the brain perfusion agent ^{99m}Tc-ethyl cysteinate dimer (ECD, or Bicisate) in patient. **Right**: molecular structure of ECD; **Center**: schematic representation of a gamma camera image acquisition; **Left**: SPECT image obtained 12 hours after ECD administration in a patient with a cerebral embolism (adapted)[27–29]

The favorable features, together with the ready and inexpensive availability of ^{99m}Tc by elution of the ^{99}Mo/^{99m}Tc generator and introduction of kits that allow fast and effective synthesis of the radioconjugates (Figure 1.7), justifies the success of ^{99m}Tc in diagnostic Nuclear Medicine.[1,25,30,31]

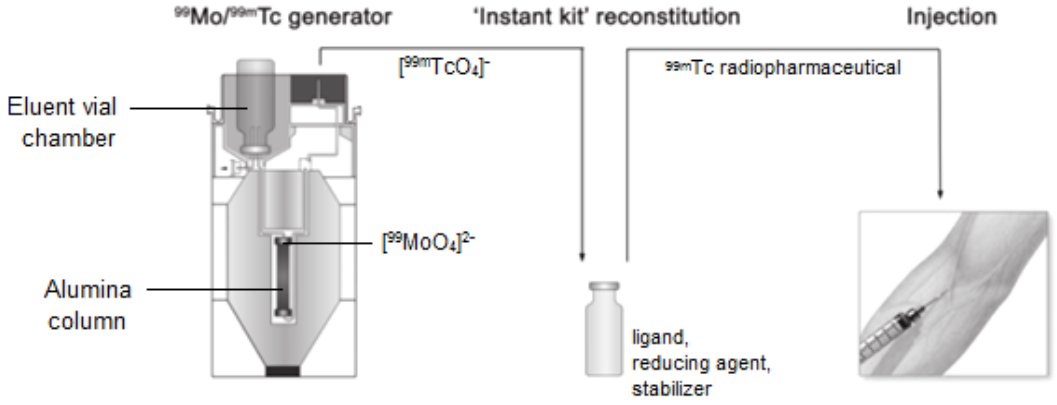

Figure 1.7 Obtention of ^{99m}Tc from a ^{99}Mo/^{99m}Tc generator followed by ^{99m}Tc radiopharmaceutical preparation and administration in patient (adapted) [30]

A typical ^{99}Mo/^{99m}Tc generator consists of $[^{99}MoO_4]^{2-}$ (molybdate) adsorbed on the top of an alumina (Al_2O_3) ion-exchange chromatographic column (Figure 1.7). The ^{99}Mo decay results in accumulation of $[TcO_4]^-$ (pertechnetate) until an equilibrium is reached, after approximately four half-lives of ^{99m}Tc, at the maximum activity. The pertechnetate on top of the column is then eluted with a 0.9% NaCl solution and collected as $[Na^{99m}TcO_4]$ (sodium pertechnetate). The molybdate stays retained in the column and the ^{99}Mo decay originates more pertechnetate that can be eluted successively.

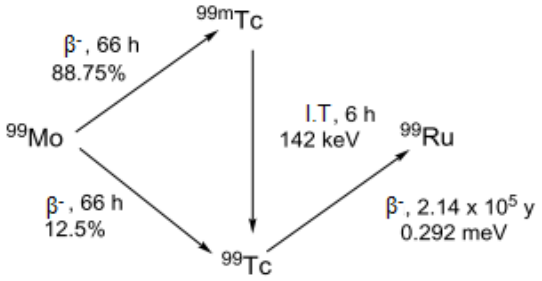

Scheme 1.1 Simplified scheme of $^{99}Mo/^{99m}Tc$ generator nuclear decays (adapted)[31]

Scheme 1.1 summarizes the relationship between the nuclear decay of the radionuclides present on the $^{99}Mo/^{99m}Tc$ generator. ^{99}Mo decays with a half-life of 66 hours by β^- emission to ^{99m}Tc (≈87%) and ^{99}Tc (≈13%). The metaestable ^{99m}Tc ($t_{1/2}$ = 6h) decays by isomeric transition of 140 keV to the ground state ^{99}Tc ($t_{1/2}$ = 2.1 x 10^5 years) which decays to the stable ^{99}Ru by β^- emission.[1,30,31]

The concentration of $[TcO_4]^-$ obtained from each elution is usually about 10^{-7} to 10^{-10} M, thus the synthesis of the radiopharmaceutical agents has to be done directly from the eluate aqueous solution. As the $^{99m}TcO_4^-$ is at +7 oxidation state it first has to be reduced to lower oxidation states by adequate reducing agents under adequate reaction conditions (temperature, pH, etc.), in order to react with the ligands to produce the radiopharmaceutical agent. The final ^{99m}Tc oxidation state determines the choice of the donor atoms and denticity of the chelator, as well as the type of metallic core.[25] Several different cores with different oxidation states and ligands of different denticity were used to obtain a variety of ^{99m}Tc agents applied in diagnostic imaging of brain, skeleton, heart, lung, bone marrow, infection, inflammation, etc., as described in the literature.[25,29,31–33] Some examples of the current approved ^{99m}Tc-radiopharmaceuticals for kidney, brain and heart imaging can be seen in Figure 1.8.

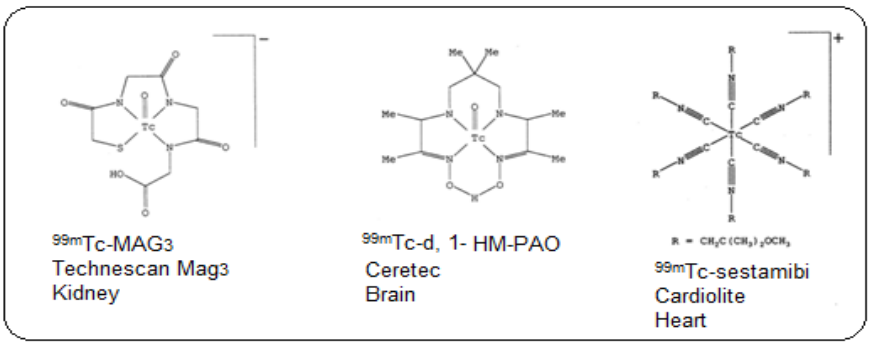

Figure 1.8 Molecular scrutures of some of the currently approved perfusion ^{99m}Tc-radiopharmaceuticals[29]

Tc(V) complexes used to be the most widely explored for the design of ^{99m}Tc radiopharmaceuticals. However, lower ^{99m}Tc oxidation states such as the Tc(I) are gaining more interest especially with the introduction by Alberto et al, 1998, of the novel *fac*-

$[^{99m}Tc(H_2O)_3(CO)_3]^+$ precursor, which can be obtained directly from $[TcO_4]^-$. Initially, the synthesis of this precursor was performed with the reducing agent $NaBH_4$ under 1 atm of CO.[34] This method is not very feasible as the gaseous CO source is considered toxic and also limiting for the fast and ready availability of the precursor in commercial radiopharmaceutical *kits*. Today this problem is overcome by the use of a boranocarbonate reducing agent $K_2[H_3BCO_2]$ that works, simultaneously, as a source of CO for the precursor (see Scheme 1.2).[35] The available *kits* allow fast (20-30 min) preparation of the tricarbonyl precursor in aqueous solution with high yield (>95%), in a single step.

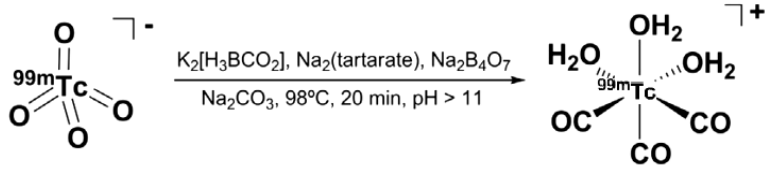

Scheme 1.2 Aqueous-based *kit* preperation of *fac*-$[^{99m}Tc(H_2O)_3(CO)_3]^+$ precursor by Alberto *et al*, 2001[36]

The *fac*-$[^{99m}Tc(H_2O)_3(CO)_3]^+$ precursor is air and water stable in a broad range of pH (1-13) for hours.[34] It is an octahedral complex with three CO ligands facially coordinated to the metal center and each one trans to a water molecules. The water molecules are highly labile and can easily be substituted by a variety of functional groups of different mono, bi or tridentate ligands, while the carbonyl groups are strongly bound to the metal center enabling stable and inert *fac*-$[^{99m}Tc(CO)_3(ligand)]$ complexes.[34,36]

Although none radiopharmaceutical containing the *fac*-$[^{99m}Tc(CO)_3]$ core has yet been applied in clinical trial, this core is of great interest due to the small and compact size, possibility of being stabilized with a large variety of ligand systems, which allows the formation of complexes with tuned physical-chemical properties, namely in terms of hydrophilicity and lipophilicity.[36]

The characterization of the ^{99m}Tc compounds is a limited process due to the very low concentration of this nuclide in aqueous solution. The only method sensitive enough to analyze these much diluted compounds is the HPLC (or other chromatographic methods) coupled to a γ-radiation detector. Otherwise only by use of ^{99}Tc nuclide it is possible to perform the characterization with conventional analytical methods such as NMR, mass spectrometry (MS) or X-ray crystallography. The comparison of the HPLC chromatograms of the ^{99m}Tc compounds with respective ^{99}Tc counterparts allows their chemical identification.[25,30,31]

^{99}Tc is a long-lived isomer of Tc, being the most abundant technetium radioisotope. It is available in macroscopic amounts, and is the most significant byproduct of ^{235}U fission. ^{99}Tc is a weak β^- emitter (0.292 MeV) with no accompanying γ-radiation, thus the HPLC studies of ^{99}Tc compounds are performed using UV and β^- detection. The handling of ^{99}Tc still has to be

performed under good laboratory practices, using glassware to block the β^- particles and taking appropriate precautions.[25,30,31]

The chemical identification of ^{99m}Tc complexes can be done by HPLC comparison with Re congeners, in alternative to the use of ^{99}Tc compounds. The use of non-radioactive Re as ^{99m}Tc analogous is advantageous as it is easier to manipulate without major precautions. The HPLC studies of Re complexes usually involves UV detection.

Rhenium also belongs to the group 7 of the Periodic Table, with atomic number of 75 (Figure 1.9), thus having rich coordination chemistry comparable to that of technetium. The existence of rhenium element, named after the river "Rhine", was confirmed by Noddack-Tacke in 1925 by X-ray spectroscopy. Soon, this element was being produced in macroscopic scale.[24] Re is one of the rarest elements in nature, consisting of a mixture of two isotopes, ^{185}Re (37.4%) and ^{187}Re (62.6%).[31] Due to the lanthanide contraction, the chemistry of Tc and Re is very similar and the respective complexes present similar physical properties, such as size and lipophilicity. Nevertheless, some differences have to be taken into consideration. The technetium compounds are easier to reduce providing faster complexation reactions with the ligands. The rhenium complexes on the other hand are easier to oxidize and more kinetically inert providing more stable complexes.[31,36]

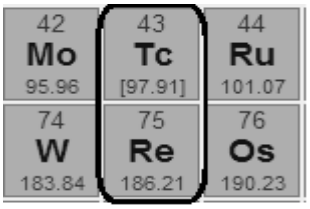

Figure 1.9 Section of the Periodic Table with the group 7 elements Tc and Re

Rhenium possesses two important radioactive isotopes, ^{188}Re ($t_{1/2}$ = 17 h; β^-, 2.1 MeV) and ^{186}Re ($t_{1/2}$ = 90 h; β^-, 1.1 MeV), which can be obtained by elution of the ^{188}W/^{188}Re generator or by neutron irradiation of ^{185}Re, respectively. These metallic radioisotopes have great interest in Nuclear Medicine and are being explored based on coordination or organometallic complexes similar to those of the congener ^{99m}Tc, in terms of available cores and chelators.[30,31,37]

1.4.2 ^{99m}Tc and cancer theranostics

The capabilities of ^{99m}Tc for in vivo imaging are well established being approved a large number of ^{99m}Tc radiopharmaceuticals for diagnostic applications, as mentioned in the previous sections. By contrast, the potential of this radionuclide for clinical therapeutic applications remains to be demonstrated. For this reason, much attention has been drawn in recent years to

the evaluation of the potential therapeutic properties of this radionuclide, as is the case of the present thesis. In particular, these studies intend to prove the relevance of ^{99m}Tc for Theranostics, which requires the combination of diagnostic and therapeutic capabilities in the same entity.

As seen in Section 1.2.2 - Table 1.4, the ^{99m}Tc nuclide is not the most promising Auger emitter candidate for therapy in terms of yield per decay. ^{99m}Tc decays by isomeric transition predominantly by γ-ray emission and the total energy per decay is about 142.6 keV, where only 0.6% of this energy is due to Auger emission and 10.8% due to IC. The number of IC and Auger electrons per decay are about 1.1 and 4, with energies around 15.4 and 0.9 keV, respectively. Only few studies have shown results that indicate some potentiality of this radionuclide for the development of therapeutic agents. Yet, the search is constant and motivated by the fact that along with all the advantages of using an Auger emitter for targeted therapy, ^{99m}Tc is the most easily available at low cost among all the known Auger-emitting radionuclides. The cheap and ready availability, versatility, ideal $t_{1/2}$ and the possibility to monitor the treatment through high resolution imaging are highly favorable characteristics of ^{99m}Tc. The fact that ^{99m}Tc is widely used in diagnosis, being available a large number of approved radiopharmaceuticals obtained with a variety of chelators and based on a well established radiochemistry, also facilitates the development of new and more efficient radiopharmaceutical agents.[10,13] These favorable features prompted several research groups to evaluate ^{99m}Tc complexes as potential radiopharmaceuticals for Auger therapy of cancer. Some of the most important results of such research work are presented bellow.

The first reported *in vitro* study involving pertechnetate as a radiocytotoxic agent was performed with a bacterial strain of *Escherichia coli*, K12S, by Silva and co-workers in 1998. The studies consisted on two assays where the bacteria were directly (in growth medium) or indirectly (separated by glass-wall) exposed to $[^{99m}TcO_4]^-$. The glass attenuates efficiently the Auger and IC electrons but not the γ-rays. They have noticed that the cells directly exposed to $[TcO_4]^-$ presented significant reduced survival fraction relative to the ones exposed only to gamma radiation (5.6 and 65% respectively, after 180 min incubation with a 37mBq/mL final activity). Thus, they concluded that the Auger and/or IC electrons were responsible for the cell cytotoxicity rather than the gamma radiation of the ^{99m}Tc decay. The high radio-cytotoxic effect in this case might be because there is greater access to the DNA in prokaryotes. Also, they showed that the introduction of free radical scavengers or metal ion chelators protected the cells against the radiotoxic effects of the ^{99m}Tc decay indicating that these effects occur partially through indirect mechanisms.[38]

In year 2000, Pedraza-López and co-workers reported *in vitro* DNA damage induced by ^{99m}Tc-radiopharmaceuticals incorporated in murine lymphocytes, as checked by single-cell gel electrophoresis. The cells were incubated with ^{99m}Tc-hexamethyl-propylene amine oxime

(^{99m}Tc-HMPAO) and ^{99m}Tc-2,5-dihydroxybenzoic acid (^{99m}Tc-gentisic acid). As expected, the ^{99m}Tc-HMPAO diffused into the cytoplasm (19.6%; with final activity ≈ 5.3 Bq per cell) while the ^{99m}Tc-gentisic acid remained bonded to the cell membrane (25.6%; with final activity ≈ 4.0 Bq per cell). Despite DNA breaks and alkali labile sites were observed in almost 100% of the cells, no cytotoxic effect was noticed. The results are consistent with the fact that, although the radio-conjugates were close to the nucleus, as it occupies a large part of lymphocyte cells, this proximity was not enough to cause solid and irreparable DNA damages.[39]

The first *in vivo* study showing cancer therapy properties of ^{99m}Tc was performed with pertechnetate, which was administred to nude mice carrying NIS (sodium/iodide symporter)-expressing neuroendocrine tumor, as reported by Behr and coworkers in 2007. They showed that the volume of the tumors decreased significantly in the presence of the radioactive compound, indicating potentiality of the this Auger emitter in therapy.[40] More recently, successful studies with ^{99m}Tc incorporated in multifunctionalized gold nanoparticles provide an extending on the use of this nuclide as a targeted therapeutic agent, through a variety of approaches and delivery systems.[41]

The earlier studies did show that the Auger electrons emitted by ^{9m}Tc can induce DNA damage but mainly emphasized the need for new complexes with the ability to target the cell DNA, in order to function as efficient therapeutic agents. Alberto and co-workers have pioneered the studies with such complexes by introducing multifunctionalized ^{99m}Tc compounds with the ability to target the cell nucleus and enhanced radiotoxic effects in eukaryotic cells. First they synthesized two ^{99m}Tc(I) complexes containing the *fac*-[^{99m}Tc(CO)$_3$] core coordinated by a triamine ligand, and functionalized with two different DNA binders, pyrene and anthraquinone (Figure 1.10). They evaluated the ability of these complexes to cause DSB as an indicator of cytotoxicity.[12]

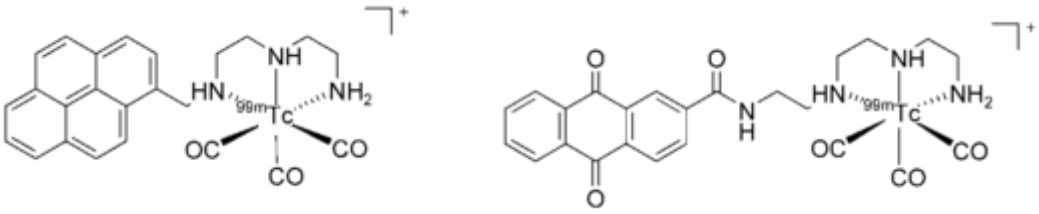

Figure 1.10 ^{99m}Tc-tricarbonyl complexes containing pyrene (**left**) or anthraquinone (**right**) DNA-binding groups[12]

The complexes induced significant amount of DSB on a ϕ174 double-stranded DNA contrary to the non-DNA-binding [^{99m}TcO$_4$]$^-$ and the respective non-radioactive Re compounds. The Re analogues were also used to evaluate the complexes interaction with the DNA molecule and showed that pyrene and anthraquinone complexes were able to interact with DNA. The authors concluded that the Auger electrons from the ^{99m}Tc decay can induce DSB on DNA when located

in its direct vicinity. To evaluate the cytotoxicity at cellular level, they functionalized the pyrene-containing ^{99m}Tc complex with the SV40 nuclear localization sequence (NLS) peptide to allow nuclear targeting and hence, the proximity to the DNA molecule.[42] They showed that the complex was able to accumulate in the nucleus of B16-F1 murine melanoma cells and induce a dose-dependent radiotoxic effect much more significant compared to that of non-nucleus/DNA-targeting complexes (such as $[^{99m}TcO_4]^-$). The cytotoxic effects through DNA damage were evident by the necrotic cell death through mitotic catastrophe pathway. Still, the doses of ^{99m}Tc radioactivity applied were too high with small/slow uptake, which can be limiting for the use of this radionuclide in therapy. This problem had to be overcome by the use of efficient delivery systems that can provide both fast and high uptake by the cells in order to minimize the applied doses.

In another study, Alberto and coworkers found out that related tricarbonyl M(I) (M = ^{99m}Tc, Re) complexes bearing acridine orange as DNA-binding group were able to target the nucleus of B16-F1 and PC3 human prostate cancer cells without the presence of the NLS peptide.[43] The complexes functionalized with a bioactive peptide bombesin (BNN) showed high specific uptake by the PC3 cells through receptor-mediated mechanisms but were not able to reach the nucleus. All the results together indicate that an efficient therapeutic ^{99m}Tc radiopharmaceutical has to be at least functionalized with a DNA-binding group, a NLS and a tumor seeking-vector. Another option is the so-called [2 +1] approach, where the bioactive peptide could be released once inside the cell, while the ^{99m}Tc complex would then reach the nucleus without the presence of the NLS.[44]

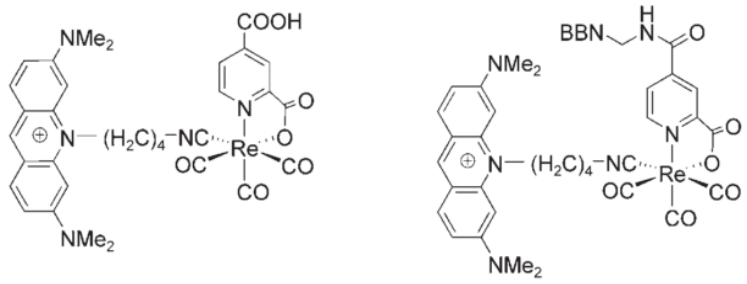

Figure 1.11 Re-tricarbonyl complexes containing acridine orange as DNA-binding group (**left**) functionalized with bombesin (BBN) bioactive peptide (**right**) introduced by Alberto and coworkers[43]

The group of Ciências Radiofarmacêuticas (CR) from C^{2}TN – IST, where the experimental work on the basis of this MSc thesis has been performed, has also been involved in the study of multifunctional ^{99m}Tc tricarbonyl complexes for specific targeting of the nucleus of cancer cells, as summarized below.[45–48]

Victor *et al*, 2008, verified by fluorescence microscopic studies that two novel Re(I) complexes containing the *fac*-$[ReCO)_3]^+$ core and an anthracenyl pyrazole-diamine ligand were able to

target and enter the nucleus of B16-F1 murine melanoma cells. The characterization of the DNA interaction of these complexes by different spectroscopic techniques has shown a moderate affinity of the compounds towards CT-DNA. Later, in 2009, the authors synthesized the congener complexes with ^{99m}Tc and demonstrated that the complexes were also able to enter the nucleus of B16-F1 cells, causing in some cases significant radio-cytotoxic effects and cell death. Most importantly, the radiotoxicity found for these anthracenyl-containing pyrazolyl-diamine ^{99m}Tc(I) tricarbonyl complexes containing against B16F1 murine melanoma cells was well correlated with their nuclear uptake. The ^{99m}Tc complex having the anthracenyl group at the 4- position of the azolyl ring (complex **Tc1**, Figure 1.12 (right)) showed the highest radio-cytotoxicity and induced cell death apparently through caspase-3 apoptotic pathways.

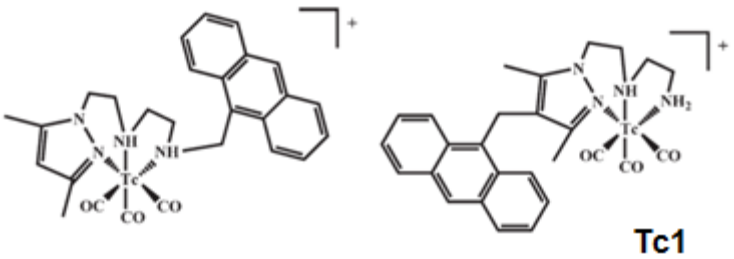

Figure 1.12 ^{99m}Tc-tricarbonyl complexes containing anthracene DNA-binding group at terminal amine of the pyrazole-diamine chelator (**left**) or at 4-position of the pyrazolyl ring (**right**) introduced by Vitor *et al*[48]

Esteves *et al* (2010) have introduced a pyrazole-diamine ^{99m}Tc(I) complex bearing acridine orange (AO) as a DNA binding group, using a butylenic spacer to attach the AO to the 4-position of the pyrazolyl ring. The authors showed that this complex was also able to target the nucleus of B16-F1 cells. Moreover, Esteves *et al* (2011) further functionalized the AO containing ^{99m}Tc(I) complex with the bombesin analogues SGS-BNN and GGG-BNN as tumor-seeking peptides. The Re and ^{99m}Tc complexes containing the GGG-BNN showed high cellular internalization and nuclear uptake in PC-3 cells expressing the GRP-receptor (see Figure 1.13). The observed cell uptake was receptor-mediated showing that the presence of the metal-complexes and/or DNA intercalator did not compromise the ability of specific cell targeting by the BBN vector. Another interesting result is the fact that the GGG-BNN complex can still reach the nucleus, most probably following the lysosomal degradation of the BBN peptide. These are the first examples of ^{99m}Tc complexes that can simultaneously have specific cell targeting and nuclear internalization, a quite encouraging result to further explore this class of compounds in the design of radiopharmaceutical agents for Auger therapy of cancer. But, unlike the **Tc1** introduced by Vitor, the new complexes do not display radio-cytotoxic effects.

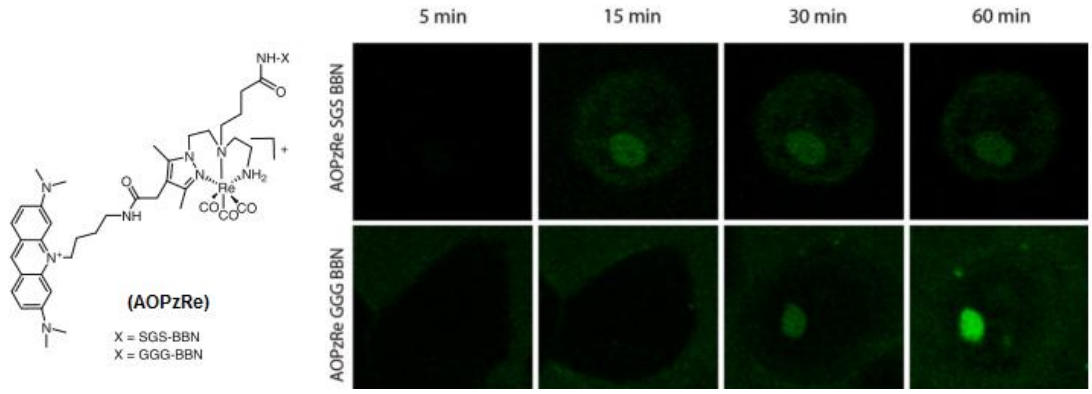

Figure 1.13 **Left**: Molecular structure of Re-tricarbonyl complexes containing acridine orange DNA-binding group at 4-position of the pyrazolyl ring and functionalized with bombesin analogues. **Right**: Single-cell fluorescence distribution of the Re-complexes in PC-3 cells, visualized by time-lapse cofocal microscopy imaging at time points of 5, 15, 30 and 60 min.[47]

1.5 **Background and aim of the thesis**

As mentioned before, the potential capability of ^{99m}Tc-labeled compounds to simultaneously function as therapeutic and diagnostic chemical entities has gained interest in recent years. To explore this potential quality, also known as theranostic property, several complexes have been synthesized and characterized chemically and biologically. For this purpose, the major challenge is to obtain compounds with selective uptake by tumor cells and with the ability to interact with its nuclear DNA, thus leading to cell death as a result of DNA damage induced by Auger electrons emitted by ^{99m}Tc. As this radionuclide is a gamma emitter as well, it could also be possible to monitor the treatment with such complexes using SPECT techniques in patients. Despite some promising *in vitro* results that have been reported, to date there is no example of ^{99m}Tc that has fulfilled the necessary requisites to be used in theranostic applications, particularly in Auger therapy of cancer.

Following some of the previous studies started by the CR group and inspired by several other studies in this field; in this project it was aimed to synthesize, characterize and evaluate biologically ^{99m}Tc(I) tricarbonyl complexes stabilized by pyrazole-diamine units functionalized with two different DNA-binding moieties, anthracene or acridine orange. In particular, it was intended to test the effect of the distance between the decaying ^{99m}Tc and the intercalator on the DNA damage and radio-cytotoxicity induced by the radiocomplexes. For these studies, it was decided to further evaluate the best performing complex introduced by the CR group, i.e. **Tc1** (see Fig. 1.12) extending its *in vitro* biological evaluation to PC-3 human prostate cancer cells, and compare its biological performance with related complexes having anthracene or AO

groups as DNA binders and different linkers to attach these groups to the pyrazolyl ring (see Figure 1.14).

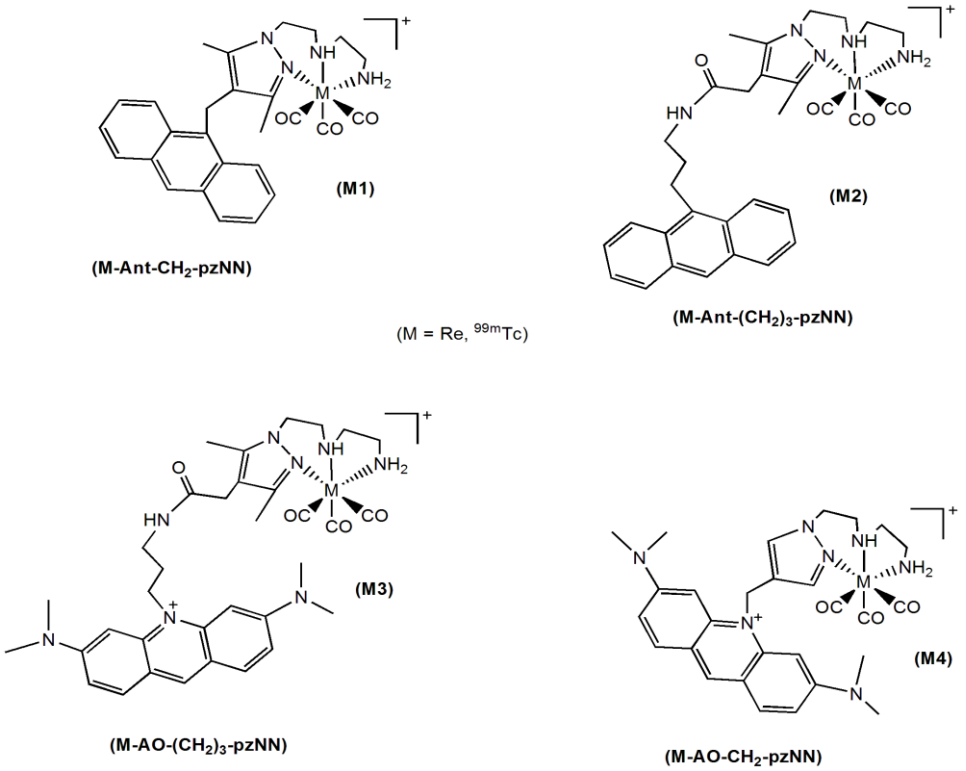

Figure 1.14 Molecular structures of the Re and ^{99m}Tc complexes proposed in this thesis

After identifying the best performing complex from those proposed in Figure 1.14, a next step would be its functionalization with a bioactive peptide (BM), such as bombesin, and a NLS, as proposed in Figure 1.15. The multi-functionalization with a NLS along with the tumor-seeking vector should improve the ability of the complexes to target the nucleus of tumor cells, in close proximity with DNA, which is a crucial issue to explore ^{99m}Tc in Auger therapy.

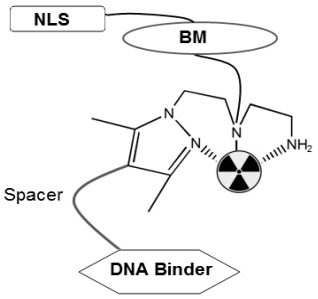

Figure 1.15 Schematic representation of ^{99m}Tc radiopharmaceuticals intended with this thesis

Briefly, a ^{99m}Tc compound that can combine specific cell targeting, nuclear internalization and significant cell killing due to the Auger electron effect is yet to be introduced. Herein, it was intended to contribute for a better understanding of the structural characteristics (e.g. nature of DNA binder, spacer length, presence of NLS and/or bioactive peptide) that are more determinant of their ability to induce DNA damage and cause radiotoxic effects against tumor cells.

1.6 Rationale for the design and evaluation of the proposed complexes

1.6.1 Pyrazole-diamine BFCs

A large variety of mono, bi or tridentate N, S, P or O-donor ligands can stabilize the *fac*-$[M(CO)_3]^+$ (M = Re, Tc) core.[49–52] Pyrazole derivatives are very versatile, have been widely used for biomedical applications and in some cases can also coordinate this organometallic core.[53] Mono and bidentate chelators give M(I) (M = Re, Tc) tricarbonyl complexes that show reduced *in vivo* and *in vitro* stability. By contrast, it has been established that tridentate NNN-donor ligands give more stable complexes.[51] In fact, various studies showed that pyrazole-diamine (pzNN) ligands are ideal tridentate BFCs for the stabilization of *fac*-$[M(CO)_3]^+$, leading to complexes with high kinetic inertness and thermodynamic stability that are obtained in high specific activity, with high yield and radiochemical purity,.[45–52,54] Pyrazolyl-diamine chelators provide three N donor atoms with great capacity to replace the water molecules of the *fac*-$[M(CO)_3]^+$ (M = Re, Tc) core. More details about its coordination chemistry can be found elsewhere.[49,50]

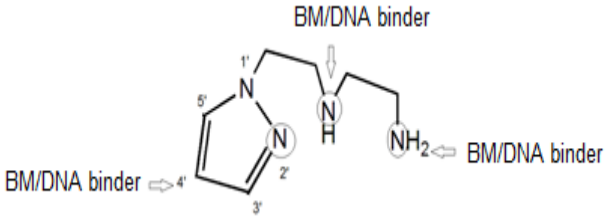

Figure 1.16 Schematic representation of different possibilities for functionalization of pyrazole-diamine BFCs with biomolecules and/or DNA-binding groups. The N donor atoms for stabilization of *fac*-$[M(CO)_3]^+$ are also featured.

The versatility of pyrazolyl-diamine ligands makes them suitable for functionalization with BMs and/or other relevant organic compounds through the amines or the pyrazolyl ring (Figure 1.16).

So far, the reported studies showed that their coordination capability towards the *fac*-$[M(CO)_3]^+$ (M = Re, Tc) is not affected by their functionalization with BMs or DNA. Usually, the resulting radio-conjugates have great *in vitro* and *in vivo* stability, and still retain its biological functions.[49,50,52,54] Favorable pharmacokinetics (i.e. fast clearance from the blood, minimal retention in the hepatobiliary tract and kidneys with rapid urinary excretion) have also been reported in mice for several pyrazole-diamine ^{99m}Tc tricarbonyl complexes bearing bioactive peptides, such as bombesin or melanocortin analogues.[52,55]

Herein, we will use pyrazole-diamine ligands containing anthracenyl or AO groups, as DNA binders that are introduced at the 4- position of the pyrazolyl ring using appropriate linkers. Then, the secondary amine can be used for further functionalization with the BBN analogue and with a nuclear localization sequence (NLS).[47,52,54] It is worthwhile to mention that in the case of anthracene derivatives of pyrazolyl-diamine ligands it has been shown that the corresponding ^{99m}Tc complexes have higher nuclear uptake and enhanced radio-cytotoxic effects on B16-F1 murine melanoma cells when the DNA binder is attached through the azolyl ring, if compared with the complexes having the anthracenyl group at the terminal amine. Studies of the interaction of this type of anthracenyl-containing ligands and their Re complexes with calf thymus (CT) DNA showed that the position used to introduce the DNA binder also influences the way how the compounds interact with DNA.

1.6.2 **DNA-binding groups and DNA interaction**

As said before, for Auger therapy it is mandatory that the radionuclide stays as close as possible to the target DNA in order to cause a significant damage by direct effect of the Auger electrons. By functionalization of the chelate with an aromatic DNA-binding group it is expected that once inside the cell nucleus, the radio-conjugate will be able to have a strong interaction with DNA and provide an enhancement on the radio-cytotoxicity effect by the short-ranged Auger electrons. The introduction of aromatic DNA-binding group in ^{99m}Tc radiopharmaceuticals is also very convenient, as its fluorescence properties allow *in vitro* studies with the Re congeners by different microscopy techniques, at cellular and subcellular level where the *in vivo* imaging by ^{99m}Tc has very poor resolution.[43]

DNA-targeted therapy is gaining much interest and a couple of anticancer, antibacterial or antiviral drugs bearing small molecules capable of interacting with DNA have been intensively studied.[56–58] The information about how these molecules interact with the DNA - the binding-mode, kinetics and the forces involved - is crucial to understand and predict the effects they will have, thus potentiating their use for biomedical applications. Some molecules interact with the DNA in a very specific way and it is important to take in consideration that this interaction is dependent on certain characteristics like its size, structure and charge.[56,59,60] So, the

conjugation with other entities more likely will change, slightly or drastically, the way this interaction occurs. Therefore, it is important to determine the binding mode of the DNA-binding moiety as well as of the whole conjugate.

1.6.2.1 **DNA binders and DNA-binding modes**

The structural conformation of DNA is very diverse, which allows the interaction with a variety of small molecules in various specific and non-specific different ways. The most important interaction modes for the design of drugs containing DNA-binding molecules are intercalation and groove binding[56–60], where the minor groove binding is the predominant among the DNA-binding drugs[58] (Figure 1.17). These binding modes are non-covalent and reversible most of the times. The drugs with this type of interaction are usually less toxic than the ones with covalent binding mode.[61]

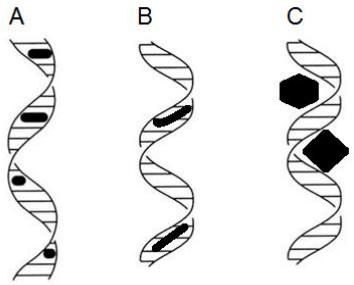

Figure 1.17 The three main binding modes of small molecules with the DNA with biomedical interest for drugs containing DNA-binding units (**A**-intercalation; **B**-minor groove binding; **C**-major groove binding)

Intercalators are usually planar fused hetero-aromatic molecules that insert, partially or entirely, between adjacent base pairs of the DNA inducing structural changes. Some non-fused aromatic rings were found capable of intercalating the DNA base pairs and are classified as atypical DNA-intercalators.[57] The interaction is stabilized mainly by van der Waals forces and hydrophobic interactions and, depending on the charge of the molecule, might include hydrogen bonding or ionic forces involving the negatively charged DNA phosphate groups.[56–60] All these contributions lead to favorable intrinsic binding constants (*K*) that compensate the free energy cost of this type of interaction.[57] These type of DNA-binders do not have sequence-specific recognition sites but usually prefer the CT-rich sequences and alternating purine-pyrimidine sequences.[58]

The groove binders generally don't cause perturbation on the DNA structure. They are mostly minor groove binders composed by non-fused aromatic rings with terminal base functions and a narrow curved shape. The interaction is also stabilized by intermolecular interactions but without any free energy cost and therefore a higher intrinsic binding constant.[57] The elected sequence-

specific sites are the AT-rich sequences because of the favorable hydrophobic contacts and accessibility of hydrogen bond receptors.[56,58]

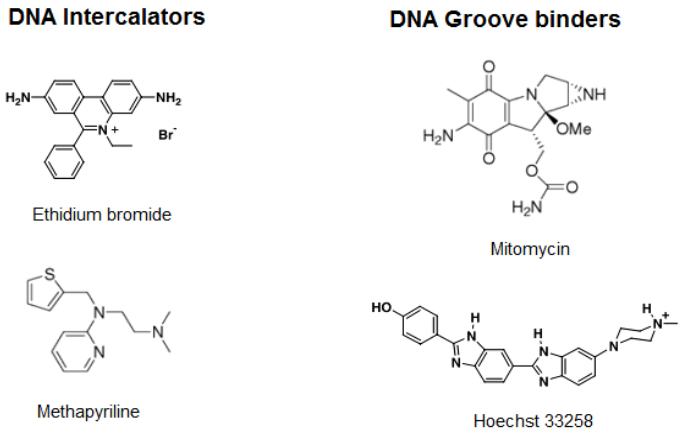

Figure 1.18 Molecular structure of some DNA-binding molecules[56,57]

Figure 1.18 shows the molecular structure of two of the most widely studied DNA-binders: the DNA-intercalator ethidium bromide and the DNA-minor groove binder Hoechst 33258. The structures of methapyriline and the mitomycin are also presented as examples of structurally atypical intercalator and groove binder, respectively.

1.6.2.2 **Acridine orange and anthracene**

Acridine was the first proposed model molecule for the study of ligand-DNA interaction by Lerman in 1961.[62] It is a versatile planar polyaromatic structure related to anthracene that allows several chemical reactions and acts as a classic DNA intercalator. Its potential as anti-tumor agent has been intensively explored, with a variety of molecular manipulations to enhance the therapeutic effects and overcame its high cytotoxicity. Acridine and its derivatives are very important for biomedical applications and several therapeutic agents based on these molecules have been developed.[63,64] The cationic derivative acridine orange (AO) (Figure 1.19) is no exception with enhanced electrostatic attraction towards the phosphate group of the DNA. It usually provides drugs with high affinity and specificity for the DNA molecules with good stability and solubility in aqueous solution. The high absorption capacity, fluorescence intensity and staining properties make this molecule and its conjugates suitable for a variety of studies by the available spectroscopic and optical techniques.[65]

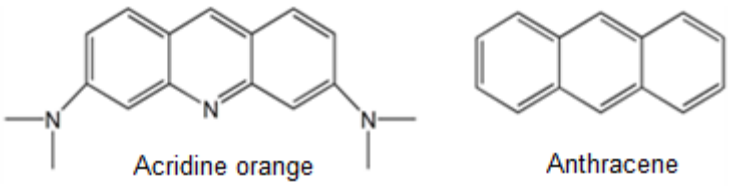

Figure 1.19 Molecular structures of acridine orange and antracene

Anthracene (Ant) is a large planar hydrophobic polyaromatic hydrocarbon constituted by three fused benzene rings (Figure 1.19). Its chemical versatility allows the functionalization with other entities and thus the alteration of its chemical and physical properties, like hydrophobicity. It is a DNA intercalator but when conjugated with other molecules its properties tend to change significantly. Yet, its derivatives and conjugates generally retain its remarkable fluorescence and absorption characteristics.[66,67]

The use of these two different DNA-binding groups, AO and anthracene, with different properties and affinity for the target molecule, was expected to give an insight on the influence of the DNA binder on the eventual radiotoxic effects of the pyrazolyl-diamine ^{99m}Tc(I) tricarbonyl complexes proposed in this thesis.

1.6.2.3 **Evaluation of DNA-binding**

The effect caused by DNA-binding units is dependent on the characteristics of the binding molecule and type of DNA, but also on the strength and mode of interaction. It can be measured by several techniques based on the chromophoric properties of the ligands, cytotoxic effects, structural changes on the DNA or thermodynamic properties of the interaction. At macroscopic level it can be detectable trough inhibition of cell growh or cell transformation as a result of disturbance in the DNA dynamics. Some examples of physical/chemical methods that can estimate the mechanism and/or the occurrence of these interactions are: structural techniques (gel electrophoresis, X-ray crystallography); spectroscopic techniques (NMR, UV-Visible, fluorescence, circular and linear dichroism), viscosity measurements[56,57,59]; thermodynamic experiments (isothermal titration calorimetry)[56] or computational molecular modeling[58].

This section will focus on the fluorescence and UV-Vis spectroscopy as these are the techniques that have been used in the studies reported in this thesis. These techniques are suitable to confirm the occurrence of interaction and for the determination of the binding constant (*K*) by titration methods. More detailed information about these techniques can be found elsewhere.[61] A brief overview is presented below.

The UV-Vis absorption spectroscopy can be used to detect changes in the absorption properties of the ligand or the DNA when the interaction occurs. The DNA molecule presents a broad absorption band at 200-250 nm with a maximum at 260 nm in the UV region. The common studied DNA-binding molecules, in general, also present a characteristic absorption band in the UV-Vis absorption spectrum. The complex ligand-DNA presents a shift on the position of the maximum absorption, in both cases, relative to the free molecule in solution. Thus, the comparison of these spectra can be used to assess the ligand-DNA interaction. The magnitude of the shifting indicates the strength of the interaction and the presence of hypochromism and bathochromism (red shift) usually indicates intercalative mode of binding.

Fluorescence spectroscopy is a very sensitive technique and very suitable for these studies as the DNA-binding drugs usually correspond to aromatic compounds that present high intensity fluorescence. The changes in environment, like the binding to the DNA molecule, can cause spectral shifts relative to the excitation and emission of the fluorescence of the ligands. The enhancement of the fluorescence intensity indicates interaction with the DNA, where higher enhancements are commonly observed for intercalative binding-mode while a decrease indicates groove-binding mode.

1.6.3 Functionalization with a bioactive peptide and a nuclear localization sequence: a perspective

The main purpose of the synthesis and evaluation of the AO- and anthracene-containing pyrazolyl-diamine ^{99m}Tc(I) tricarbonyl complexes proposed in this thesis was to find organometallic building blocks that could reach the cell nucleus and target the DNA of any cell. If shown some ability to induce significant cell death, the next step would be the functionalization of these building blocks with a peptidic BM and a NLS for targeted cancer therapy.

1.6.3.1 Bioactive peptide

The identification and characterization of BMs, their molecular targets and mechanisms of action, allow advances in pharmacological applications based on drug delivery systems. This is a multidisciplinary area that involves organic chemistry, biochemistry and molecular biology focused on the isolation of the natural occurring BMs as well as its mimicking by synthetic congeners. There is a constant search for new BMs and its targets and some have been well characterized and successfully applied as biologically active targeting vectors.[68]

Bioactive peptides are part of the class of biomolecules that mediate the intercellular signalling process. This signalling occurs upon development and regulation of physiological processes in response to external conditions. The bioactive peptides are very specific and efficient messengers and require fewer resources from the cells compared to the proteins. They are synthesized then activated by post-translational modification and stored in secretory vesicles. When released they bind to their target (usually G-protein coupled receptors (GPCR)) that initiates the process of cellular response, which depends on the type of cell. The same cell can express and respond to a variety of different bioactive peptides from neighbour or distant cells. The receptors also present different subtypes that provide different response to the same peptide.[69]

Bombesin (BBN) is an amphibian tetradecapeptide that binds to a GPCR which comprise four receptor subtypes (see Table 1.5). In this work, it was intended to functionalize the ^{99m}Tc(I) tricarbonyl complexes with BBN analogues for the targeting of gastrin-releasing peptide (GRP) (subtype BB2) receptor that is overexpressed in several tumor cells, such as prostate, breast, pancreatic, and small-cell lung cancer cells.[70–73] The well characterized bombesin peptide analogues can be used as tumor-seeking vectors for both diagnostic and (radio/chemo)-therapy of those tumors. In nuclear medicine, these BMs can be radiolabeled directly or through the use of a bi/multifunctional ligands, as seen in previous sections. An overview of radiolabeled BBN conjugates that seek GRP-receptor can be found in several reviews[72,74–77].

Table 1.5 Bombesin receptor subtypes and the respective native peptide sequences[77]

Subtype	Native Peptide		Origin
BB1	Neuromedin B (NMB)	Gly-Asn-Leu-Trp-Ala-Thr-Gly-His-Phe-Met-NH_2	Mammalian
BB2	Gastrin Releasing Peptide (GRP)	Val-Pro-Leu-Pro-Ala-Gly-Gly-Gly-Thr-Val-Leu-Thr-Lys-Met-Tyr-Pro-Arg-Gly-Asn-His-Trp-Ala-Val-Gly-His-Leu-Met-NH_2	Mammalian
BB3	BRS-3	Not identified	Mammalian
BB4	Bombesin (BBN):	Pyr-Gln-Arg-Leu-Gly-Asn-Gln-Trp-Val-Gly-His-Leu-Met-NH_2 Pyr-Gln-Arg-Leu-Gly-Asn-Gln-Trp-Ala-Val-Gly-His-Phe-Met-NH_2	Amphibian

1.6.3.2 **Nuclear localization sequence**

All the translation process occurs outside the nucleus but some proteins that regulate important cell functions in eukaryotic cells are required by this organelle. The traffic of macromolecules into the nucleus is a controlled and restricted active transport, mediate by nuclear receptors and other proteins of the nuclear pore complex (NPC) as well as the GTPase Ran that generates energy. Small molecules can diffuse through the NPC by passive transport, but for macromolecules up to 45-50 kDa the required signal to translocate through the NPC is the NLS. The NLS is recognized by members of the cytosolic Importin/Karyopherin super family of

proteins which sets the beginning of the import process.[78–82] This signal sequence is of great interest for nuclear delivery systems design and it has been explored in areas like gene therapy researches but with limited success. The delivery of peptidic drugs on the other hand presents more encouraging platforms.[80,81]

Table 1.6 Exemples of nuclear localization sequences of the different classes[80,81]

SV40 large T-antigen	PKKKRKV	(classical monopartite)
Nucleoplasmin	KRPAATKKAGQA- KKKK	(classical bipartite)
hnRNPA1 (M9)	NQSSNFGPMKGGNFGGRSSGPYGGGGQYEAKPRNQGGY	(non-classical)

Table 1.6 shows some examples of the most studied sequences of each of the different NLS's classes. The main difference between the classical and non-classical NLSs is that the classical NLSs possess short stretch (s) of basic amino acids. Those stretches can be continuous (monopartite) or separated by a spacer (bipartite).[80,81]

2 Results and discussion: synthesis and characterization of the ligands and complexes

2.1 **Synthesis and characterization of the ligands**

Pyrazole-diamine ligands bearing anthracene or acridine orange as DNA-binding groups were synthesized in order to obtain stable ^{99m}Tc compounds with the ability to intercalate the DNA and display enhanced radiotoxic effect through Auger electrons emission. The ligands were expected to position the radionuclide at different distances to the target by introduction of two different spacers between the chelator backbone and the DNA-binding moiety.

As illustrated in Scheme 2.1, the synthesis of **L1** was performed using a multistep synthetic strategy as reported in the literature, starting from the commercially available 9-anthracene aldehyde.[45]

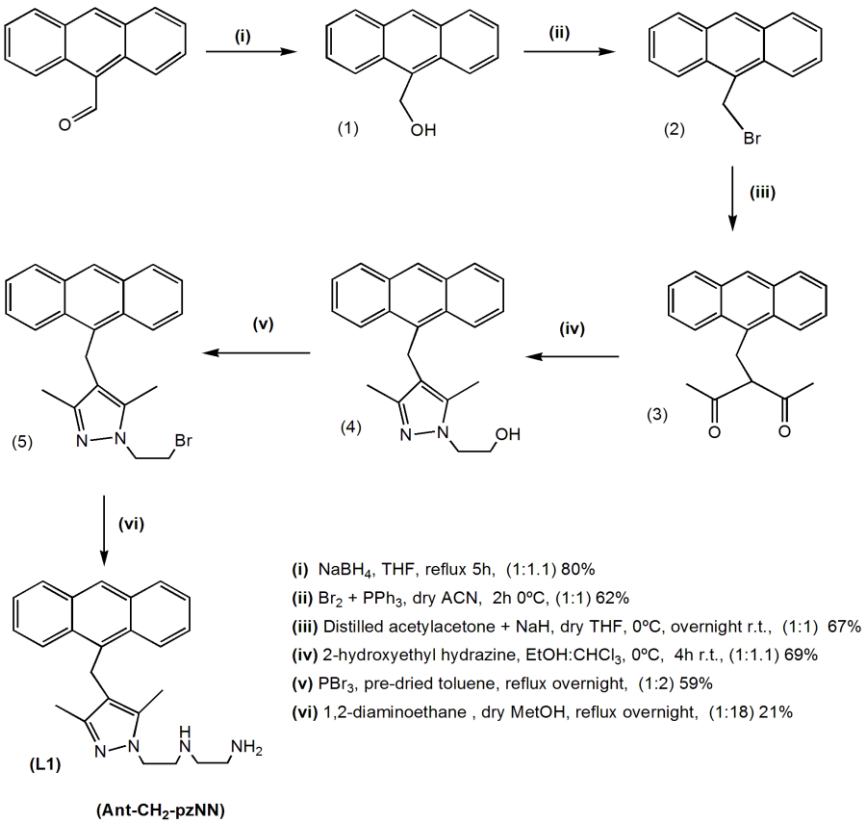

Scheme 2.1 Synthesis of Ant-CH_2-pzNN **(L1)**

The multistep synthesis of **L1** started with the reduction of 9-anthracene aldehyde with sodium borohydride in tetrahydrofuran (THF), which afforded 9-anthracenemethanol (**1**). The

bromination of the latter with liquid bromine (Br_2) was carried out in dry acetonitrile (ACN) in presence of the reducing agent triphenylphosphine (PPh_3) at 0°C. The resulting brominated derivative, compound **2,** was then alkylated with acetylacetone in THF in presence of the base sodium hydride (NaH) to give **3** in *keto* form. Cyclisation of **3** with 2-hydroxyethyl hydrazine in a mixture of ethanol and chloroform (1:1) at 0°C afforded compound **4**, which was brominated with phosphorus tribromide (PBr_3) under reflux in toluene giving compound **5**. **L1** was obtained by treatment of **5** with an excess of 1,2-diaminoethane in methanol (MeOH) under reflux. **L1** was purified by silica-gel (SiO_2) column chromatography, and obtained as a yellow oil in low to moderate yield (21%). The characterization of **L1** was done by ^{1}H-NMR spectroscopy and HPLC (see experimental section), and confirmed the formation of the desired anthracenyl-containing chelator as checked by comparison with the spectroscopic data reported in the literature for **L1**.[45]

The synthesis of Ant-$(CH_2)_3$-pzNN (**L2**) and AO-$(CH_2)_3$-pzNN (**L3**), which contain anthracenyl or acridine orange moieties and a longer propylenic linker to attach these DNA binding moieties to the chelator framework, was performed according to the literature. This was done using a similar strategy that involved the use of a common N-hydroxysuccinimine (NHS) activated ester pyrazole-diamine derivative, containing a terminal tert-butyloxycarbonyl (BOC)-protected amine group, which was coupled to 3-(anthracen-9-yl)propan-1-amine or 10-(3-aminopropyl)-3,6-bis(dimethylamino)acridinium through their amine groups.[83] The syntheses of the activated ester derivative, amine precursors of the DNA binding molecules and final chelators are described below.

The N-hydroxysuccinimine (NHS) activated ester was synthesized as described previously, according to the reactions presented in Scheme 2.2.[84] Its multistep synthesis started with the preparation of compound **6**, undergoing a *keto-enol* equilibrium, which was obtained by C-alkylation reaction between 2,4-pentanodione and ethyl bromoacetate in presence of NaH in THF at 0°C. The cyclocondensation of **6** with 2-hydroxiethylhydrazine in EtOH at 0°C originated **7**. The latter was brominated with PBr_3 under reflux in toluene to give **8**. Another method that has been used to obtain **8** was the bromination of **7** with tetrabromomethane (CBr_4) in presence of PPh_3 in THF. Compound **8** was N-alkylated with tert-butyl 2-aminoethylcarbamate (**9**) in presence of potassium carbonate (K_2CO_3) and potassium iodide (KI) in ACN to give compound **10**. Then, the protection of the secondary amine of **10** was carried out by treatment of this compound with Boc_2O in THF at 0°C, which led to the formation of the BOC-protected derivative **11**. The alkaline hydrolysis of **11** with aqueous NaOH under reflux in THF originated **12** that was activated by NHS in presence of 1-Ethyl-3-(3-dimethylaminopropyl)-carbodiimide (EDC) in dichloromethane (DCM) at 0°C, yielding the desired activated ester **13**.

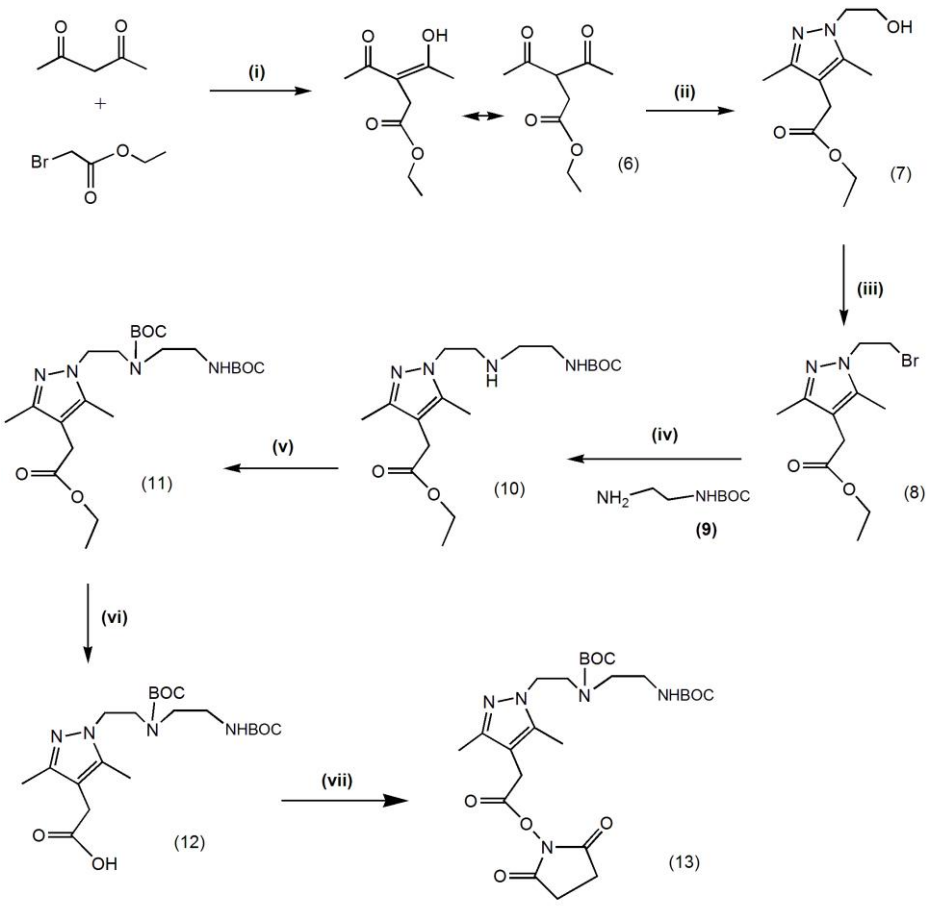

(i) NaH, dry THF, 0°C, overnight r.t., (1:1) 82%
(ii) 2-hydroxiethylhydrazine, EtOH, 0°C, overnight r.t., (1:1) 89%
(iii) PBr_3, toluene, reflux overnight, (1:2.4) 67% **or** CBr_4 + PPh_3, pre-dried THF, 48h r.t., (1:2) 47%
(9) 1,2-diaminoethane + Boc_2O, dioxane, 22h r.t., (1:8) 84%
(iv) K_2CO_3 + KI, dry ACN, reflux overnight, (1:1.5) 48%
(v) Boc_2O, dry THF, 0°C, overnight r.t., (1:1) 93%
(vi) NaOH aq., THF, reflux overnight, (1:12) 92%
(vii) NHS + EDC, dry DCM, 0°C, 72h r.t., (1:1) 75%

Scheme 2.2 Synthesis of the N-hydroxysuccinimine (NHS) activated ester pyrazole-diamine derivative (**13**)

The next step was the synthesis of already described amine precursors functionalized with the DNA binding molecules anthracene and acridine orange (AO). Both precursors were obtained by the methods reported in the literature.[83]

The anthracene-containing precursor 3-(anthracen-9-yl)propan-1-amine (**14**) was obtained by hydrogenation of the commercially available 2-(anthracen-9-yl)acrylonitrile with lithium aluminum hydride ($LiAlH_4$) in diethyl ether (Et_2O) under reflux as shown in Scheme 2.3.

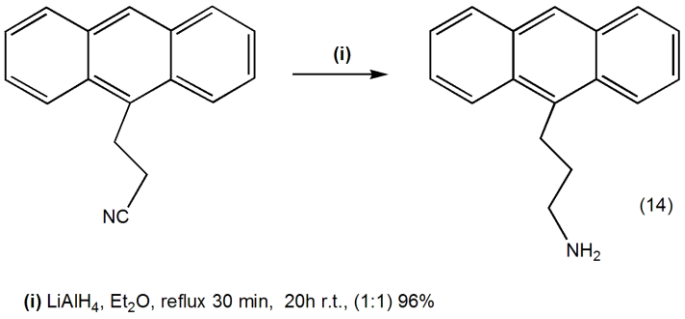

Scheme 2.3 Synthesis of 3-(anthracen-9-yl)propan-1-amine (**14**)

The synthesis of 10-(3-aminopropyl)-3,6-bis(dimethylamino)acridinium (**18**) was more demanding and involved several steps, as shown in Scheme 2.4.[83] Briefly, compound **15** was obtained by alkylation of phthalimide with dibromopropane under reflux in acetonitrile. Then, its iodination with KI in acetone under reflux originated **16**. The latter was reacted with commercial acridine orange to give **17**. Removal of the phthalimide group with excess of hydrazine monohydrate in MeOH gave **18**, which has been isolated in low yield.

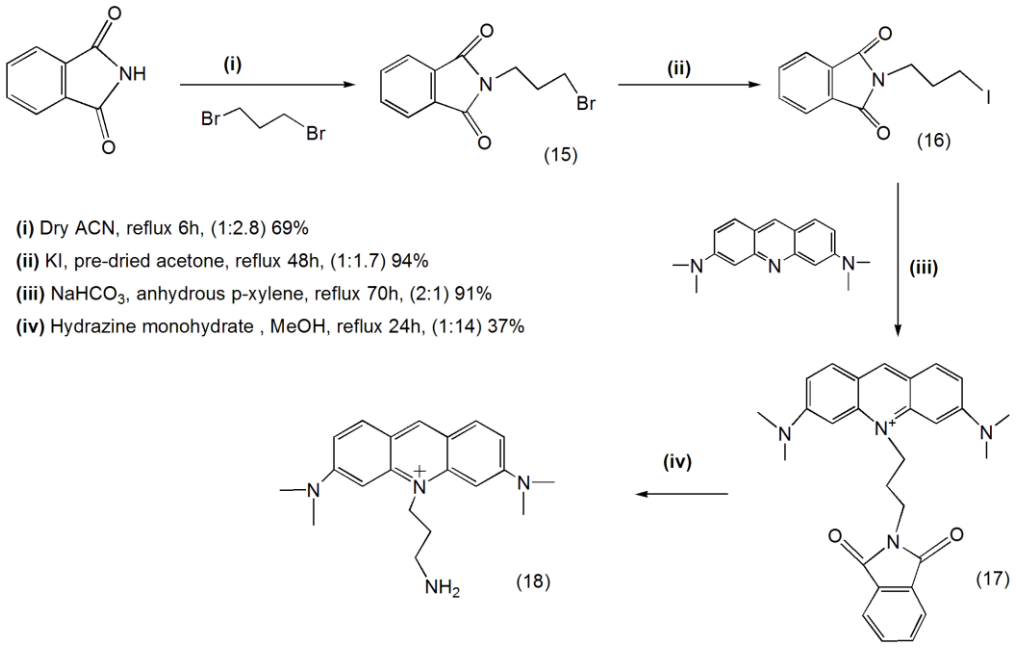

Scheme 2.4 Syntheis 10-(3-aminopropyl)-3,6-bis(dimethylamino)acridinium (**18**)

As presented in Scheme 2.5, the conjugation of the activated ester **13** with compounds **14** and **18** led to the synthesis of BOC-protected pyrazolyl-diamine derivatives, **19** and **20** respectively. These conjugation reactions were performed in presence of the base *N*,*N*-diisopropylethylamine (DIPEA) in dichloromethane (**19**) or dimethylformamide (**20**). The deprotection of the amine groups of **19** with an excess of trifluoroacetic acid (TFA) in DCM gave **L2**, which was isolated as a yellow solid. Compound **20** was deprotected with hydrochloric acid (HCl) in MeOH to give **L3**,

which was isolated as a dark red solid after purification by alumina (Al_2O_3) column chromatography.

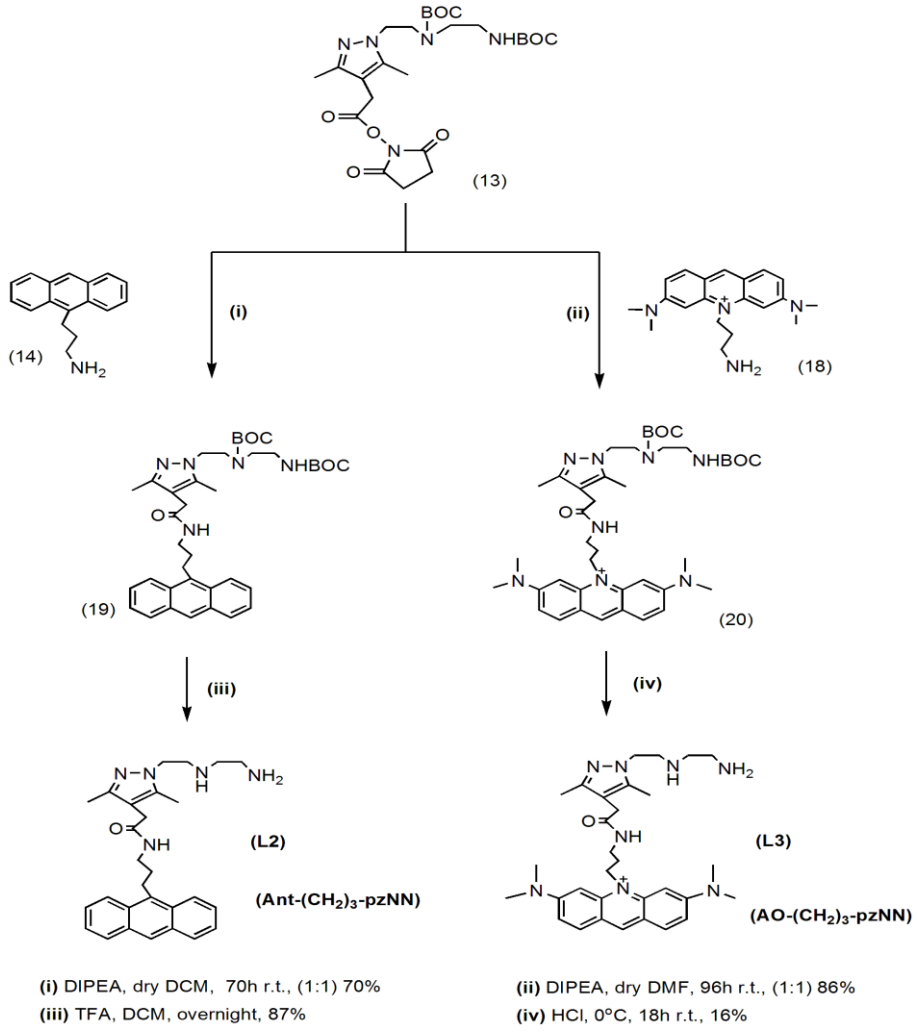

Scheme 2.5 Synthesis of Ant-$(CH_2)_3$-pzNN (**L2**) and AO-$(CH_2)_3$-pzNN (**L3**)

L2 and **L3** were characterized by ^{1}H-NMR spectroscopy and by HPLC. Unlike **L2**, **L3** was obtained with very low yield in very low amount (10 mg). For this reason, it was not further used to synthesize the corresponding ^{99m}Tc(I) and Re(I) tricarbonyl complexes. The lack of available time also did not allow the possibility of repeating the synthesis of **L3**.

If synthesized with success, the fourth ligand (**L4**) would be a new AO-containing chelator. Two strategies have been devised to synthesize **L4**. The first strategy that has been studied involved the direct coupling of a brominated BOC-protected pyrazole-diamine derivative with acridine orange, as proposed in Scheme 2.6. **L4** would be obtained after deprotection of the amine groups.

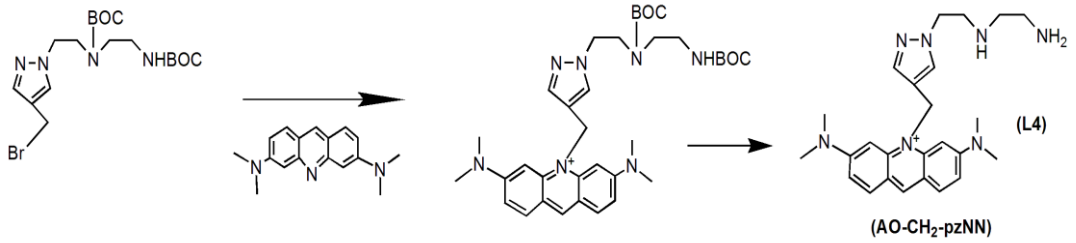

Scheme 2.6 First strategy for the synthesis of AO-CH_2-pzNN (**L4**)

The second strategy was based on the prior functionalization of a tritylated pyrazole derivative with AO, followed by the building-up of the pyrazolyl-diamine backbone and removal of the trityl protecting group, as shown in Scheme 2.7.

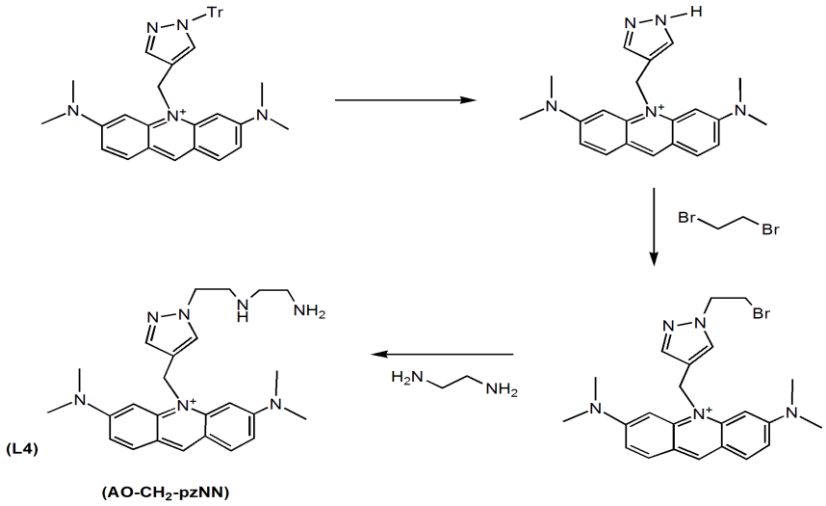

Scheme 2.7 Second strategy for the synthesis of AO-CH_2-pzNN (**L4**)

In the first strategy, two approaches were attempted to obtain the starting brominated BOC-protected pyrazole-diamine derivative (Scheme 2.8). Both approaches involved the synthesis of compound **23** as a key intermediate. In one of these approaches, the central amine was protected with BOC before conversion of the alcohol function to a bromide, while in the other one such protection was not performed.

The multistep synthesis of **23** started with the formation of a 2-hydroxyethylpyrazole derivative, compound **21**, which was obtained as described in the literature, by cyclocondensation of ethyl 2-formyl-3-oxopropanoate with 2-hydroxyethylhydrazine in EtOH at 0°C.[85] The new compound ethyl 1-(2-bromoethyl)-1H-pyrazole-4-carboxylate (**22**) was obtained with a moderate-high yield of 66%, by bromination of **21** with CBr_4 in presence of PPh_3 in THF at 0°C. Then, **23** was obtained by treatment of **22** with excess of **9** in presence of K_2CO_3 and KI in dry ACN under reflux.

In the first approach, the reduction of the ester group of **23** with $LiAlH_4$ in THF successfully afforded compound **24**, which contains a hydroxymethyl group at the 4-position of the pyrazolyl ring and does not present the central amine group protected with BOC (Scheme 1.8). However, the bromination of the hydroxymethyl group of **24** with CBr_4 in THF in presence of PPh_3 did not afford the desired compound. Thus, a second approach involved the protection of the secondary amine of **23** with Boc_2O in THF at 0°C. The resulting ethyl 1-(2-(tert-butoxycarbonyl(2-(tert-butoxycarbonylamino)ethyl)amino)ethyl)-1H-pyrazole-4-carboxylate (**25**) was isolated with a very high yield of 99%. Reduction of **25** with $LiAlH_4$ gave 1-(2-(tert-butoxycarbonyl(2-(tert-butoxycarbonylamino)ethyl)amino)ethyl)-1H-pyrazol-4- hydroxymethyl (**26**), which was obtained as a yellow oil with moderate yield (54%). Likewise in the first approach, bromination of **26** with CBr_4 in THF in presence of PPh_3 also did not provide the desired brominated derivative.

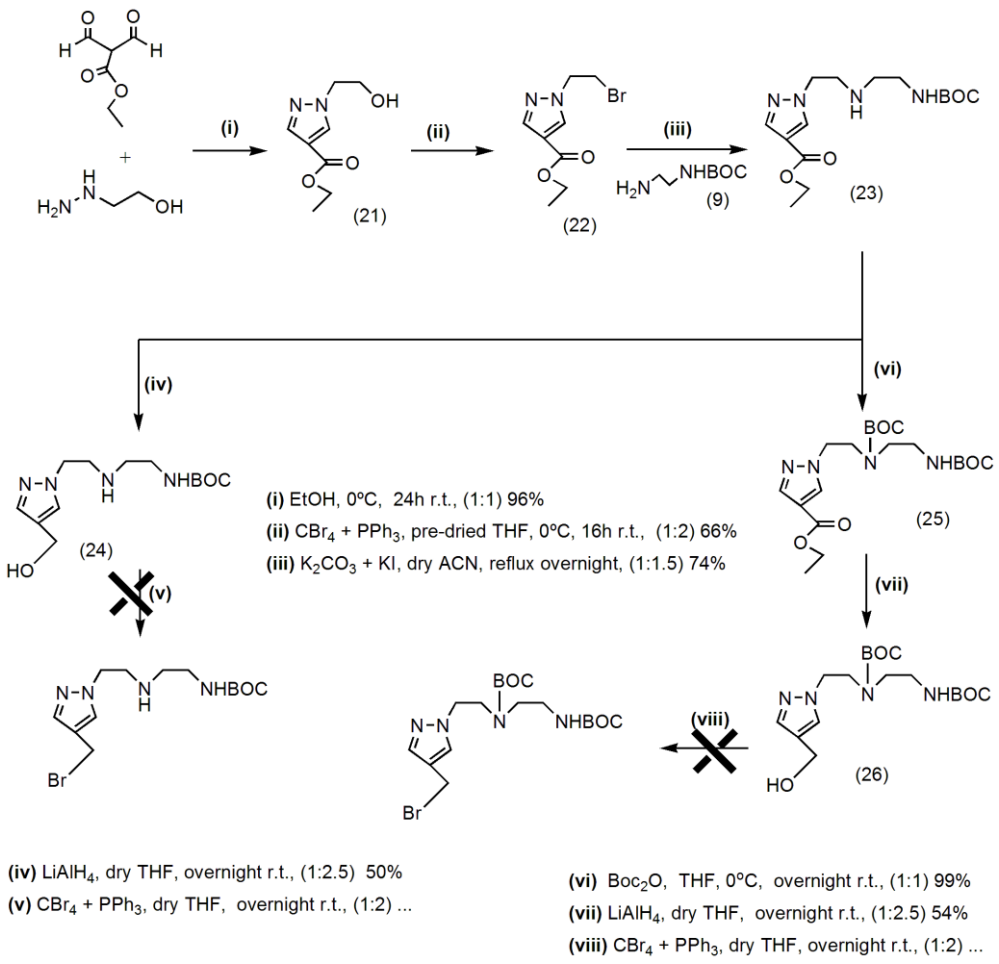

Scheme 2.8 Synthesis of tert-butyl 2-(2-(4-(hydroxymethyl)-1H-pyrazol-1-yl)ethylamino)ethylcarbamate (**24**) and 1-(2-(tert-butoxycarbonyl(2-(tert-butoxycarbonylamino)ethyl)amino)ethyl)-1H-pyrazol-4-hydroxymethyl (**26**)

The new compounds involved in the attempted synthesis of **L4** (see Scheme 2.8) were characterized by ^{1}H and ^{13}C-NMR spectroscopy, as exemplified for compounds **22**, **25** and **26** in

Figure 2.1-Figure 2.4. The NMR characterization of all the compounds confirmed the proposed formulations and the presence of highly pure compounds.

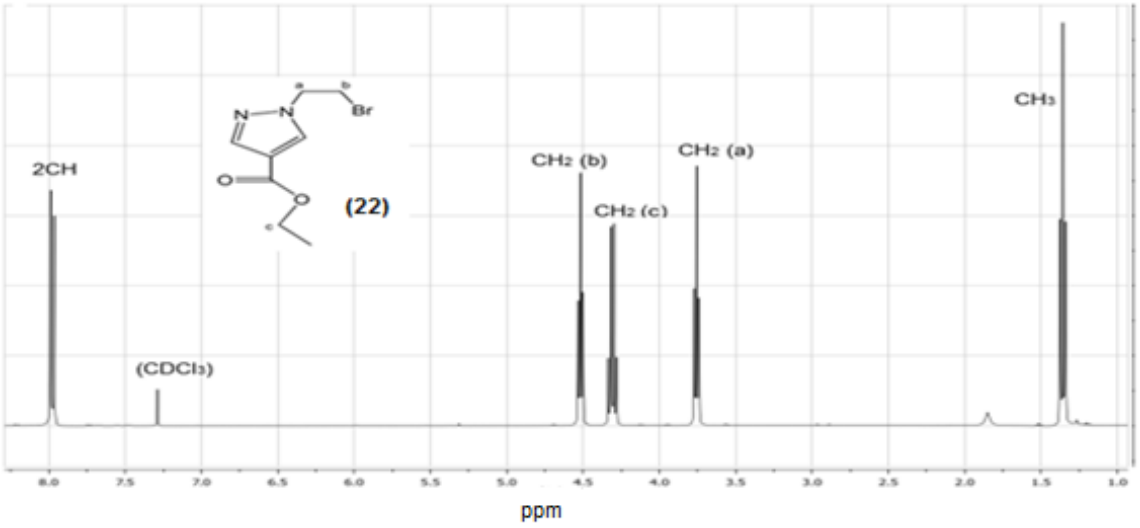

Figure 2.1 ^{1}H-NMR spectrum of ethyl 1-(2-bromoethyl)-1H-pyrazole-4-carboxylate (**22**)

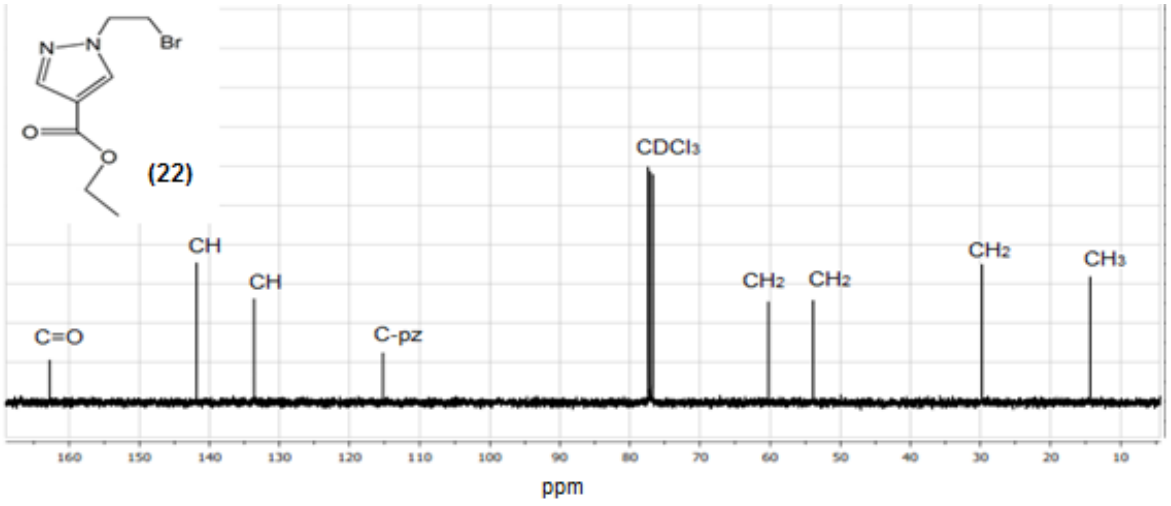

Figure 2.2 ^{13}C-NMR spectrum of ethyl 1-(2-bromoethyl)-1H-pyrazole-4-carboxylate (**22**)

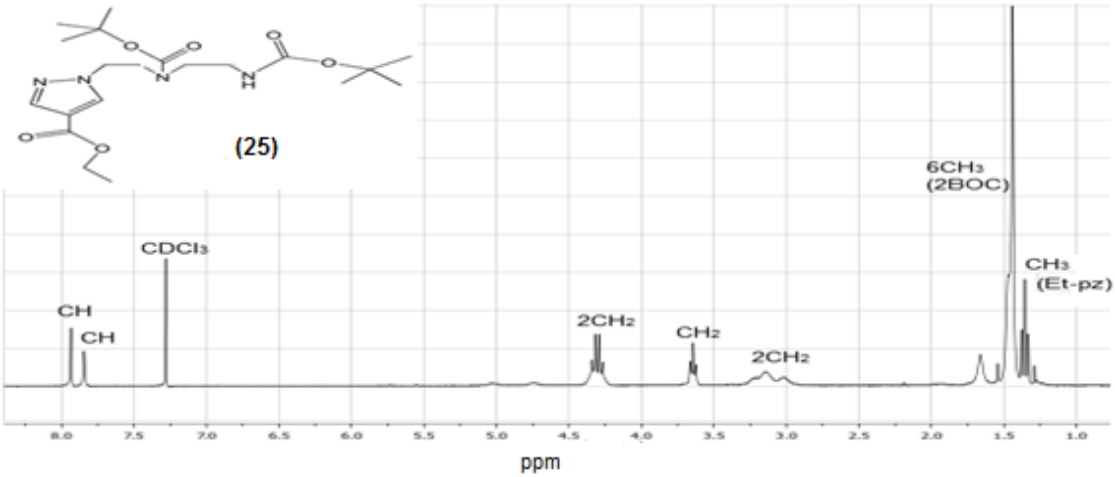

Figure 2.3 ^{1}H-NMR spectrum of ethyl 1-(2-(tert-butoxycarbonyl(2-(tert-butoxycarbonylamino)ethyl)amino)ethyl)-1H-pyrazole-4-carboxylate (**25**)

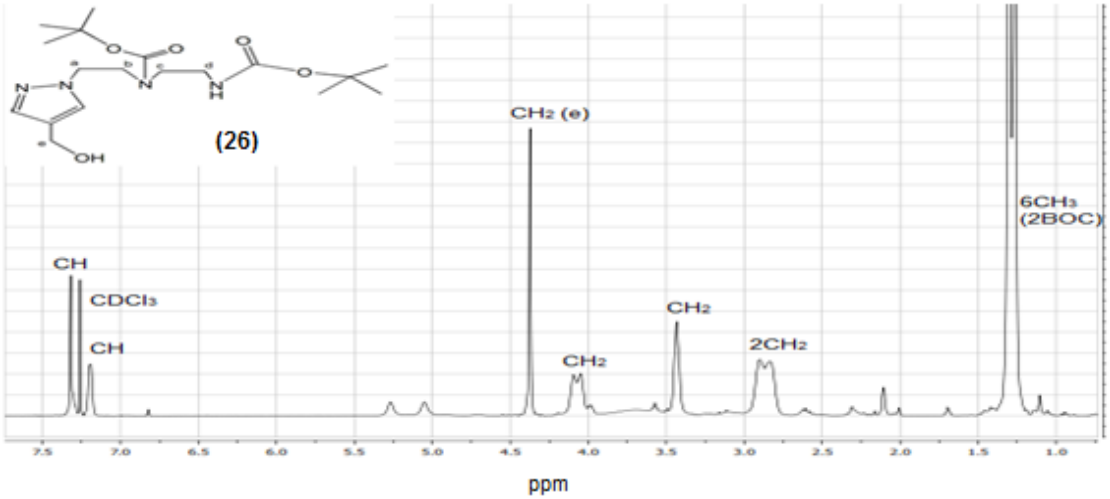

Figure 2.4 ^{1}H-NMR spectrum of 1-(2-(tert-butoxycarbonyl(2-(tert-butoxycarbonylamino)ethyl)amino)ethyl)-1H-pyrazol-4- hydroxymethyl (**26**)

Finally, it has been explored the above mentioned second strategy to obtain **L4**. As presented in Scheme 2.9, this strategy involved the synthesis of 4-(bromomethyl)-1-trityl-1H-pyrazole (**28**). This involved the use of ethyl 1-trityl-1H-pyrazole-4-carboxylate, already described in the literature,[85] as the starting material. This compound was converted to **27** by reduction of the ester group with $LiAlH_4$ in THF at 0°C. **27** was brominated with PBr_3 in toluene under reflux leading to **28**. The coupling of **28** with commercial available acridine orange in xylene under reflux was not successful and did not lead to the desired AO-containing pyrazole derivative.

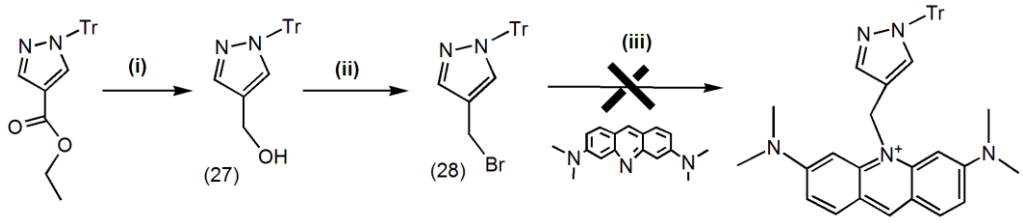

(i) $LiAlH_4$, dry THF, 0ºC, overnight r.t., (1:1.5) 84%
(ii) PBr_3, toluene, reflux overnight, (1:1.5) 82%
(iii) Xylene, reflux overnight, (1:1) ...

Scheme 2.9 Synthesis of 4-(bromomethyl)-1-trityl-1H-pyrazole (**28**)

2.2 Synthesis and characterization of the Re(I) and ^{99m}Tc(I) tricarbonyl complexes

To have an insight on the potential of the Auger emitter ^{99m}Tc for the design of DNA-target radiotherapeutic agents, ^{99m}Tc complexes containing a bifunctional chelator to stabilize the *fac*-$[^{99m}Tc(CO)_3]^+$ core and a DNA-binding moiety that ensure close proximity to the target, were synthesized.

As seen in chapter 1, the Re congeners are used for characterization of the ^{99m}Tc complexes by conventional analytical methods, which could not be possible for the very low concentration of the ^{99m}Tc complexes that are produced from the $[^{99m}TcO_4]^-$ obtained from the ^{99}Mo/^{99m}Tc generator. As seen before, only the ligands with the anthracenyl moieties, **L1** and **L2**, could be successfully obtained in adequate amounts. Therefore, the synthesis of Re and ^{99m}Tc complexes was uniquely performed for these two ligands. The respective complexes, **Re1** and **Re2**, were obtained by reacting the corresponding ligands (**L1** or **L2**) with the precursors $[Re(CO)_5Br]$ or $[Re(H_2O)_3(CO)_3]Br$, respectively.[86]

Re1 was synthesized as previously described, by an equimolar reaction of $[Re(CO)_5Br]$ with **L1** in MeOH under reflux (Scheme 2.10).[45] After washing with hexane, **Re1** was obtained as a yellow solid with a relatively high yield of 76% and characterized by ^{1}H-NMR spectroscopy and HPLC (t_R = 22.90 min). The characterization of **Re1** provided ^{1}H NMR data consistent with those reported in the literature for this complex, confirming the presence of a pyrazolyl-diamine ligand coordinated in a N,N,N-tridentate fashion to the *fac*-$[Re(CO)_3]^+$ core.

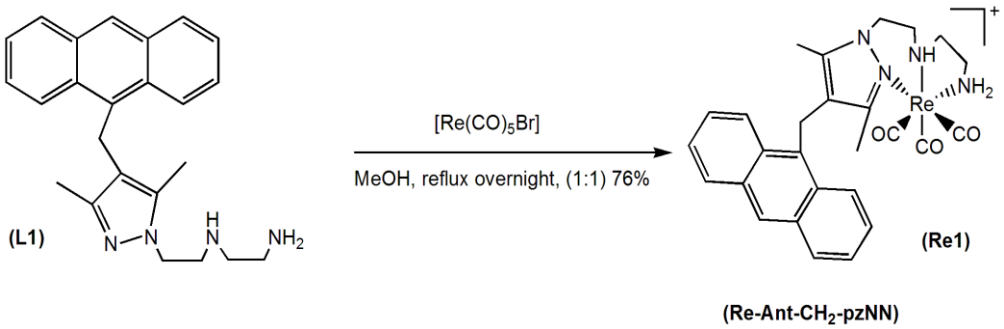

Scheme 2.10 Synthesis of Re-Ant-CH_2-pzNN (**Re1**) by reaction of **L1** with the precursor $[Re(CO)_5]Br$

Re2 was synthesized by reacting equimolar amounts of $[Re(H_2O)_3(CO)_3]Br$ with **L2** in MeOH under reflux (Scheme 2.11), as previously described for similar compounds.[46] The purification of **Re2** was done by washing with Et_2O and $CHCl_3$. After purification, **Re2** was obtained as a yellow solid in a moderate yield of 62%. Like **Re1**, **Re2** is an air and water stable compound, with good solubility in aqueous solution but low solubility in common organic solvents such as $CHCl_3$. The characterization of **Re2** was performed by ^{1}H and ^{13}C-NMR spectroscopy, HPLC and ESI-MS.

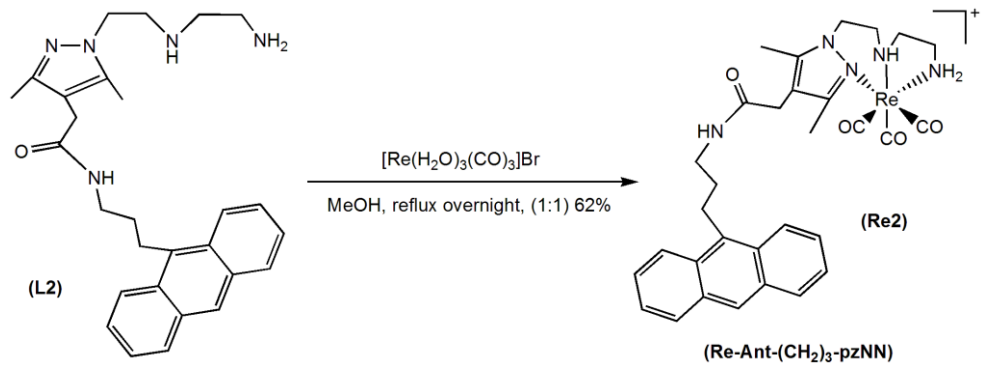

Scheme 2.11 Synthesis of Re-Ant-$(CH_2)_3$-pzNN (**Re2**) by reaction of **L2** with the precursor $[Re(H_2O)_3(CO)_3]Br$

As shown in Figure 2.5, the ESI-MS spectrum of **Re2** shows a prominent peak corresponding to the expected molecular ion ($[M]^+$) at m/z = 728.5) with the correct isotopic distribution pattern.

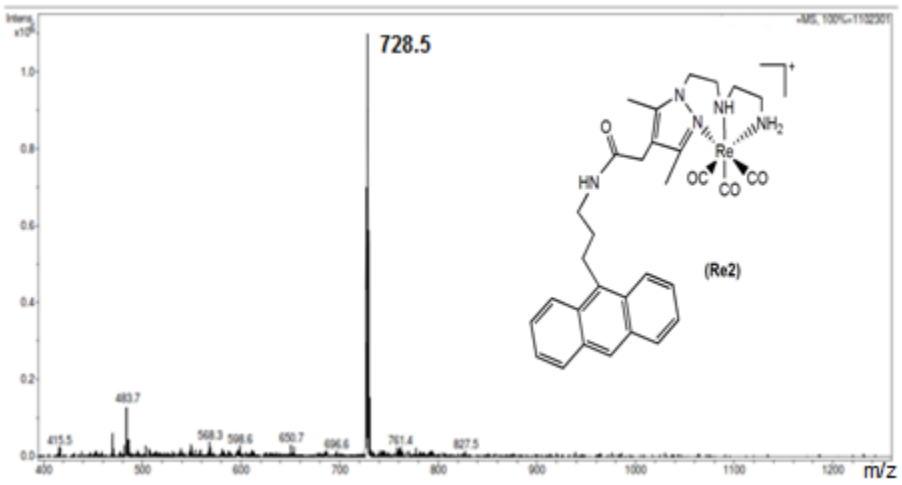

Figure 2.5 ESI-MS spectrum of Re-Ant-$(CH_2)_3$-pzNN (**Re2**)

The NMR characterization of **Re2** confirmed the proposed formulation. The assignments of the different signals on the ^{1}H and ^{13}C-NMR spectra were done based on the 2D experiments COSY ([^{1}H, ^{1}H]) and HSQC ([^{1}H, ^{13}C]). The results of the experiments are presented below (Figure 2.6 to Figure 2.9).

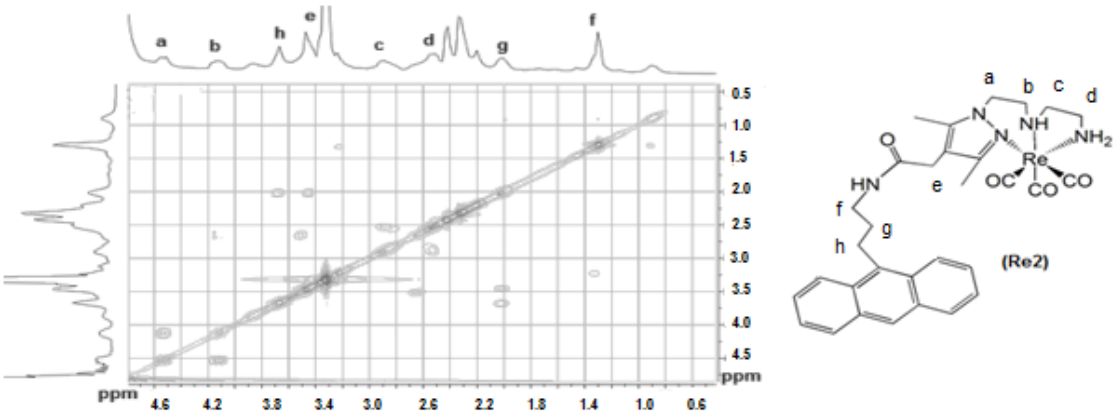

Figure 2.6 [^{1}H, ^{1}H] COSY spectra of **Re2** in CD_3OD (ampliation of the aliphatic region)

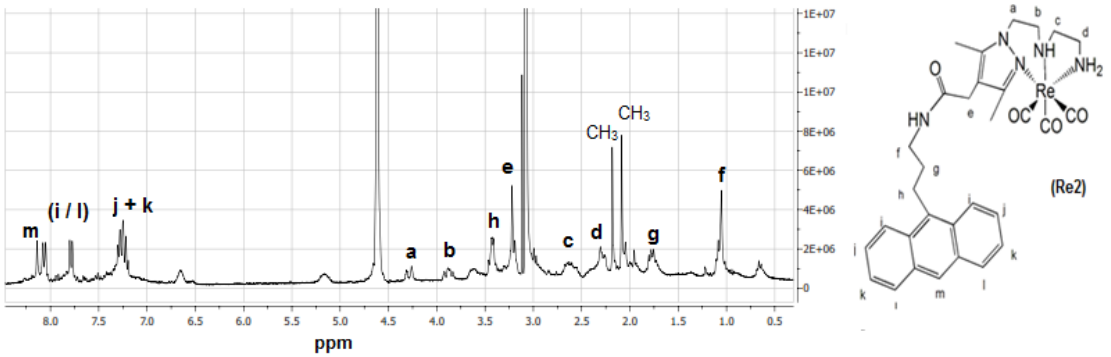

Figure 2.7 ^{1}H-NMR spectra of **Re2** in CD_3OD

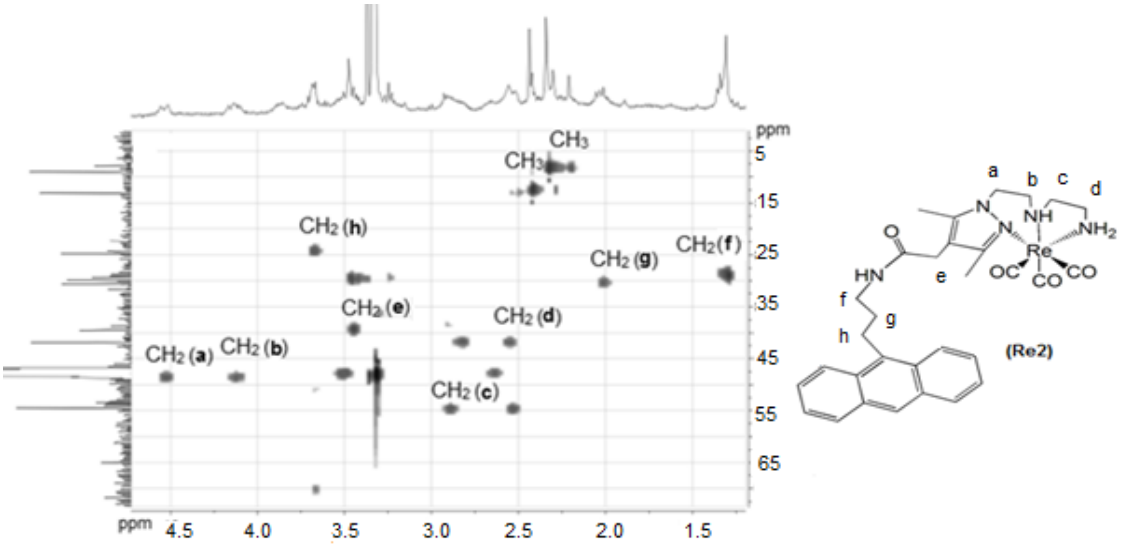

Figure 2.8 [^{1}H, ^{13}C] HSQC spectra of **Re2** in CD_3OD (ampliation of the aliphatic region)

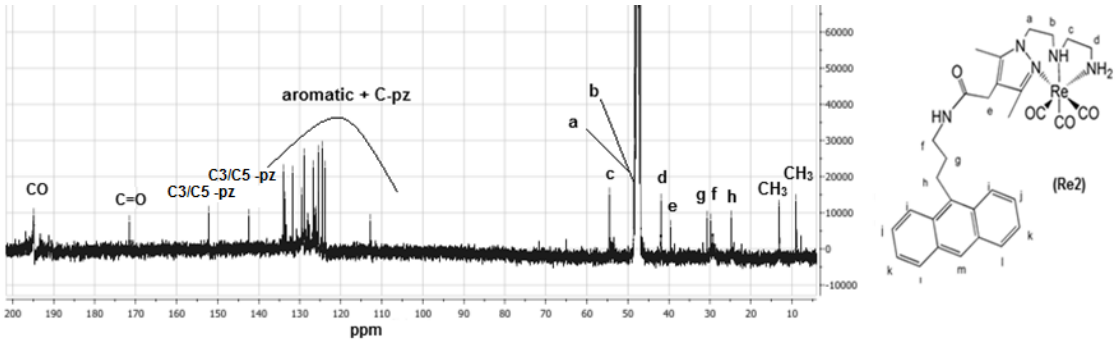

Figure 2.9 ^{13}C-NMR spectra of **Re2** in CD_3OD

The ^{99m}Tc congeners of complexes **Re1** and **Re2** were obtained by reacting the respective ligands with the precursor *fac*-[^{99m}Tc$(H_2O)_3(CO)_3]^+$ in aqueous solution. The aqueous *fac*-[^{99m}Tc$(H_2O)_3(CO)_3]^+$ was synthesized using pertechnetate obtained from the ^{99}Mo/^{99m}Tc generator. Briefly, the Na[^{99m}TcO_4] solution was added to an Isolink kit and the mixture heated for 30 min at 100°C and pH = 11. The precursor (t_R = 6-7 min) was obtained with high yield and

purity (> 95 %) as can be verified in the HPLC chromatogram presented in Figure 2.10, with negligible or non-existing amount of unreacted $[^{99m}TcO_4]^-$ (t_R = 3-4 min).

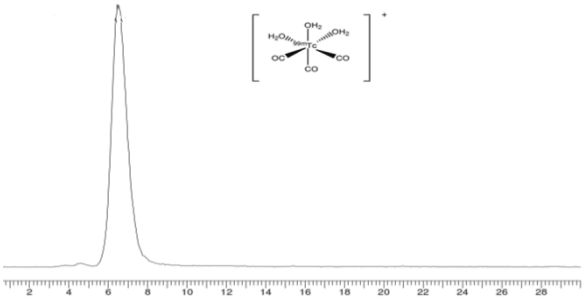

Figure 2.10 HPLC trace of the precursor $[^{99m}Tc(H_2O)_3(CO)_3]^+$

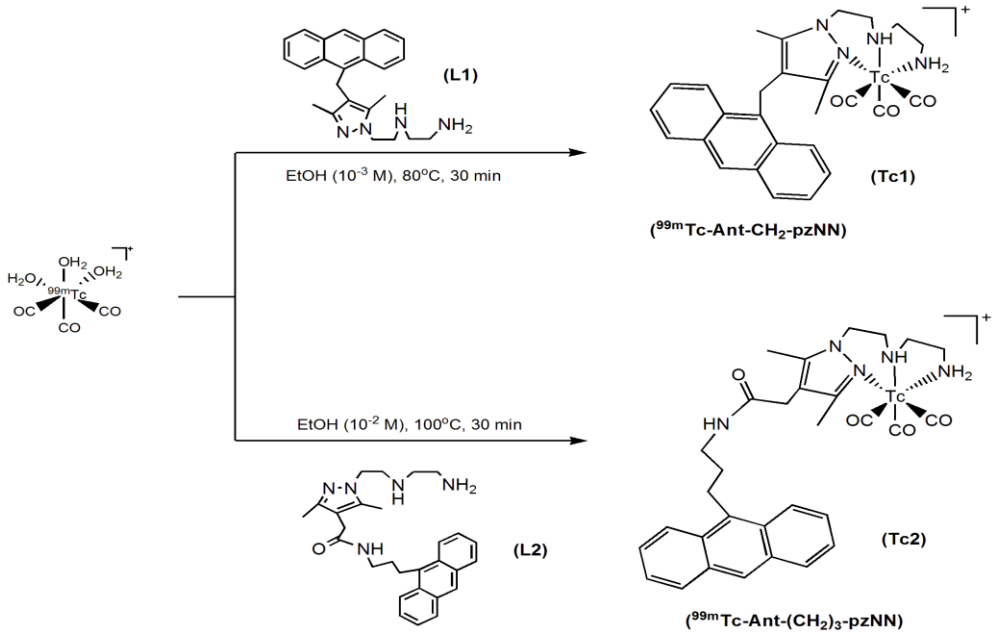

Scheme 2.12 Synthesis of **Tc1** and **Tc2** with the precursor *fac*-$[^{99m}Tc(H_2O)_3(CO)_3]^+$

As shown in Scheme 2.12, **L1** and **L2** were reacted with an aqueous solution of the tricarbonyl precursor to give **Tc1** and **Tc2**. Ethanolic solutions of the ligands were added to an aqueous solution of the precursor at pH = 7.4. The resulting mixtures, having 10^{-4} or 10^{-3} M concentrations of **L1** and **L2**, were heated for 30 min at 80°C and 100°C, respectively. The synthesized complexes, **Tc1** and **Tc2**, were analyzed by HPLC and their retention times compared with those of the Re congeners (Figure 2.11 and Figure 2.12).

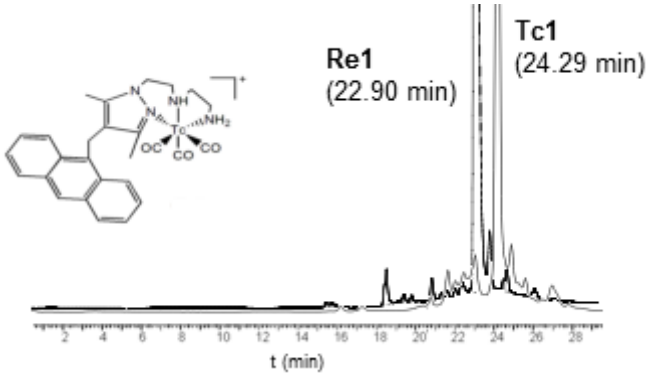

Figure 2.11 HPLC chromatograms of **Tc1** and **Re1** obtained by γ- and UV-detection, respectively

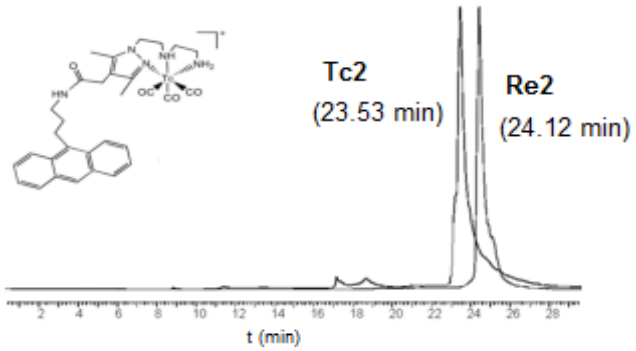

Figure 2.12 HPLC chromatograms of **Tc2** and **Re2** obtained by γ- and UV-detection, respectively

The HPLC analysis confirmed that **Tc1** and **Tc2** were obtained in high radiochemical purity. Moreover, the retention times of **Tc1** and **Tc2** are almost superimposed with those of **Re1** and **Re2**, respectively (see Figure 2.11 and Figure 2.12), showing that we are in the presence of isostructural complexes. The small difference in retention time between the ^{99m}Tc complexes and respective Re counterparts is due to the flow of the analyte in the HPLC system which passes through the UV detector first, and then through the gamma detector.

Both ^{99m}Tc complexes, **Tc1** and **Tc2**, were purified by HPLC before further *in vitro* and biological studies presented in the next chapter. The analytical control revealed high purity of the purified complexes.

3.1 **Spectroscopic studies of the interaction of the ligands and corresponding Re(I) complexes with the DNA molecule**

The interaction of the ligands and Re complexes with the DNA was evaluated by UV-Vis and fluorescence spectroscopic studies with CT-DNA. The use of these techniques for DNA-binding studies has been reviewed in Section 1.6.2.3.

Spectroscopic studies (UV-Vis, Fluorescence, Linear and Circular Dichromism) of interaction of **L1** and **Re1** with the DNA have been described in the literature.[45]

The spectra of the **L2** and **Re2** were obtained for different CT-DNA/probe ratios. The CT-DNA was added to the probes until no change was observed in the spectra, meaning that all the probes were bounded to the DNA molecule. The comparison is done with the spectra of the free probe in solution. All the measurements were carried in phosphate buffer saline (PBS) (10 mM, pH = 7.2).

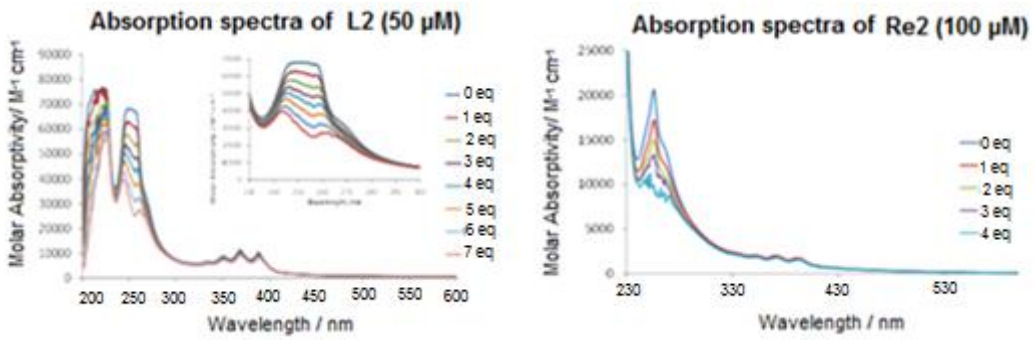

Figure 3.1 Absorption spectra of solutions containing 50 µM of **L2** (**left**) or 100 µM of **Re2** (**right**) in PBS (10 mM, pH = 7.2) with different equivalent amounts of CT-DNA.

By analyzing the obtained spectra shown in Figure 3.1, slight hypochroism and red shifting can be observed on the bands of the anthracenyl chromophores upon addition of CT-DNA for both **L2** and **Re2**. A negligible broadening on the vibronic strcture of the anthracene absorption bands can be noticed. No isosbestic points, which are indicator of the conversion of free probes to the bound ones, could be observed, in any of the cases.

The intrinsic binding constants (*K*) were estimated by Scatchard model through UV-vis spectra.[45,67] The *K* was determined from the plot of $D/\Delta\varepsilon_{ap}$ *vs* D, where D is the concentration of DNA in base pairs and $\Delta\varepsilon_{ap} = [\varepsilon_B - \varepsilon_F]$. ε_{ap} is the apparent extinction coefficient and it can be

calculated as the ratio of the observed absorbance of the sample and the total concentration of the probe (A_{obs}/[probe]). ε_B and ε_F are the extinction coefficients of the bound and the free forms of the probe, respectively.

The absorption data were fitted to the following equation:

$$D / \Delta\varepsilon_{ap} = D / \Delta\varepsilon + 1 / D/\Delta\varepsilon K$$

Where $\Delta\varepsilon = [\varepsilon_B - \varepsilon_F]$ ε_B was confirmed through an independent method, in which the absorbance was extrapolated from a linear plot of the absorbance *vs* 1/[DNA] for [DNA] >>[probe].

Table 3.1 Intrinsic binding constants (*k*) of **L1**, **Re1**, **L2** and **Re2**

***K* [M^{-1}]**	
L1*	(1.06 ± 0.01) x 10^4
Re1*	(1.95 ± 0.01) x 10^4
L2	8.37 x 10^2 ± 1.32 x 10^{-6}
Re2	2.20 x 10^3 ± 1.0 x 10^{-6}

*Data from the literature[45,87]

In general all the compounds present low to moderate affinity for the DNA molecule, but with the obtained results alone it is not possible to determine the type of interaction. By analysis of the values presented in Table 3.1, we can consider that **L1** and **Re1** have higher affinity for DNA than **L2** and **Re2,** as they present higher *K* values. In both cases the Re complexes present higher affinity than the respective ligands most likely due to their intrinsic cationic character.

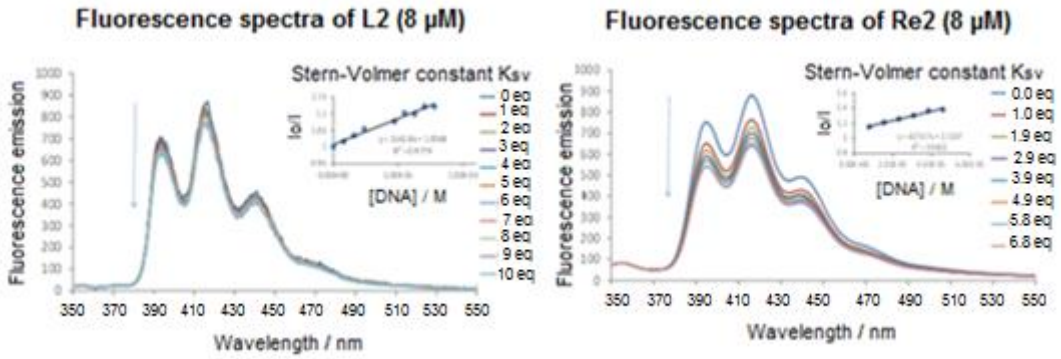

Figure 3.2 Fluorescence spectra of solutions containing 8 µM of **L2** (**left**) or **Re2** (**right**) in PBS (10 mM, pH = 7.2) with different equivalent amounts of CT-DNA

A decrease in fluorescence intensity upon addition of increasing amounts of CT-DNA can be observed for both compounds, but more significant for **Re2** than for **L2** (Figure 3.2). This quenching in the fluorescence indicates interaction with the DNA molecule as usually observed for anthracenyl chromophores.[67]

The Stern-Volmer constant (K_{sv}) could be estimated for **L2** and **Re2** based on the respective fluorescence spectra obtained in the presence of DNA.[67,88] This parameter measures the efficiency of quenching by DNA and can be obtained using the following equation:

$$I_o / I = 1 + K_{sv} [DNA]$$

where I_o and I are the fluorescence intensities in the absence and in the presence of DNA.

Table 3.2 Stern-Volmer constant (K_{sv}) of **L2** and **Re2**

K_{sv} [M^{-1}]	
L2	(1.55 ± 0.09) x 10^3
Re2	(5.56 ± 0.42) x 10^3

By the linearity of the obtained plots (Figure 3.2) and the K_{sv} values presented in Table 3.2, moderate affinity of both ligand and Re complex for the DNA can be considered. Once again **Re2** seems to present higher affinity for the DNA as indicated by the higher K_{sv}.

3.2 Lipophilicity of the ^{99m}Tc complexes

Biodistribution and efficient delivery of therapeutic drugs can be limiting for its clinical application. To estimate the capability of the drug to cross biological barriers and/or interact with biological entities such as receptors, transporters or other macromolecules, several physical-chemical properties can be evaluated, where the lipophilicity is of major interest. The lipophilicity can be measured by the partition coefficient (log P) in a two-phase system of two immiscible liquids, usually water and n-octanol (log $P_{o/w}$). [89,90]

It is assumed that drugs can be separated into three categories according to the log $P_{o/w}$ values: low lipophilicity, log $P_{o/w} \leq 1.5$; moderate lipophilicity, $1.5 \leq \log P_{o/w} \leq 4$; and high lipophilicity, log $P_{o/w} \geq 4$.[91] Table 3.3 presents the log $P_{o/w}$ values of the synthesized ^{99m}Tc complexes, determined by the classical shaken-flask method which is adequate for moderately lipophilic compounds.[89]

Table 3.3 Partition coefficient (log $P_{o/w}$) values of **Tc1** and **Tc2**

Log $P_{o/w}$	
Tc1*	1.41 ± 0.01
Tc2	2.62 ± 0.19

*Data from the literature[48]

Both complexes present moderate lipophilicity.[91,92] **Tc2** presents higher log $P_{o/w}$ value and, thus, it is more lipophilic than **Tc1**. This can be attributed to the presence of the additional propylenic linker introduced as a spacer between the anthracenyl and the pyrazolyl unit.

3.3 *In vitro* stability and protein binding of the ^{99m}Tc complexes

Stability studies in presence of natural chelators that present affinity for the *fac*-$[^{99m}Tc(CO)_3]^+$ core, such as amino acids and proteins that are very abundant in tissues and body circulation, are very important to predict reoxidation and transchelation reactions with the potential radiopharmaceuticals.

Previously, it has been shown that **Tc1** presents a good stability under physiological conditions and in presence of natural chelators such as cysteine and histidine.[87] Herein we tested also the ability of the complex **Tc2** to resist in the presence of human serum and in presence of an excess of the amino acid histidine, at physiological temperature and pH. For this purpose, solutions of **Tc2** were incubated with a solution of histidine in PBS (pH = 7) for 2 hours and with human serum for 6 hours, both at 37°C. The solutions were analyzed by HPLC and the obtained chromatograms were compared with the HPLC chromatographic profile of **Tc2** (Figure 3.3 and Figure 3.4).

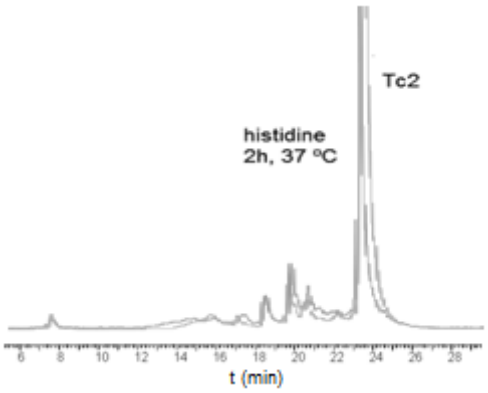

Figure 3.3 Stability of **Tc2** in presence of histidine in PBS (pH = 7) after 2 hours of incubation at 37°C

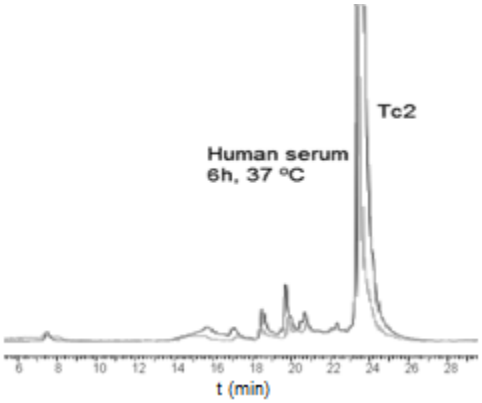

Figure 3.4 Stability of **Tc2** in presence human serum after 6 hours of incubation at 37°C

Tc2 is stable in presence of histidine for at least 2 hours. No transchelation or other degradation was observed by analyzing the chromatographic profile of the incubated solution, which remained unchanged compared to the free **Tc2** in solution as shown in Figure 3.3.

Tc2 is also stable in the presence of human serum for at least 6 hours, as seen by analysis of the chromatograms presented in Figure 3.4. This assay was also used to estimate the binding of **Tc2** with serum protein**.** To determine the percentage of protein binding of **Tc2**, the proteins were precipitated with ethanol and centrifuged. The activity of the precipitate (proteins) and supernatant were measured. It has been found that **Tc2** shows a protein binding of 26 %, after 6 h of incubation at 37 º C, which can be considered a low to moderate value.

3.4 Cellular uptake and subcellular distribution of the ^{99m}Tc complexes

As seen in previous section, the physical-chemical properties of the complexes, such as its lipophilicity, are very important to determine its ability to diffuse through the cell membrane without the need of active transport mechanisms. On the other hand, the polar and hydrophobic interactions with the constituents of the cell membrane such as lipids and proteins can dictate whether the complex will enter the cell or stay bounded to the membrane surface by intermolecular forces.[90] It has been studied the cell uptake of **Tc1** and **Tc2 i**n murine and human tumor cells, as well as their subcellular distribution (nuclear and mitochondria uptake). In particular, the nuclear uptake is a crucial factor that was expected to strongly influence the potential radiotoxicity of the complexes, which is also reported below.

3.4.1 **Cell uptake and cell internalization**

The studies were performed using the purified ^{99m}Tc complexes, **Tc1** and **Tc2**, using B16-F1 murine melanoma and PC-3 human prostate cancer cells. The assays were performed after incubation of each compound with the desired cell line at 37°C, in the presence of cell medium, for different intervals of time (5 min-4h). After incubation, the non-bounded compounds were washed away so the cell uptake could be determined. These experiments were used to determine the total cell uptake, which corresponds to the total amount of ^{99m}Tc complex internalized or bounded to the surface membrane of the cells. The same assays were also used to determine the cell internalized and membrane bound fractions, as described in detail in the experimental section.

As seen in Figure 3.5, the cell internalization of the complex **Tc1** is not significantly different for the two cell lines with a total internalization of about 17% for B16-F1 and 18% for PC-3 cells, after 4h incubation, which is about 55% of the total cell uptake in both cases. This means that about half of the total ^{99m}Tc complex uptake by the cells is able to diffuse through the cell membrane, while 45% is retained at the membrane surface. Similar results were obtained for the complex **Tc2** in both cell lines (Figure 3.6), i.e. 50% of the total ^{99m}Tc complex is internalized by the cells after 4h incubation. However, the amount of internalized complex is about 5% for **Tc2** in both cell lines, which is significantly lower that the values observed for **Tc1**. A comparison of the total cell uptake of **Tc1** and **Tc2** in the two cell lines is also shown in Figure 3.7.

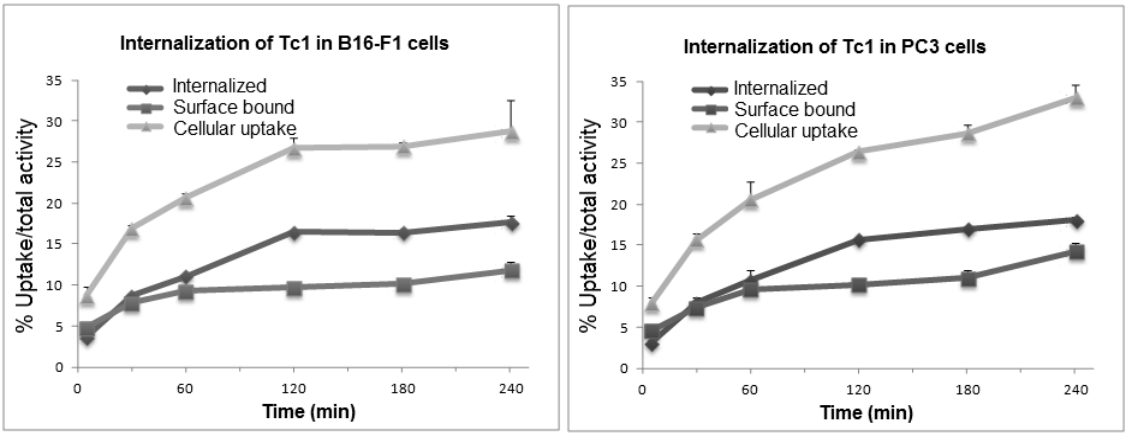

Figure 3.5 Cell internalization of **Tc1** in function of time, after 4 hours incubation at 37°C, in B16-F1 cells (**left**) and PC-3 cells (**right**)

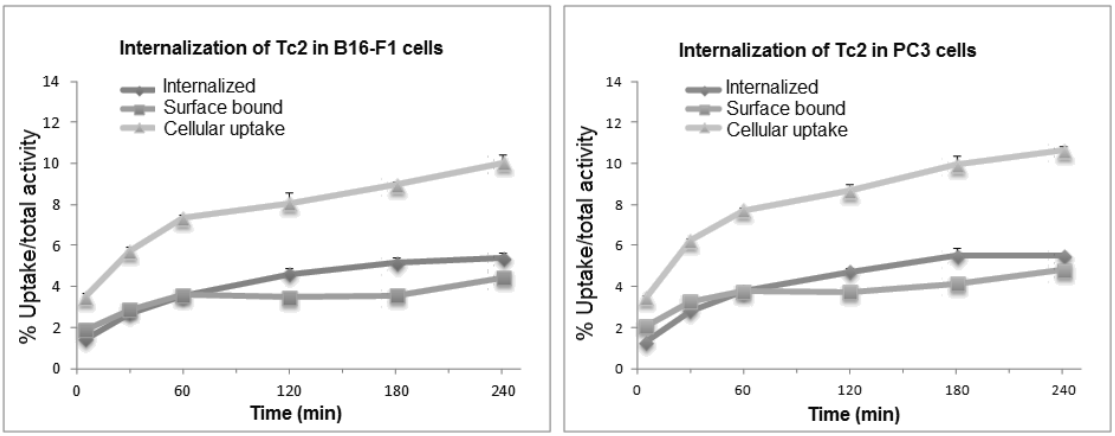

Figure 3.6 Cell internalization of **Tc2** in function of time, after 4 hours incubation at 37°C, in B16-F1 cells (**left**) and PC-3 cells (**right**)

.

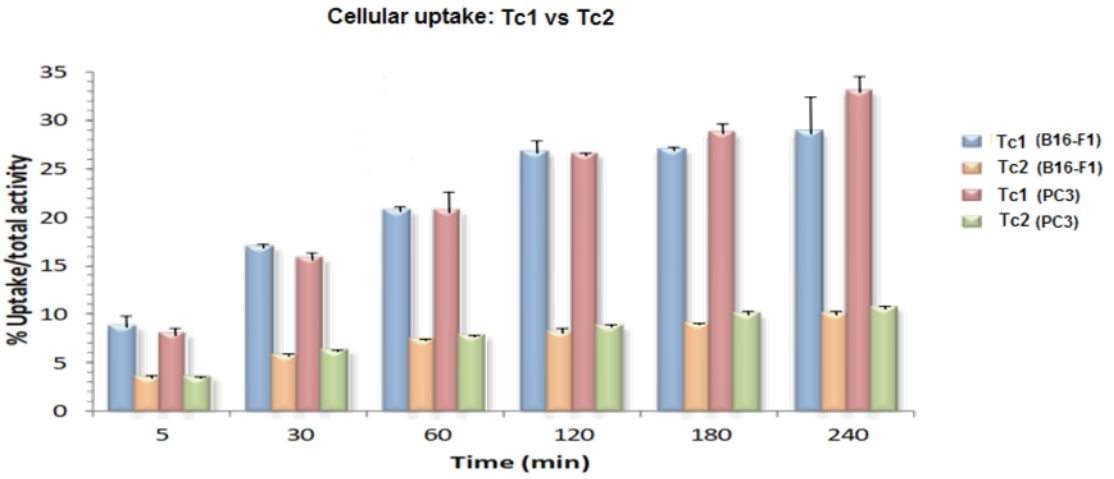

Figure 3.7 Cell uptake of **Tc1** and **Tc2** as a function of time, after 4 hours incubation at 37°C, in B16-F1 and PC-3 cells

In summary, a rapid time-dependent uptake is observed for **Tc1** and **Tc2**, as can be seen in Figure 3.7. However, after 4 of incubation, **Tc1** presents significantly higher uptake, about 35% in PC-3 cells and 30% in B16-F1 cells, if compared with **Tc2** that shows an uptake of ca. 10% in both cell lines. These results are not consistent with the lipophilicity of the complexes determined in section 3.2, as **Tc2** presented higher log $P_{o/w}$ than **Tc1** (log $P_{o/w}$ = 1.41 for **Tc1** and 2.62 for **Tc2**) thus being more lipophilic. It is important to mention that there are several factors that influence the ability of the compounds to diffuse through biological membranes or to interact with its components other than lipophilicity, such as for example charge, size and topology of the molecules. Eventually, the lower molecular weight of **Tc1** can justify its enhanced cellular uptake in comparison with **Tc2**.

3.4.2 Nuclear and mitochondrial uptake

The evaluation of the ability of the synthesized ^{99m}Tc compounds to reach the nucleus and ensure closer proximity to the DNA is of major interest to determine its potential as therapeutic agents as seen in chapter 1. We also decided to evaluate if the compounds were able to accumulate in other organelles such as mitochondria by its isolation using the commercial kit *Mitochondria Isolation Kit for Cultured Cells*. This organelle is key for oxidative metabolism and apoptosis in eukaryotes. Studies have shown that several changes occur in structure and function of mitochondria of the cancer cells, making these organelles important targets for cancer diagnosis and therapy.[93]

The nuclear and mitochondrial uptakes of the ^{99m}Tc complexes in function of total cell uptake were evaluated on B16-F1 and PC-3 cells and the results are presented below. The results

were obtained after 2 hours incubation at 37°C of the purified ^{99m}Tc complexes with the cells, and are expressed in percentage of the total added activity.

Table 3.4 Cellular, nuclear and mitochondrial uptakes of **Tc1** in B16-F1 and PC-3 cells after 2 hours incubation at 37°C

% Uptake/total activity (Tc1)	**B16-F1**	**PC-3**
Cell	30.0 (2.50)*	19.5 (2.30)
Nucleus	23.6 (2.00)	15.6 (1.80)
Mitochondria	0.9 (0.07)	0.2 (0.03)

*The numbers in brackets represent the %uptake/total activity per million cells

The nucleus uptake of **Tc1** is about 80% of the total cellular uptake in both cell lines, while the mitochondrial uptake represents only about 3% of the total uptake for B16-F1 and 1% for PC-3 cells (Table 3.4) after 2 hours. These results indicate that the majority of the internalized ^{99m}Tc complex is able to reach the cell nucleus.

Table 3.5 Cellular, nuclear and mitochondrial uptakes of **Tc2** by B16-F1 and PC-3 cells after 2 hours incubation at 37°C

% Uptake/total activity (Tc2)	**B16-F1**	**PC-3**
Cell	12.9 (1.00)*	8.8 (1.30)
Nucleus	10.8 (0.80)	6.6 (0.90)
Mitochondria	0.2 (0.01)	0.4 (0.06)

*The numbers in brackets represent the %uptake/total activity per million cells

Tc2 presents similar results at the same time point, with a nuclear uptake that corresponds to ca. 90% and 75% of the total cellular uptake in B16-F1 and PC-3 cells, respectively, while the mitochondrial uptake is minimal corresponding only to about 2% and 5% of the total uptake in B16-F1 and PC-3 cells, respectively (Table 3.5).

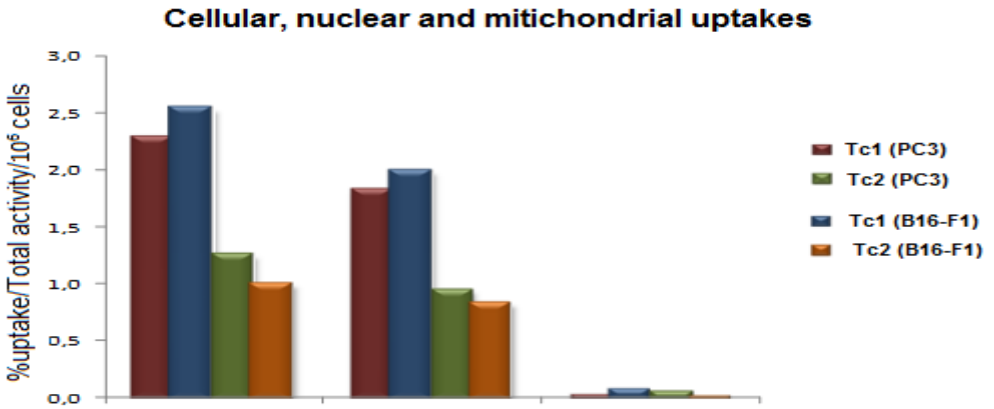

Figure 3.8 Cellular, nuclear and mitochondrial uptakes of **Tc1** and **Tc2** by B16-F1 and PC-3 cells per million cells after 2 hours incubation at 37°C

In summary, there is a minimal accumulation of the complexes in the mitochondria but extremely high uptake by the nucleus in B16-F1 and PC-3 cells, after 2 hour incubation (Figure 3.8). **Tc1** presents higher nuclear targeting than **Tc2**, which certainly reflects its higher cell uptake.

3.5 Cytotoxicity of the tricarbonyl complexes and respective ligands

The cytotoxicity of the ligands and corresponding Re and ^{99m}Tc complexes was evaluated by MTT (3-[4,5-dimethylthiazol-2-yl]-2,5-diphenyl tetrazolium bromide) assay on B16-F1 and PC-3 cells.

The MTT assay is a good indicator of cell viability by measurement of mitochondria activity.[94] In normal cells the mitochondria enzymes are able to provide the conversion of tetrazolium salt MTT into formazan crystals, whose concentration can be determined by the lecture of absorbance at 540 and 720 nm in solution. A decrease in formazan crystals production reflects a decrease in mitochondria activity, and thus in cell viability.

Usually the cytotoxicity of the drugs at different concentrations is determined by comparison with the controls (non-exposed cells). For rapid dividing cells, such as cancer cells, 50% inhibitory concentration (IC_{50}) can be calculated which corresponds to the compound concentration inhibiting cell growth by 50%.

3.5.1 Cytotoxicity of the ligands and Re complexes

The cytotoxicity of the ligands (**L1** and **L2**) and Re complexes (**Re1** and **Re2**) was evaluated to estimate whether the chemical nature of the congener ^{99m}Tc complexes would also contribute for cell toxicity in the range of concentrations (10^{-7}-10^{-9} M) involved in the synthesis of non-carrier added ^{99m}Tc complexes.

The cells were incubated with solutions of the tested compounds at increasing concentrations at 37°C for 40 hours. The cell viability was assessed by the MTT assay and compared with that of controls, i.e. cells not exposed to the compounds. The results obtained are presented in Figure 3.9 and Figure 3.10.

For concentrations lower than 5 µM and 10 µM, respectively, **L1** and **Re1** can be considered non-toxic for B16-F1 cells, as seen in Figure 3.9 (left). At higher concentrations there is a significant inhibition in cell growth with reduced cell survival of almost 0%. For PC-3 cells, cytotoxic effects are observed only at concentrations higher than 10 µM and 20 µM for **L1** and **Re1**, respectively (Figure 3.9 (right)). For **L2** and **Re2**, the cytotoxic effects are observed at concentrations higher than 20 µM and 50 µM for B16-F1 cells and 50 µM and 100 µM for PC-3 cells, respectively (see Figure 3.10).

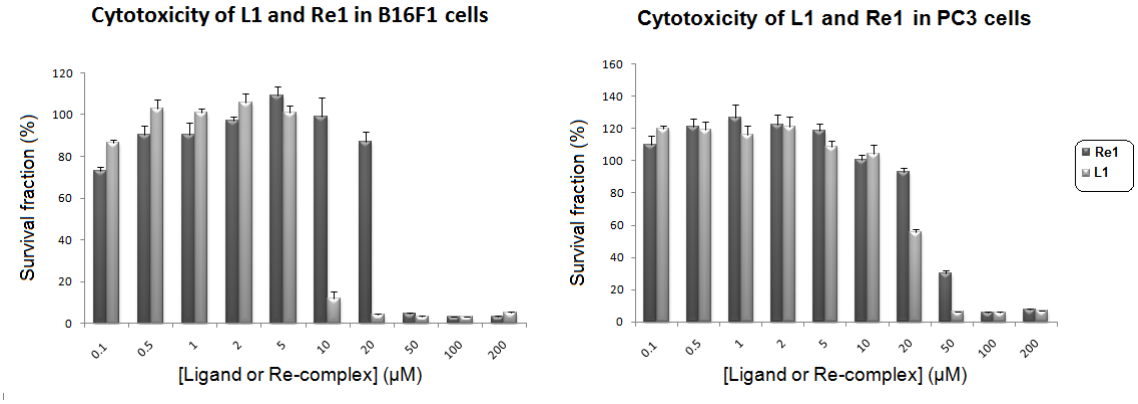

Figure 3.9 Cytotoxicity of **L1** and **Re1** at different concentrations, after 40 hours incubation at 37°C, in B16-F1 cells (**left**) and PC-3 cells (**right**)

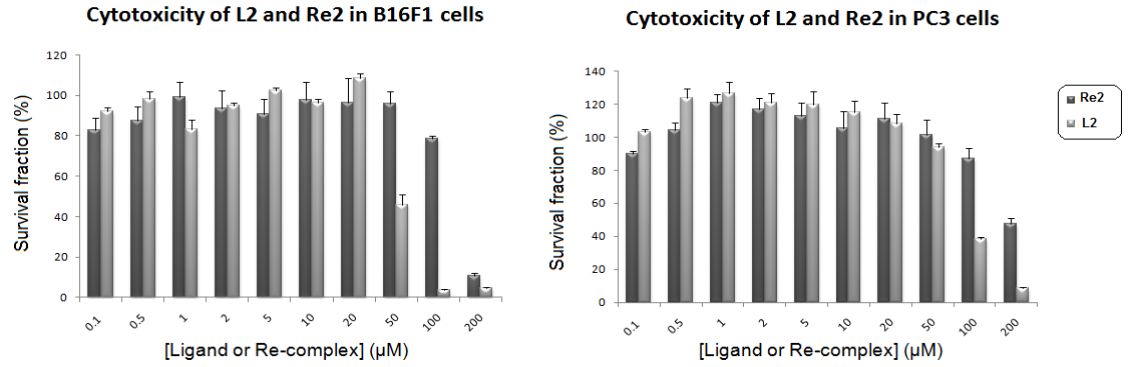

Figure 3.10 Cytotoxicity of **L2** and **Re2** at different concentrations, after 40 hours incubation at 37°C, in B16-F1 cells (**left**) and PC-3 cells (**right**)

Table 3.6 50% inhibitory concentration (IC_{50}) of **L1**, **Re1**, **L2** and **Re2** in B16-F1 and PC-3 cells

IC_{50} [μM] 40h	**B16-F1**	**PC3**
L1	8.1 ± 4.1	28.9 ± 16
Re1	31.3 ± 16.9	46.6 ± 14
L2	56.6 ± 31.8	119.8 ± 80
Re2	153.0 ± 110.0	377 ± 307

The cytotoxicity assays allowed the determination of IC_{50} values (Table 3.6). In both cases, the ligands are more cytotoxic than the Re complexes as lower concentration is needed to reduce cell growth by 50%. This could be due to the facility of the compounds to enter the cells, which is dependent on their structural characteristics, showing that the presence of the metal influences the ability of the ligands to interact with biological systems. The results also indicate that B16-F1 cells are more susceptible to the toxic effects of the ligands and Re complexes than PC-3 cells.

L1 and **Re1** show significantly higher cytotoxic effects than **L2** and **Re2** respectively, which is consistent with the cell uptake and internalization studies with the corresponding ^{99m}Tc complexes. It is possible that, similarly to the corresponding ^{99m}Tc complexes, **L1** and **Re1** have enhanced ability to enter the cells and accumulate into the nucleus, leading to higher cytotoxic effect via disturbance in the structure and dynamics of the DNA molecule. This possibility is more plausible for the isoestrutural Re congeners, as the substitution of ^{99m}Tc for this metal wouldn't change significantly the intrinsic properties of the final organometallic complex. Nevertheless, this discussion has to be done with caution since the standard deviation values of the measured IC_{50} values are rather high.

3.5.2 **Radio-cytotoxicity of the ^{99m}Tc complexes**

Once the synthesized ^{99m}Tc complexes were able to enter the cells and reach the nucleus, their radio-cytotoxicity was evaluated in the same cell lines. Moreover, the cytotoxicity studies with the ligands and Re congeners also showed that at concentrations lower than 10^{-6} M the non-radioactive congeners are not cytotoxic. Therefore any toxic effect presented by the ^{99m}Tc complexes will be due to the radioactive decay of the ^{99m}Tc radionuclide, as the excess of free ligands has been separated by HPLC.

The cells were incubated with solutions of the ^{99m}Tc tricarbonyl complexes (**Tc1** and **Tc2**) with increasing activities, at 37°C for 40 hours. The radio-cytotoxicity of the complexes was then determined by MTT assay. The viability of the cells was compared to that observed in controls and the inhibitions of cell growth were calculated in percentage.

Solutions of the non-nucleus/DNA targeting pertechnetate were also used as controls at the highest activities used for the ^{99m}Tc complexes and as expected, did not show radio-cytotoxic effects in any of the cases.

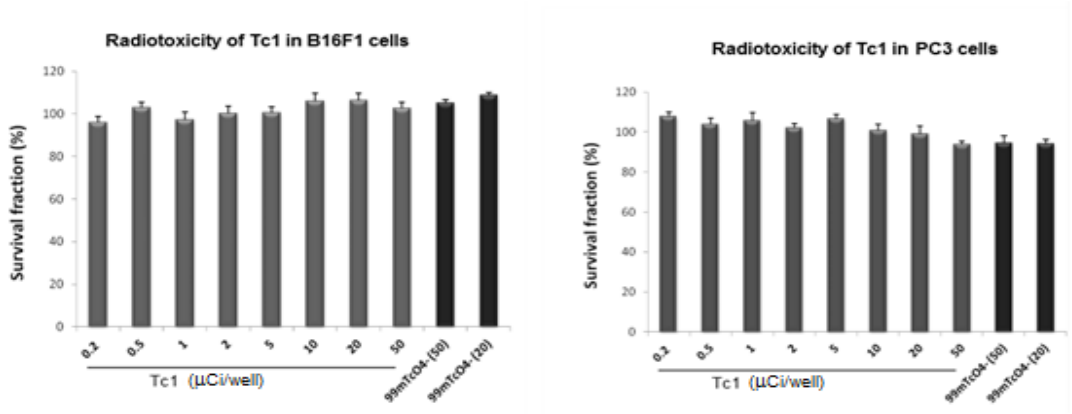

Figure 3.11 Radio-cytotoxicity of **Tc1** at different activities, after 40 hours incubation at 37°C, in B16-F1 cells (**left**) and PC-3 cells (**right**)

The complex **Tc1** did not show any radio-cytotoxic effect in the range of the studied activities (0.2-50 µCi/9 x 10^3 cells per 200 µL of culture medium), which are considered relatively high, with almost 100% of cell survival in both B16-F1 and PC-3 cell lines after 40 hours (Figure 3.11). These results are very different from the ones obtained in the previous studies where the same compound showed great radio-cytotoxic effect towards B16-F1 cells even, at low activities, with about 100% inhibition of cell growth after 2 hours incubation.[48] These previous results can be attributed to matrix effect in the medium, as studies with related compounds show much less or no radio-cytotoxic effect even though these compounds were as efficient to enter the cells and target the nucleus.[46,48]

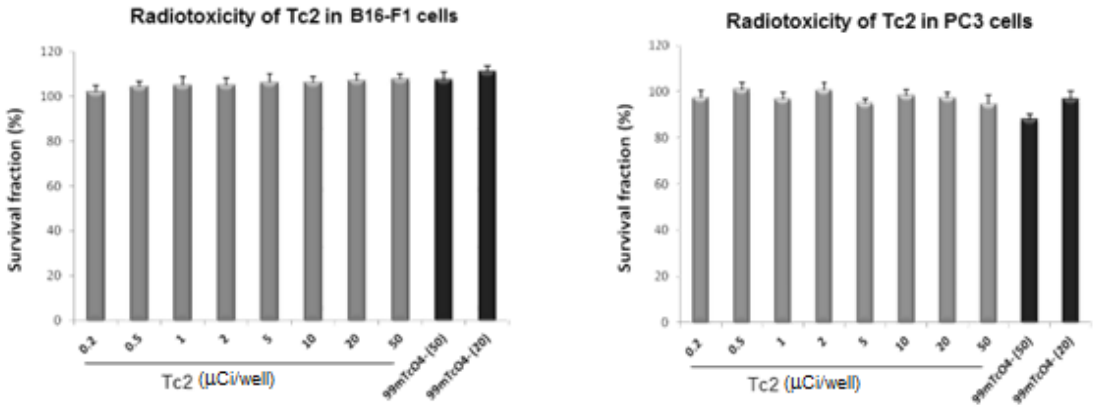

Figure 3.12 Radio-cytotoxicity of **Tc2** at different activities, after 40 hours incubation at 37°C, in B16-F1 cells (**left**) and PC-3 cells (**right**)

As seen in Figure 3.12, **Tc2** also has no radio-cytotoxic effect in the range of the studied activities (0.2-50 µCi/9 x 10^3 cells per 200 µL of culture medium), with almost 100% of cell survival in both B16-F1 and PC-3 cell lines after 40 hours.

4 Conclusions and future prospects

This work falls within the ongoing research at CR group in the design and evaluation of multifunctional radioactive ^{99m}Tc(I) organometallic compounds with the ability to target tumor cells and reach the nucleus for enhanced radiotoxic effects, due to Auger electron emission. A more specific goal of this thesis was to assess the influence of different structural factors that might determine the efficiency of cell internalization, nuclear targeting and radio-cytotoxic effects, such as the DNA-binding nature and the distance between the radionuclide and the target. The synthesis and evaluation of four ^{99m}Tc complexes stabilized by pyrazole diamine ligands, bearing anthracene (**L1** and **L2**) or acridine orange (**L3** and **L4**) as DNA-binding units, were envisaged to elucidate the influence of those structural factors.

The synthesis of the ligands was demanding with moderate to low yields. **L1** and **L2** were successfully obtained and the respective Re and ^{99m}Tc complexes (**Re1**, **Tc1**, **Re2**, and **Tc2**) were synthesized and characterized. After several tries, **L3** was finally obtained but in very low amount and could not be used for further studies. Two novel strategies to synthesize **L4** were tried without success, so this ligand could not be obtained.

Like **Tc1**/**Re1**, **Tc2**/**Re** were obtained with high yield and chemical/radiochemical purity. In the same way as **Tc1, Tc2** has shown a high stability towards challenge reactions with the natural chelator histidine and in the presence of human serum.

Both **Tc1** and **Tc2** showed the ability to enter into B16-F1 murine melanoma cells and PC-3 human prostate cancer cell with significant high accumulation of the total internalized activity in the nucleus. Despite being more lipophilic, **Tc2** present significantly lower uptake by both cell lines than **Tc1,** and thus lower accumulation in the nucleus.

Although fluorescence and UV-Vis spectroscopic studies with the Re congeners showed that the complexes were also able to interact with CT-DNA, no cytotoxic effects of the ^{99m}Tc complexes (**Tc1** and **Tc2**) were observed at activities up to 50 µCi per 10^3 cells in B16-F1 and PC-3 cells after 40 hours of incubation. These results contrast with ones reported previously in the literature for **Tc1**, which showed high radio-cytotoxic effect towards B16-F1 cells with almost 100% of cell death in 24 hours. We attribute these conflicting results to matrix effects that might occurred in the previous studies.

The obtained results indicate that the spacer influences the physical-chemical properties of the complexes, and thus its ability to penetrate through biological barriers. In this case, the longer spacer led to lower cell and nuclear uptake. As none of the complexes was able to cause cytotoxic effects, it was not possible to conclude whether the spacer could also affects the cell killing ability of the synthesized complexes by positioning the radionuclide at different distances

to the DNA. For the same reason we did not proceed with the functionalization of the synthesized complexes with a bioactive peptide and a NLS to enhance its potential as a targeted therapeutic agent. As the AO-containing ^{99m}Tc complexes, **Tc3** and **Tc4**, could not be synthesized we were not able to test the effect of the DNA-binding group either.

From our results we conclude that an efficient delivery system of ^{99m}Tc at single cell level could be provided but the radionuclide did not exert enhanced radiotoxic effects. In other words, the synthesized compounds were able to provide delivery of ^{99m}Tc to its target but the Auger electrons emission did not display sufficient energy for significant cell killing.

The use of Auger emitters for target radionuclide therapy is a very complex issue. In the particular case of ^{99m}Tc complexes, several questions remain to be addressed: i) influence of DNA-binding mode in DNA damage and radiotoxicity; ii) role of direct or indirect effects in DNA damage and cell killing ability if compared with other Auger emitters; iii) relashionship between DNA damage, generation of ROS species and cell death outcome; iv) minimum threshold of accumulated radioactivity per cell nucleus to obtain significant radiotoxic effects, etc.

Our complexes did not show any radio-cytotoxic activity for the tested radioactivity values, but we consider that it is worthwhile to evaluate their ability of inducing DNA damage using naked DNA (e.g. plasmid DNA) and using single-cell gel electrophoresis experiments (e.g comet assay), while assessing also the formation of ROS both *in vitro* (plasmid DNA) and in vivo (tumor cell lines). By extending such studies to the initially proposed AO-containing congeners, which are being synthesized by other students at the RS Group, we expect to address some of the above mentioned questions. Thus, we anticipate that our research will have a better ability of contributing to clarify whether ^{99m}Tc has relevance for targeted Auger Therapy, which remains an unanswered scientific question.

5.1 **General aspects**

The manipulation of chemical compounds was performed according to good laboratory practice. Protective lead barriers were used in the manipulation of all the radioactive compounds. The control of the radiation dose absorbed by the handler was performed by reading individual dosimeters.

All the chemical reactions were performed at room temperature except when indicated. In those cases, ice bath was used to lower the temperature to 0ºC and dry or water bath was used to rise to the required temperature.

Compounds sensitive to air or humidity were treated with distilled and dry solvents and were handled under nitrogen (N_2) atmosphere using Schlenk line techniques. The work-ups were performed under air.

5.2 **Materials and methods**

5.2.1 **Solvents and reagents**

All chemical and solvents were of analytical grade (Sigma-Aldrich) and were used without further purification unless stated otherwise.

Dry solvents used were distilled and dried according to the literature procedures then kept under nitrogen atmosphere and molecular sieves.[95]

The compounds ethyl 1-trityl-1H-pyrazole-4-carboxylate, 2-(anthracen-9-yl)acrylonitrile; and the rhenium precursors *fac*-[$Re(H_2O)_3(CO)_3$]Br and *fac*-[$Re(CO)_5Br$] were prepared as described in the literature.[85,86]

5.2.2 Techniques for purification and/or characterization

Nuclear Magnetic Resonance Spectrometry (NMR)

^{1}H and ^{13}C NMR spectra were recorded on a Bruker Avance 400 MHz or 300 MHz spectrometers (IST, Lisbon, Portugal); the chemical shifts are given in ppm and were referenced to the residual solvent resonances relative to tetramethylsilane ($SiMe_4$). For complex **Re2**, the assignment of the ^{1}H and ^{13}C NMR resonances was done based on COSY and HSQC techniques.

Mass Spectrometry (MS)

Mass spectra were obtained on a spectrometer ESI/QITMS Bruker HCT with electrospray ionization by Dr. Célia Fernandes (CR Group, C^2TN). The samples were prepared in MeOH.

Thin Layer Chromatography (TLC)

TLC was used to monitor chemical reactions and analyze the products obtained.

Silica-gel (SiO_2) plates (0.20 mm 60 Å-UV_{254}, ALUGRAM® aluminum sheets from Macherey-Nagel) were used to run the chromatograms, with exception of the acridine orange derivatives that were analyzed using aluminum oxide (Al_2O_3) matrices (0.25 mm 60 Å, glass support from Sigma-Aldrich); the chromatograms were revealed by UV radiation (254 nm) or and/or using I_2 chambers.

Column Chromatography

This technique was used to purify some of synthesized compounds with silica gel (60 Å with granulometry of 70 - 230 mesh ASTM (Merck)) or aluminum oxide (Sigma-Aldrich) as chromatographic supports. These supports were prepared with the appropriate solvent/eluent (s) and filled into glass columns with the proper dimensions. The choice of the eluents depended on the characteristics of the compounds to separate, and the column glass size on the amount used for the purification. The compounds were applied on the top of the column and eluted through gravity effect, and then collected as several small fractions. Those fractions were analyzed by TLC and separated in different sets according to the respective retardation factor

(R_f). The purified compounds were dried under reduced pressure and characterized by common analytical techniques.

High Performance Liquid Chromatography (HPLC)

HPLC was used to characterize and purify the ^{99m}Tc compounds. It was also used to characterize the respective Re congeners and ligands. These studies were performed on a HPLC system constituted by a Perkin-Elmer LC 200 pump with an UV-Vis detector (Perkin-Elmer LC 290) and a radiation detector (Berthold-LB 507A). The solvents were of HPLC grade and were purged with helium. The water was bidistilled from a quartz distillation unit and filtered by Millipore (0.22 µm) filters. The different methods used in the HPLC separations described in this thesis are presented below.

HPLC conditions

Analytical control of the ligands and Re complexes

UV detection: λ = 254 nm
Column A: Macherey-Nagel EC 250/4 Nucleosil 100-10 C18
Flow: 1 mL/min
Eluents: **A**- 0.1% aqueous TFA; **B**- MeOH

Method A

Step	**Time (min)**	**% A**	**% B**	**Curve**
0	5.0	100	0	-
1	3.0	100	0	1
2	0.1	75	25	-
3	5.9	75	25	-
4	0.1	66	34	1
5	10.9	0	100	-
6	5.0	0	100	-
7	0.1	100	0	1
8	4.9	100	0	-

Purification and/or analytical control of solutions containing ^{99m}Tc compounds

Radiation detection: γ radiation

Column B: Macherey-Nagel EC 250/3 Nucleosil 100-5 C18
Flow: 0.5 mL/min
Eluents: **A**- 0.1% aqueous TFA; **B**- ACN

Method B

Step	**Time (min)**	**% A**	**% B**	**Curve**
0	5.0	100	0	-
1	0.3	100	0	-
2	0.1	75	25	1
3	5.9	75	25	-
4	0.1	66	34	1
5	8.9	0	100	-
6	17.0 (7.0)*	0	100	-
7	0.1	100	0	1
8	4.9	100	0	-

*In some cases, the running time of this step was reduced as it does not affect the retention time and separation of the compounds

Purification of ^{99m}Tc complexes

When needed, the purification of the ^{99m}Tc complexes consisted on applying a higher amount (0.5-1 mL) of the sample into the HPLC system, and the run performed using the same conditions as for the analytical control of the complexes. The fractions corresponding to the desired complexes were collected in falcon tubes containing a small amount of phosphate buffered saline (PBS) 0.1 M (pH=7) (100 µL). Then, the eluent (ACN) was evaporated under N_2. The purity of the collected complexes was checked by analytical HPLC using the same elution conditions.

Activity measurements of radioactive solutions

The activity of the radioactive solutions was measured in an ionization chamber (Aloka, Curiemeter IGC-3). The samples with lower activity (less than 2 µCi) were measured in a Gamma counter (Berthold, LB2111).

5.3 Synthesis and characterization of the ligands

5.3.1 Synthesis and characterization of the pyrazol units

(Z)-ethyl 3-acetyl-4-hydroxypent-3-enoate (6)

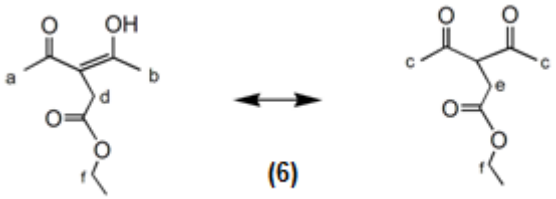

2,4-pentanodione (1.50 mL, 14.58 mmol) was added, drop wise, to a suspension of NaH (0.65 g, 27.09 mmol) in dry THF (20 mL) at 0ºC. The mixture was stirred for 1 h followed by slow addition of ethyl bromoacetate (1.60 mL, 14.49 mmol) at the same temperature. The stirring mixture was left overnight at room temperature. HCl 2M was added at 0ºC and the compound was extracted with Et_2O. The organic phase was then separated, dried with $MgSO_4$ and filtered. The solvent was evaporated under reduced pressure and the product dried under vacuum.
Yield: 82% (2.23 g) of a yellow oil.

^{1}H NMR (300 MHz, $CDCl_3$) δ_H (ppm): 1.64 (m, 6H, $2CH_3$ (Et-ester, *keto* and *enol* forms)); 1.99 (s, 3H, CH_3 (b)); 2.11 (s, 3H, CH_3 (a)); 2.18 (s, 6H, $2CH_3$ (c)); 2.80 (d, 2H, CH_2 (e)); 3.20 (s, 2H, CH_2 (d)); 4.03 (m, 4H, $2CH_2$ (f, *keto* and *enol* forms)).

Ethyl 2-(1-(2-hydroxyethyl)-3,5-dimethyl-1H-pyrazol-4-yl)acetate (7)

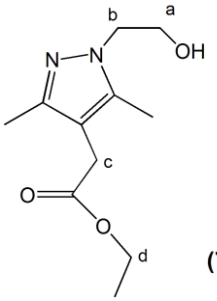

(7)

A solution of 2-hydroxyethylhydrazine (0.84 mL, 12.39 mmol) in EtOH (20 mL) was added to a solution of compound **6** (2.23 g, 12.46 mmol) in EtOH (10 mL) at 0ºC and the mixture was stirred overnight at room temperature. The product was concentrated under reduced pressure and dried under vacuum.
Yield: 89% (2.50 g) of a brown oily solid.

^{1}H NMR (400 MHz, $CDCl_3$) δ_H (ppm): 1.15 (t, 3H, CH_3 (Et-ester)); 2.13 (s, 6H, $2CH_3$ (Me_2pz)); 3.30 (s, 2H, CH_2 (c)); 3.61 (q, 2H, CH_2 (d)); 3.85 (t, 2H, CH_2); 4.04 (m, 2H, CH_2); 4.50 (s br, 1H, OH).

Ethyl 2-(1-(2-bromoethyl)-3,5-dimethyl-1H-pyrazol-4-yl)acetate (8)

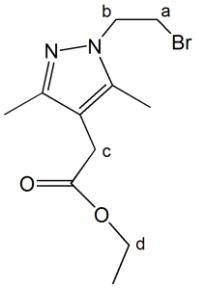

(8)

Method 1

PBr_3 (1mL, 10.61 mmol) was added to a solution of compound **7** (1.00 g, 4.42 mmol) in toluene (30 mL) and the reaction mixture was heated under reflux overnight. The solvent was evaporated under reduced pressure and the residue extracted with an aqueous solution of $NaHCO_3$ and chloroform. The organic phase was dried with $MgSO_4$ and filtered, then concentrated under reduced pressure and dried under vacuum.
Yield: 67% (0.86 g) of brownish oil.

Method 2

CBr_4 (4.97 g, 14.99 mmol) and PPh_3 (3.93 g, 14.98 mmol) were added to a solution of compound **7** (1.60 g, 7.07 mmol) in dry THF (50 mL) and the reaction mixture was stirred for 48h. The precipitate was filtered off and the filtrate was concentrated under reduced pressure. The product was purified by SiO_2 column chromatography (eluent: DCM (100-96%)/EtOH (0-4%)). The final product was washed with Et_2O and filtered to remove the O-PPh_3. The filtrate was concentrated and dried under vacuum.
Yield: 47% (0.96 g) of brownish yellow oil.

^{1}H NMR (300 MHz, $CDCl_3$) δ_H (ppm): 1.95 (t, 3H, CH_3 (Et-ester)); 2.23 (s, 6H, $2CH_3$ (2Met-pz)); 3.34 (s, 2H, CH_2 (c)); 3.66 (t, 2H, CH_2); 4.09 (q, 2H, CH_2 (d)); 4.39 (t, 2H, CH_2).

Tert-butyl 2-aminoethylcarbamate (9)

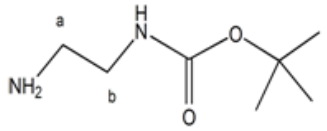

(9)

A solution of Boc_2O (7.00 g, 32.07 mmol) in dioxane (30 mL) was added drop wise to a solution of 1,2-diaminoethane (17 mL, 257 mmol) in dioxane (40 mL) and the reaction mixture was stirred for 22 h. The solvent was evaporated under reduced pressure and then water was added to the residue. The white precipitate formed was filtered off and the filtrate was extracted with chloroform. The organic phase was dried with Na_2SO_4, filtered and concentrated under reduced pressure. The final product was dried under vacuum.
Yield: 84% (4.30 g) of colorless oil.

^{1}H NMR (400 MHz, $CDCl_3$) δ_H (ppm): 1.13 (s, 2H, NH_2); 1.23 (s, 9H, $3CH_3$ (BOC)); 2.56 (t, 2H, CH_2 (a)); 2.94 (t, 2H, CH_2 (b)); 5.46 (s br, 1H, NH).

Ethyl 2-(1-(2-(2-(tert-butoxycarbonylamino)ethylamino)ethyl)-3,5-dimethyl-1H-pyrazol-4-yl)acetate (10)

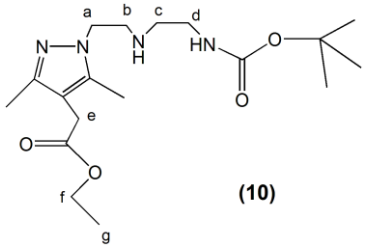

(10)

A solution of compound **8** (0.4 g, 1.38 mmol) in dry ACN (5 mL) was added drop wise to a suspension of compound **9** (0.33 g, 2.07 mmol), K_2CO_3 (0.19 g, 1.38 mmol) and KI (0.01 g, 0.07 mmol) in dry ACN (10 mL), and the resulting mixture was heated overnight under reflux. The solid was filtered off and the filtrate was concentrated under reduced pressure. The product was purified by SiO_2 column chromatography (eluent: chloroform (90%)/MeOH (10%)).
Yield: 48% (0.24 g) of yellow oil.

^{1}H NMR (400 MHz, $CDCl_3$) δ_H (ppm): 1.10 (t, 3H, CH_3 (Et-ester)); 1.30 (s, 9H, $3CH_3$ (BOC)); 2.06 (s, 6H, $2CH_3$ (Me_2pz)); 2.57 (t, 2H, CH_2); 2.85 (t, 2H, CH_2); 3.05 (t, 2H, CH_2); 3.19 (s, 2H, CH_2 (e)); 3.91 (t, 2H, CH_2 (a)); 3.98 (q, 2H, CH_2 (f)); 5.46 (s, 1H, NH).

Ethyl 2-(1-(2-(tert-butoxycarbonyl(2-(tert-butoxycarbonylamino)ethyl)amino)ethyl)-3,5-dimethyl-1H-pyrazol-4-yl)acetate (11)

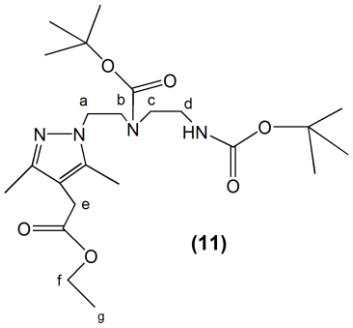

(11)

To a stirring solution of compound **10** (0.47 g, 1.28 mmol) in dry THF (20 mL) at 0ºC was added, drop wise, a solution of Boc_2O (0.30 g, 1.38 mmol) in dry THF (15 mL), and the resulting mixture was stirred overnight at room temperature. The solvent was evaporated under reduced pressure and the residue was extracted with an aqueous solution of Na_2CO_3 and chloroform. The organic phase was dried with Na_2SO_4, filtered and evaporated under reduced pressure. The final product was dried under vacuum.

Yield: 93% (0.56 g) of yellow oil.

^{1}H NMR (300 MHz, $CDCl_3$) δ_H (ppm): 1.22 (t, 3H, CH_3 (Et-ester)); 1.42 (s, 18H, $6CH_3$ (2BOC)); 2.07 (m, 6H, $2CH_3$ (Me_2pz)); 3.06 (m, 4H, $2CH_2$); 3.33 (s, 2H, CH_2 (e)); 3.52 (t, 2H, CH_2); 4.08 (m, 4H, $2CH_2$ (f + a)).

2-(1-(2-(tert-butoxycarbonyl(2-(tert-butoxycarbonylamino)ethyl)amino)ethyl)-3,5-dimethyl-1H-pyrazol-4-yl)acetic acid (12)

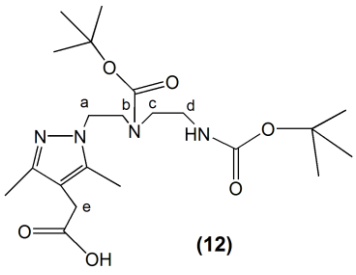

(12)

A solution of NaOH (0.58 g, 14.60 mmol) in water (15 mL) was added to a solution of compound **11** (0.58 g, 1.23 mmol) in THF (15 mL) and the stirring mixture was heated overnight under reflux. The mixture was then neutralized with HCl 4M at 0ºC. THF was evaporated under reduce pressure and the product extracted with DCM. The organic phase was dried with Na_2SO_4, filtered, evaporated under reduced pressure and finally dried under vacuum.

Yield: 92% (0.50 g) of a yellow solid.

^{1}H NMR (400 MHz, $CDCl_3$) δ_H (ppm): 1.38 (s, 18H, $6CH_3$ (2BOC)); 2.13 (s, 6H, $2CH_3$ (Me2pz)); 2.99 (m, 4H, $2CH_2$); 3.29 (s, 2H, CH_2 (e)); 3.48 (t, 2H, CH_2); 4.07 (m, 2H, CH_2 (a)); 5.03 (s br, 1H, OH/NH); 5.18 (s br, 1H, NH).

2,5-dioxopyrrolidin-1-yl 2-(1-(2-(tert-butoxycarbonyl(2-(tert-butoxycarbonylamino)ethyl)amino)ethyl)-3,5-dimethyl-1H-pyrazol-4-yl)acetate (13)

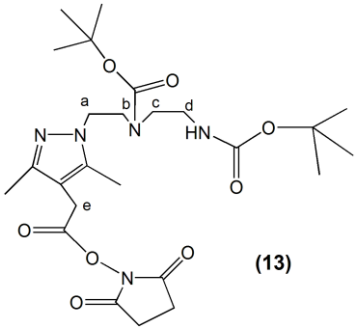

(13)

To a stirring solution of compound **12** (0.45 g, 1.02 mmol) in dry DCM (20 mL) at 0ºC was added NHS (0.14 g, 1.24 mmol). After 15 min at this temperature EDC (0.24 g, 1.24 mmol) was added and the reaction mixture was stirred for 72 h at room temperature. The product was then extracted with water and DCM. The organic phase was separated, dried with Na_2SO_4, filtered and concentrated under reduced pressure. The final product was dried under vacuum.
Yield: 75% (0.41 g) of a yellow solid.

^{1}H NMR (400 MHz, $CDCl_3$) δ_H (ppm): 1.40 (s, 18H, $6CH_3$ (2BOC)); 2.16 (s, 6H, $2CH_3$ (Me_2pz)); 2.79 (s, 4H, $2CH_2$ (NHS)); 2.84 (m, 4H, $2CH_2$); 3.51 (t, 2H, CH_2); 3.62 (s, 2H, CH_2 (e)); 4.07 (m, 2H, CH_2 (a)).

Ethyl 1-(2-hydroxyethyl)-1H-pyrazole-4-carboxylate (21)

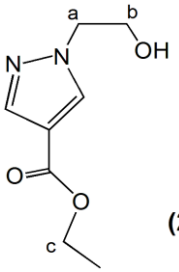

(21)

A solution of 2-hydroxyethylhydrazine (0.95 mL, 13.80 mmol) in EtOH (76 mL) was added drop wise to a solution of ethyl 2-formyl-3-oxopropanoate (2.00 g, 13.88 mmol) in EtOH (16 mL) at 0ºC. The mixture was stirred for 40 h and the solvent was then evaporated under reduced pressure. The final product was dried under vacuum.
Yield: 96% (2.45 g) of yellow oil.

^{1}H NMR (300 MHz, $CDCl_3$) δ_H (ppm): 1.11 (t, 3H, CH_3); 3.73 (t, 2H, CH_2 (a/b)); 4.02 (m, 4H, $2CH_2$ (c + a/b)); 4.56 (s br, 1H, OH); 7.64 (s, 1H, CH); 7.82 (s, 1H, CH).

Ethyl 1-(2-bromoethyl)-1H-pyrazole-4-carboxylate (22)

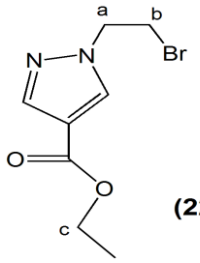

(22)

CBr_4 (8.80 g, 26.65 mmol) and PPh_3 (6.97 g, 26.57 mmol) were added to a solution of compound **21** (2.45 g, 13.30 mmol) in pre-dried THF (90 mL) at 0ºC and the mixture was stirred for 16 h. The solvent was evaporated under reduced pressure and the mixture was extracted with DCM and water. The organic phase was dried with Na_2SO_4, filtered and concentrated under reduced pressure. The product was purified by SiO_2 column chromatography (eluent: gradient elution with Hexane (90-30%)/Acetyl acetate (10-70%)).
Yield: 66% (2.17 g) of yellow solid.

^{1}H NMR (300 MHz, $CDCl_3$) δ_H (ppm): 1.32 (t, 3H, CH_3); 3.72 (t, 2H, CH_2 (a)); 4.26 (m, 2H, CH_2 (c)); 4.48 (t, 2H, CH_2 (b)); 7.94 (s, 2H, 2CH).

^{13}C NMR (100.61 MHz, $CDCl_3$) δ (ppm): 14.25 (CH_3); 29.52 (CH_2); 53.82 (CH_2); 60.21 (CH_2); 115.14 (C, pz); 133.53 (CH, pz); 141.82 (CH, pz); 183.07 (C=O).

Ethyl 1-(2-(2-(tert-butoxycarbonylamino)ethylamino)ethyl)-1H-pyrazole-4-carboxylate (23)

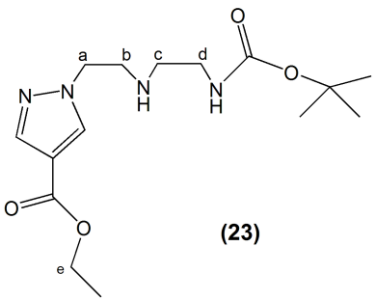

(23)

A solution of compound **22** (2.20 g, 8.90 mmol) in dry ACN (20 mL) was added drop wise to a stirring suspension of compound **9** (2.14 g, 13.35 mmol), K_2CO_3 (1.23 g, 8.90 mmol) and KI (0.07 g, 0.44 mmol) in dry ACN (40 mL), and the mixture was heated under reflux overnight. The solid was filtered off and the solvent was evaporated under reduced pressure. The product

was purified by SiO_2 column chromatography (eluent: gradient elution with DCM (100-94%)/MeOH (0-6%)).

Yield: 74% (2.15 g) of yellow oil.

^{1}H NMR (300 MHz, $CDCl_3$) δ_H (ppm): 1.30 (t, 3H, CH_3 (Et-pz)); 1.37 (s, 9H, $3CH_3$ (BOC)); 2.68 (t, 2H, CH_2); 3.03 (t, 2H, CH_2); 3.13 (t, 2H, CH_2); 4.16 (t, 2H, CH_2); 4.18 (m, 2H, CH_2 (e)); 4.98 (s br, 1H, NH); 7.85 (s, 2H, 2CH).

Tert-butyl 2-(2-(4-(hydroxymethyl)-1H-pyrazol-1-yl)ethylamino)ethylcarbamate (24)

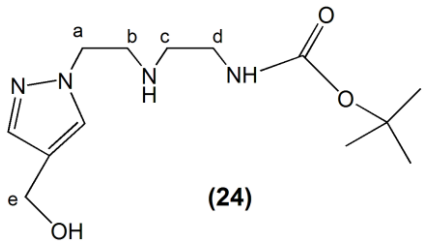

(24)

$LiAlH_4$ 1 M/THF (1.50 mL, 1.50 mmol) was added drop wise to a solution of compound **23** (0.20 g, 0.61 mmol) in dry THF (30 mL) at 0ºC and the mixture was stirred overnight at room temperature. Cold water (3 mL) was slowly added at 0ºC and after 5 min stirring at the same temperature, NaOH 10% (0.5 mL) was added. The white precipitate formed was filtered off, while the filtrate was concentrated under reduced pressure and extracted with DCM. The organic phase was dried with Na_2SO_4, filtered and concentrated under reduced pressure. The product was purified by SiO_2 column chromatography (eluent: gradient elution with chloroform (100-95%)/MeOH (0-5%)).

Yield: 50% (0.09 g) of a yellow oil.

^{1}H NMR (400 MHz, $CDCl_3$) δ_H (ppm): 1.40 (s, 9H, 3CH3 (BOC)); 2.51 (m, 2H, CH_2); 3.03 (m, 2H, CH_2); 3.19 (m, 2H, CH_2); 4.18 (t, 2H, CH_2); 4.50 (s, 2H, CH2 (e)); 7.43 (s, 2H, 2CH).

ESI/MS (m/z) ($C_{13}H_{24}N_4O_3$) = **[M^+ + H]** calculated 284.18, found 285.5.

Ethyl 1-(2-(tert-butoxycarbonyl(2-(tert-butoxycarbonylamino)ethyl)amino)ethyl)-1H-pyrazole-4-carboxylate (25)

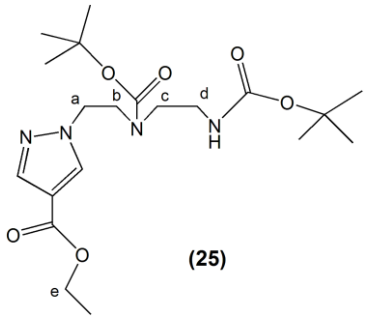

(25)

A solution of Boc_2O (1.25 g, 5.75 mmol) in THF (30 mL) was added drop wise to a solution of compound **23** (1.88 g, 5.75 mmol) in THF (30 mL) at 0ºC and the mixture was stirred overnight at room temperature. The solvent was evaporated under reduced pressure and the mixture was extracted with chloroform and a saturated aqueous solution of Na_2CO_3. The organic phase was dried with Na_2SO_4, filtered, concentrated under reduced pressure and the final product was dried under vacuum.

Yield: 99% (2.44 g) of yellow oil

^{1}H NMR (400 MHz, $CDCl_3$) δ_H (ppm): 1.14 (t, 3H, CH_3 (Et-pz)); 1.23 (s, 18H, $6CH_3$ (2BOC)); 2.84 (m br, 4H, $2CH_2$); 3.45 (m br, 2H, CH_2); 4.08 (m, 4H, $2CH_2$); 4.96 (s br, 1H, NH); 7.69 (s, 2H, 2CH).

^{13}C NMR (75.47 MHz, $CDCl_3$) δ (ppm): 14.53 (CH_3, Et-pz); 28.08 ($9CH_3$, 2BOC); 39.09 (CH_2); 47.43 (CH_2); 59.98 ($2CH_2$); 79.60 (2C, 2BOC); 80.61 (CH_2); 115.09 (C, pz); 134.90 (C-O, BOC); 141.46 (2CH, pz); 162.86 (2C=O, BOC + Ester-pz).

1-(2-(tert-butoxycarbonyl(2-(tert-butoxycarbonylamino)ethyl)amino)ethyl)-1H-pyrazol-4-hydroxymethyl (26)

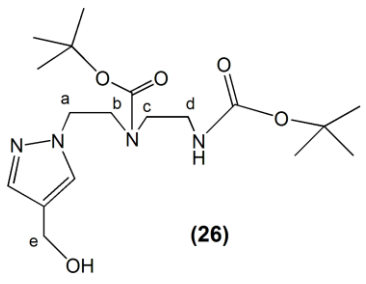

(26)

1 M $LiAlH_4$ in THF (14.50 mL, 14.50 mmol) was added drop wise to a solution of compound **25** (2.43 g, 5.68 mmol) in THF (30 mL) at 0ºC and the mixture was stirred overnight at room temperature. Cold water (15 mL) was slowly added at 0ºC and after 5 min stirring at the same temperature, NaOH 10% (2 mL) was added. The white precipitate formed was filtered off and

the filtrate was concentrated under reduced pressure. The mixture was extracted with diethyl ether and then with chloroform. The combined organic phase was dried with Na_2SO_4, filtered and concentrated under reduced pressure. The final product was dried under vacuum.
Yield: 54% (1.18 g) of a yellow oil

^{1}H NMR (400 MHz, $CDCl_3$) δ_H (ppm): 1.26 (s, 18H, $6CH_3$ (2BOC)); 2.84 (m br, 4H, $2CH_2$); 3.43 (m br, 2H, CH_2); 4.05 (m br, 2H, CH_2); 4.37 (s, 2H, CH_2 (e)); 5.06 (s br, 1H, OH/NH); 5.28 (s br, 1H, OH/NH); 7.19 (s, 1H, CH); 7.32 (s, 1H, CH).

^{13}C NMR (85.47 MHz, $CDCl_3$) δ (ppm): 28.92 ($9CH_3$, 2BOC); 39.16 (CH_2); 48.79 (CH_2); 55.95 ($2CH_2$); 79.68 (2C, 2BOC); 80.88 (CH_2); 121.97 (C, pz); 129.28 (C=O, BOC); 139.34 (2CH, pz); 165.84 (C=O, BOC).

(1-trityl-1H-pyrazol-4-yl)methanol (27)

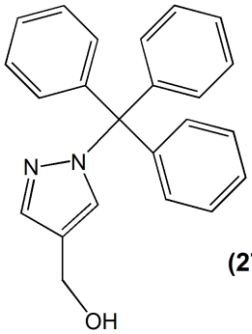

(27)

1 M $LiAlH_4$ in THF (5.8 mL, 5.8 mmol) was added drop wise to a solution of compound ethyl 1-trityl-1H-pyrazole-4-carboxylate (2.90 g, 7.58 mmol) in dry THF (55 mL) at 0ºC and the mixture was stirred overnight at room temperature. Cold water (2 mL) was slowly added at 0ºC and after 5 min stirring at the same temperature, NaOH 10% (0.53 mL) was added. The precipitate formed was filtered off and the filtrate was concentrated under reduced pressure and extracted with DCM. The organic phase was dried with Na_2SO_4, filtered, concentrated under reduced pressure and the final product was dried under vacuum.
Yield: 84% (2.15 g) of a white solid

^{1}H NMR (300 MHz, $CDCl_3$) δ_H (ppm): 4.35 (s, 2H, CH_2); 4.53 (s br, 1H, OH); 7.21 (m, 12H, 12 CH (Tr)); 7.36 (m, 3H, 3CH (Tr)); 7.73 (s, 2H, 2CH (2CH-pz)).

4-(bromomethyl)-1-trityl-1H-pyrazole (28)

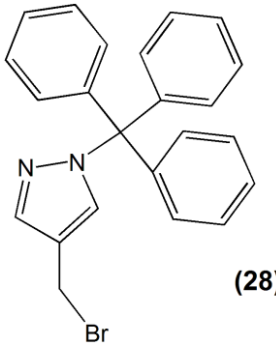

(28)

PBr_3 (0.11 mL, 1.17 mmol) was added to a stirring solution of compound **27** (0.58 g, 1.70 mmol) in toluene (9 mL) and the reaction mixture was heated under reflux overnight. The solvent was then evaporated under reduced pressure and the residue extracted with an aqueous solution of $NaHCO_3$ and chloroform; the organic phase was dried in Na_2SO_4, filtered, concentrated under reduced pressure and the final product was dried under vacuum.
Yield: 82% (0.56 g) of a white solid

^{1}H NMR (300 MHz, $CDCl_3$) δ_H (ppm): 4.52 (s, 2H, CH_2); 7.16 (m, 6H, 6CH (Tr)); 7.25 (m, 9H, 9CH (Tr)); 7.69 (s, 2H, 2CH (2CH-pz)).

5.3.2 Synthesis and characterization of the DNA-binding units

Anthracen-9-ylmethanol (1)

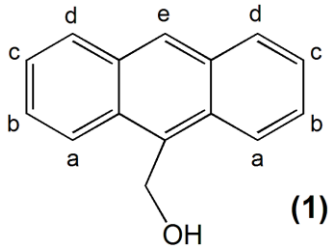

(1)

To a stirring solution of 9-anthracene aldehyde (5.00 g, 24.24 mmol) in THF (25 mL) was added drop wise, a solution of $NaBH_4$ (1.00 g, 26.43 mmo) in THF (10 mL) and the mixture was heated under reflux for 5 h. The solvent was evaporated under reduced pressure. HCl 37% (25 mL) and water (50 mL) with crushed ice (25 g) were added to the residue and the suspension was stirred for 15 min. The precipitate was filtered and dried under vacuum.
Yield: 80% (4.04 g) of yellow solid.

^{1}H NMR (300 MHz, $CDCl_3$) δ_H (ppm): 5.58 (s, 1H, OH); 5.67 (s, 2H, CH_2); 7.49 (m, 4H, 4CH (b + c)); 8.03 (d, 2H, 2CH (a/d)); 8.42 (m, 3H, 3CH (e + a/d)).

9-(bromomethyl)anthracene (2)

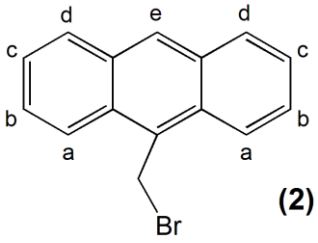

(2)

Liquid Br_2 (0.64 mL, 12.43 mmol) and compound **1** (2.50 g, 12.00 mmol) were added, slowly, to a suspension of PPh_3 (3.30 g, 12.58 mmol) in dry ACN (60 mL) and the mixture was stirred for 2 h at 0ºC. The precipitate was filtered and dried under vacuum to afford the final product.
Yield: 62% (2.03 g) of yellow solid.

^{1}H NMR (300 MHz, $CDCl_3$) δ_H (ppm): 5.52 (s, 2H, CH_2); 7.45 (t, 2H, 2CH (b/c)); 7.58 (t, 2H, 2CH (b/c)); 7.80 (d, 2H, 2CH (a/d)); 8.26 (d, 2H, 2CH (a/d)); 8.47 (s, 1H, CH (e)).

3-(anthracen-9-ylmethyl)pentane-2,4-dione (3)

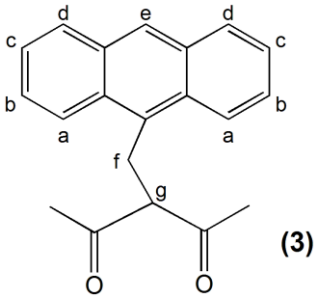

(3)

Distilled acetylacetone (0.24 mL, 2.34 mmol) was added to a suspension of NaH (0.06 g, 2.57 mmol) in dry THF (30 mL) at 0ºC and the mixture was stirred for 2 h at room temperature. Compound **2** (0.63 g, 2.34 mmol) was added at 0ºC and the mixture was stirred for 40 min at this temperature and then overnight at room temperature. HCl 1 M (60 mL) was added at 0ºC and the compound was extracted to Et_2O, dried with Na_2SO_4, filtered and evaporated under reduced pressure. The product was purified by SiO_2 column chromatography (eluent: chloroform (100-99%)/MeOH (0-1%)).
Yield: 67% (0.46 g) of yellow solid.

^{1}H NMR (300 MHz, $CDCl_3$) δ_H (ppm): 1.97 (s, 6H, $2CH_3$); 4.17 (d, 2H, CH_2); 4.25 (t, 1H, CH (g)); 7.45 (m, 4H, 4CH (b + c)); 8.05 (d, 2H, 2CH); 8.15 (d, 2H, 2CH); 8.40 (s, 1H, CH (e)).

3-(anthracen-9-yl)propan-1-amine (14)

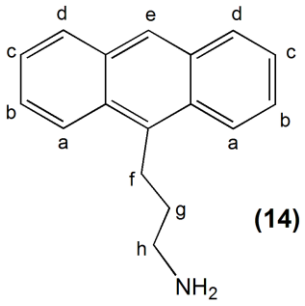

(14)

To a solution of 2-(anthracen-9-yl)acrylonitrile (0.45 g, 1.95 mmol) in dry Et_2O (10 mL) was added $LiAlH_4$ 1M/THF (1.95 mL, 1.95 mmol). The stirring mixture was heated under reflux for 30 min and then left at room temperature for 20 h. After this time, water (2 mL) was added followed by addition of an aqueous solution of NaOH 20% (0.76 mL) 5 min later. The product was extracted with water and Et_2O and the emulsion formed was washed with more Et_2O. The combined organic phase was dried with Na_2SO_4, filtered, concentrated under reduced pressure and the product dried under vacuum.

Yield: 96% (0.44 g) of brown oily solid.

^{1}H NMR (300 MHz, $CDCl_3$) δ_H (ppm): 1.70 (s br, 2H, NH_2); 1.93 (m, 2H, CH_2 (g)); 2.89 (t, 2H, CH_2 (f/h)); 3.62 (t, 2H, CH_2 (f/h)); 7.45 (m, 4H, 4CH (b + c)); 7.56 (d, 2H, 2CH (a/d)); 8.03 (m, 3H, 3CH (e + a/d)).

2-(3-bromopropyl)isoindoline-1,3-dione (15)

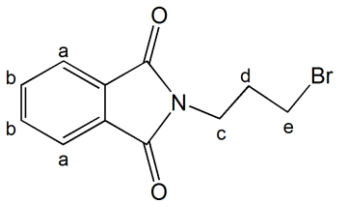

(15)

To a stirring solution of potassium phthalimide (12.70 g, 68.56 mmol) in dry ACN was added 1,3 dibromopropane (20 mL, 197.00 mmol) and the mixture was heated under reflux for 6h. The precipitate was filtered off and the filtrate was partially concentrated under reduced pressure and left in the fridge for 72 h. The precipitate formed was filtered and washed with cold MeOH. The MeOH was left in the fridge until a crystalline precipitate was formed. The latter was separated and dried under vacuum.

Yield: 69% (12.68 g) of a yellow solid

^{1}H NMR (300 MHz, $CDCl_3$) δ_H (ppm): 2.24 (m, 2H, CH_2 (d)); 3.40 (t, 2H, CH_2); 3.80 (t, 2H, CH_2); 7.73 (m, 2H, 2 CH); 7.84 (m, 2H, 2CH).

2-(3-iodopropyl)isoindoline-1,3-dione (16)

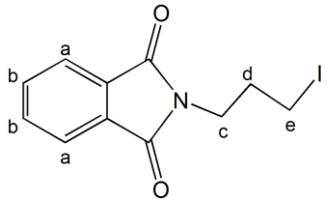

(16)

KI (3.13 g, 18.86 mmol) was added to a stirring solution of compound **15** (3.00 g, 11.19 mmol) in pre-dried acetone (60 mL) and the mixture was heated under reflux for 48 h. The solid was filtered off and the filtrate was concentrated under reduced pressure and dried under vacuum.
Yield: 94% (3.33 g) of a yellow solid.

^{1}H NMR (300 MHz, $CDCl_3$) δ_H (ppm): 2.25 (m, 2H, CH_2 (d)); 3.17 (t, 2H, CH_2 (e)); 3.77 (t, 2H, CH_2 (c)); 7.73 (m, 2H, 2 CH); 7.84 (m, 2H, 2CH).

3,6-bis(dimethylamino)-10-(3-(1,3-dioxoisoindolin-2-yl)propyl)acridinium (17)

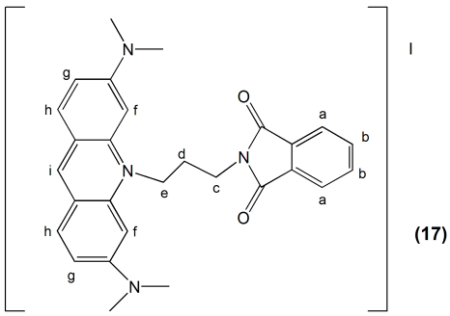

(17)

Acridine orange (0.63 g, 2.37 mmol) and a pinch of $NaHCO_3$ were added to a solution of compound **16** (1.50 g, 4.76 mmol) in anhydrous *p*-xylene (30 mL) and the stirring mixture was heated under reflux for 70 h. The precipitate was filtered, washed with Et_2O and dried under vacuum.
Yield: 91% (1.26 g) of brownish red solid.

^{1}H NMR (400 MHz, $CDCl_3$) δ_H (ppm): 2.63 (m, 2H, CH_2 (d)); 3.47 (m, 12H, $4CH_3$); 4.24 (t, 2H, CH_2); 4.97 (t, 2H, CH_2); 6.89 (s, 2H, 2CH (f)); 7.47 (d, 2H, 2CH); 8.06 (m, 6H, 6CH); 8.87 (s, 1H, CH (i)).

10-(3-aminopropyl)-3,6-bis(dimethylamino)acridinium (18)

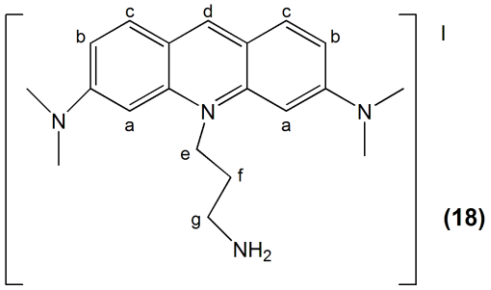

(18)

Hydrazine monohydrate (0.69 mL, 14.00 mmol) was added to a solution of compound **17** (0.60 g, 1.03 mmol) in MeOH (30 mL) and the stirring mixture was heated under reflux for 24 h. HCl 37% was added until a white precipitate was formed. The latter was filtered off and the filtrate was alkalized to pH 12 with an aqueous solution of NaOH 4M. The solvent was evaporated under reduced pressure and the residue extracted with water and chloroform. The organic phase was dried with Na_2SO_4, filtered and concentrated under reduced pressure. The final product was dried under vacuum.

Yield: 37% (0.17 g)

^{1}H NMR (300 MHz, CD_3OD) δ_H (ppm): 1.18 (m, 2H, NH_2); 2.14 (m, 2H, CH_2 (f)); 2.99 (t, 2H, CH_2 (g)); 3.31 (m, 12H, $4CH_3$); 4.79 (t, 2H, CH_2 (e)); 6.77 (s, 2H, 2CH (a)); 7.26 (d, 2H, 2CH (b/c)); 7.90 (d, 2H, 2CH (b/c)); 8.67 (s, 1H, CH (d)).

5.3.3 Synthesis and characterization of Ant-CH_2-pzNN (L1)

2-(4-(anthracen-9-ylmethyl)-3,5-dimethyl-1H-pyrazol-1-yl)ethanol (4)

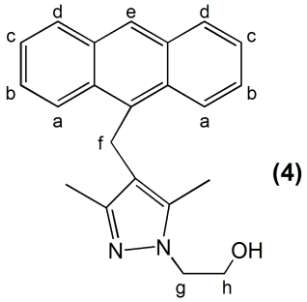

(4)

A solution of 2-hydroxyethyl hydrazine (0.11 mL, 1.63 mmol) in EtOH (8mL) was added drop wise to a solution of compound **3** (0.46 g, 1.57 mmol) in a mixture of chloroform and EtOH (1:1) (8 mL) at 0ºC. The mixture was stirred for 5 h at room temperature and the solvent was then evaporated under reduced pressure and the product dried under vacuum.

Yield: 69% (0.36 g) of a yellow solid.

^{1}H NMR (300 MHz, $CDCl_3$) δ_H (ppm): 1.71 (s, 3H, CH_3 (Mepz)); 1.92 (s, 3H, CH_3 (Mepz)); 4.19 (t, 2H, CH_2 (g/h)); 4.31 (t, 2H, CH_2 (g/h)); 4.73 (s, 2H, CH_2 (f)); 4.98 (s br, 1H, OH); 7.47 (m, 4H, 4CH (b + c)); 8.06 (m, 4H, 4CH (a + d)); 8.45 (s, 1H, CH (e)).

4-(anthracen-9-ylmethyl)-1-(2-bromoethyl)-3,5-dimethyl-1H-pyrazole (5)

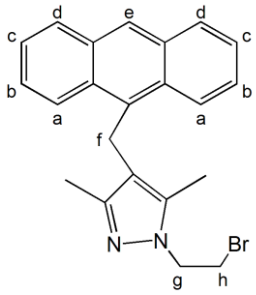

(5)

PBr_3 (0.08 mL, 0.83 mmol) was added to a stirring solution of compound **4** (0.15 g, 0.45 mmol) in pre-dried toluene (8 mL) and the mixture was heated under reflux overnight. The solution was washed with a saturated aqueous solution of $NaHCO_3$ and then with water. The organic phase was separated, dried with Na_2SO_4, filtered and concentrated under reduced pressure. The final product was dried under vacuum.
Yield: 59% (0.11 g) of a yellow solid.

^{1}H NMR (300 MHz, $CDCl_3$) δ_H (ppm): 1.65 (s, 3H, CH_3 (Mepz)); 1.89 (s, 3H, CH_3 (Mepz)); 3.58 (t, 2H, CH_2 (g/h)); 4.23 (t, 2H, CH_2 (g/h)); 4.70 (s, 2H, CH_2 (f)); 7.44 (m, 4H, 4CH (b + c)); 8.19 (m, 2H, 2CH (a/d)); 8.28 (m, 2H, 2CH (a/d)); 8.43 (s, 1H, CH (e)).

N^1-(2-(4-(anthracen-9-ylmethyl)-3,5-dimethyl-1H-pyrazol-1-yl)ethyl)ethane-1,2-diamine (L1)

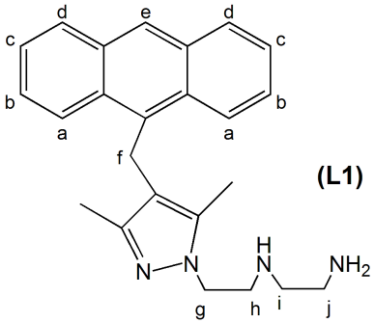

(L1)

A solution of compound **5** (0.11 g, 0.27 mmol) in dry MeOH (5 mL) was added drop wise to a stirring solution of 1,2-diaminoethane (0.32 mL, 4.80 mmol) in MeOH (20 mL) and the mixture was heated under reflux overnight. The solvent was evaporated under reduced pressure and

the compound was extracted with chloroform and water. The organic phase was separated, dried with Na_2SO_4, filtered and concentrated under reduced pressure. The product was purified by SiO_2 column chromatography (eluent: gradient elution with MeOH (100-96%)/ NH_4OH(0-4%)).

Yield: 21% (0.02 g) of yellow oily solid.

^{1}H NMR (300 MHz, $CDCl_3$) δ_H (ppm): 1.58 (s, 6H, $2CH_3$ (2Met-pz)); 2.58 (t, 2H, CH_2 (h/i/j)); 2.66 (t, 2H, CH_2 (h/i/j)); 2.89 (t, 2H, CH_2 (h/i/j)); 3.95 (t, 2H, CH_2 (g)); 4.67 (s, 2H, CH_2 (f)); 7.43 (m, 4H, 4CH (b + c)); 7.99 (m, 2H, 2CH (a/d)); 8.13 (m, 2H, 2CH (a/d)); 8.30 (s, 1H, CH (e)).

HPLC: t_R (column **A**; method **A**) = 21.04 min

5.3.4 Synthesis and characterization of Ant-$(CH_2)_3$-pzNN (L2)

2-(1-(2-(2-tert-butoxycarbonyl(2-(tert-butoxycarbonylamino)ethyl)amino)ethyl)-3,5-dimethyl-1H-pyrazol-4-yl)-N-(3-(anthracen-9-yl)propyl)acetamide (19)

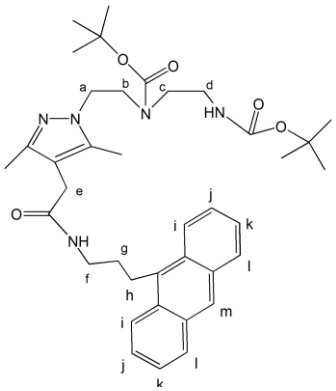

(19)

DIPEA (0.17 mL, 0.98 mmol) was added to a stirring solution of compound **14** (0.10 g, 0.43 mmol) in dry DCM followed by a slow addition of a solution of compound **13** in dry DCM and the mixture was stirred for 70 h. The compound was extracted with DCM and water. The organic phase was separated, dried with Na_2SO_4, filtered and concentrated under reduced pressure. The final product was dried under vacuum.

Yield: 70% (0.20 g) of a yellow oily solid

^{1}H NMR (300 MHz, $CDCl_3$) δ_H (ppm): 1.25 (m, 22H, $6CH_3$ (2BOC) + 2 CH_2); 2.11 (m, 6H, $2CH_3$ (2Met-pz)); 3.05 (m, 2H, CH_2); 3.27 (s, 2H, CH_2 (e)); 3.38 (m, 2H, CH_2); 3.46 (m, 2H, CH_2); 3.60 (m, 2H, CH_2); 4.05 (m, 2H, CH_2); 7.38 (m, 4H, 4CH (j + k)); 7.95 (d, 2H, 2CH (i/l)); 8.20 (m, 3H, 3CH (m + i/l)).

2-(1-(2-(2-aminoethylamino)ethyl)-3,5-dimethyl-1H-pyrazol-4-yl)-N-(3-(anthracen-9-yl)propyl)acetamide (L2)

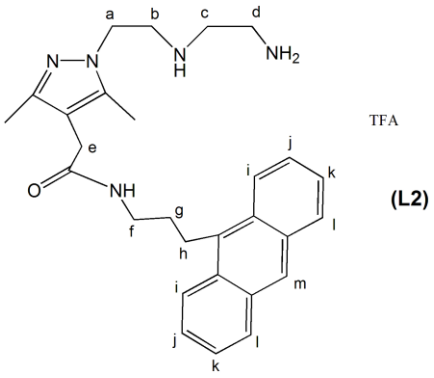

TFA (1.8 mL, 23.50 mmol) was added to a solution of compound **19** (0.20 g, 0.30 mmol) in DCM (2 mL) and the mixture was stirred overnight. The product was dried under vacuum.
Yield: 87% (0.14 g) of a yellow oily solid

^{1}H NMR (300 MHz, $CDCl_3$) δ_H (ppm): 1.19 (m, 2H, NH_2); 1.85 (m, 4H, $2CH_2$); 2.15 (s, 3H, CH_3 (Met-pz)); 2.57 (m, 3H, CH_3 (Met-pz)); 2.89 (t, 2H, CH_2); 3.22 (s, 2H, CH_2 (e)); 3.38 (q, 2H, CH_2); 3.55 (t, 2H, CH_2); 4.04 (t, 2H, CH_2); 5.76 (d br, 1H, NH); 7.42 (m, 4H, 4CH (j + k)); 7.98 (d, 2H, 2CH (i/l)); 8.13 (d, 2H, 2CH (i/l)); 8.26 (s, 1H, CH (m)).

HPLC: t_R (column **A**; method **A**) = 21.99 min

5.3.5 Synthesis and characterization of AO-$(CH_2)_3$-pzNN (L3)

10-(3-(2-(1-(2-(tert-butoxycarbonyl(2-(tert-butoxycarbonylamino)ethyl)amino)ethyl)-3,5-dimethyl-1H-pyrazol-4-yl)acetamido)propyl)-3,6-bis(dimethylamino)acridinium (20)

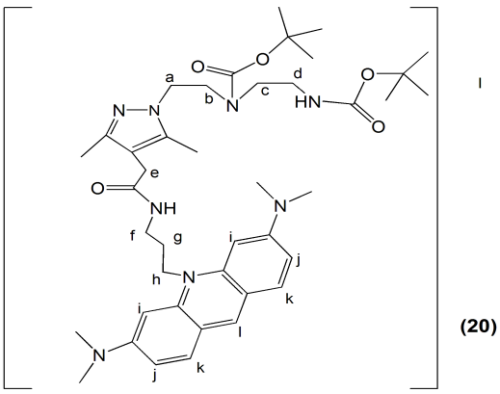

A solution of compound **18** (0.06 g, 0.13 mmol) in dry DMF was stirred for 1 hour, and then DIPEA (35 µL, 0.20 mmol) was added followed by a slow addition of a solution of compound **13**

(0.07 g, 0.13 mmol) in dry DMF. The mixture was stirred for 96 h. The solvent was evaporated under vacuum and a dry final product was obtained.
Yield: 86% (0.10 g) of a brownish oily solid

^{1}H NMR (300 MHz, CD_3OD) δ_H (ppm): 1.44 (m, 22H, $6CH_3$ (2BOC) + $2CH_2$); 2.23 (m, 6H, $2CH_3$ (Met-pz)); 3.02 (s, 12H, $4CH_3$ (AO)); 3.53 (m br, 6H, $3CH_2$); 4.14 (m br, 4H, $2CH_2$); 4.65 (m br, 2H, CH_2); 6.62 (s br, 2H, 2CH (i)); 7.18 (m br, 2H, 2CH (j/k)); 7.84 (m br, 2H, 2CH (j/k)); 8.59 (s br, 1H, CH (l)).

10-(3-(2-(1-(2-(2-aminoethylamino)ethyl)-3,5-dimethyl-1H-pyrazol-4-yl)acetamido)propyl)-3,6-bis(dimethylamino)acridinium (L3)

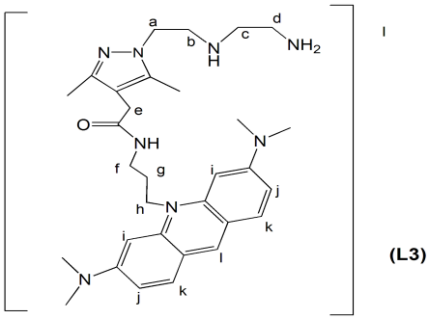

HCl 37 % (2 mL) was added to a solution of compound **20** (0.10 g, 0.12 mmol) in MeOH (5 mL) at 0ºC and the mixture was stirred for 18 h at room temperature. The pH was adjusted to 12 with an aqueous solution of NaOH 2.5 M and the mixture was extracted with chloroform. The organic phase was separated, dried with Na_2SO_4, filtered and concentrated under reduced pressure. The product was purified by Al_2O_3 column chromatography (eluent: gradient elution with MeOH (100-96%)/ NH_4OH (0-4%)).
Yield: 16% (0.01 g) of a brownish red solid.

^{1}H NMR (300 MHz, CD_3OD) δ_H (ppm): 2.12 (m, 6H, $2CH_3$ (Me-pz)); 2.19 (m, 4H, $2CH_2$); 2.66 (m, 2H, CH_2); 2.92 (m, 2H, CH_2); 3.13 (m, 2H, CH_2); 3.32 (s, 12H, $4CH_3$ (AO)); 3.49 (m, 2H, CH_2); 4.07 (m, 2H, CH_2); 4.65 (m, 2H, CH_2); 6.69 (s, 2H, 2CH (i)); 7.25 (d, 2H, 2CH (j/k)); 7.89 (d, 2H, 2CH (j/k)); 8.66 (s, 1H, CH (l)).

5.4 Synthesis and characterization of the Re complexes

5.4.1 *fac*-[Re(CO)$_3$(Ant-CH$_2$-pzNN)]Br (Re1)

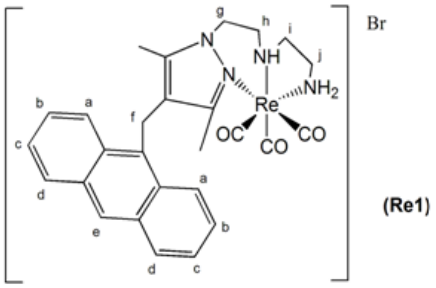

[Re(CO)$_5$Br] (20 mg; 0.054 mmol) was reacted with Ant-CH$_2$-pzNN **(L1)** (22 mg, 0.054 mmol) in MeOH and the reaction mixture was heated under reflux overnight. After removing the solvent under reduced pressure, the product was washed with hexane and dried under vacuum.
Yield: 76% (30 mg) of brownish yellow solid.

^{1}H NMR (300 MHz, CD_3OD) δ_H (ppm): 3.09 (s, 3H, CH_3 (Met-pz)); 3.64 (s, 3H, CH_3 (Met-pz)); 3.91 (t br, 2H, CH_2 (h/i/j)); 4.27 (m br, 2H, CH_2); 4.82 (t, 2H, CH_2); 5.20 (m br, 2H, CH_2); 6.23 (s, 2H, CH_2 (f)); 8.91 (m, 4H, 4CH (b + c)); 9.48 (d, 2H, 2CH (a/d)); 9.58 (d, 2H, 2CH (a/d)); 9.92 (s, 1H, CH (e)).

HPLC: t_R (column **A**; method **A**) = 22.90 min

5.4.2 *fac*-[Re(CO)$_3$(Ant-(CH$_2$)$_3$-pzNN)]Br (Re2)

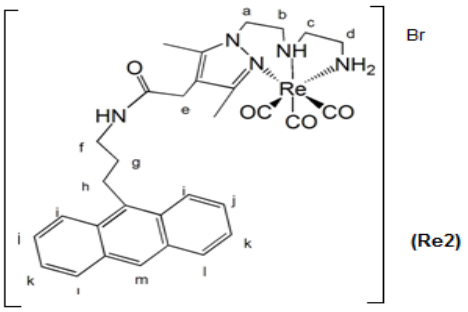

[Re(H$_2$O)$_3$(CO)$_3$]Br (49 mg; 0.12 mmol) was reacted with Ant-(CH$_2$)$_3$-pzNN **(L2)** (55 mg, 0.12 mmol) in MeOH and the reaction mixture was heated under reflux overnight. After removing the solvent under reduced pressure, the product was washed with Et_2O, then with $CHCl_3$ and centrifuged. The final product (supernatant) was dried under vacuum.
Yield: 62% (54 mg) of yellow solid.

^{1}H NMR (300 MHz, CD_3OD) δ_H (ppm): 1.05 (m, 2H, CH_2 (f)); 1.74 (m, 2H, CH_2 (g)); 2.09 (s, 3H, CH_3 (Met-pz)); 2.18 (m, 3H, CH_3 (Met-pz)); 2.25 (m, 2H, CH_2 (d)); 2.52 (m, 2H, CH_2 (c)); 3.12 (s, 2H, CH_2 (e)); 3.22 (m, 2H, CH_2 (h)); 3.55 (m, 2H, CH_2 (b)); 4.50 (m, 2H, CH_2 (a)); 7.20 (m, 4H, 4CH (j + k)); 7.77 (d, 2H, 2CH (i/l)); 8.05 (d, 2H, 2CH (i/l)); 8.14 (s, 1H, CH (m)).

^{13}C NMR (75.47 MHz, CD_3OD) δ (ppm): 9.04 (CH_3); 13.07 (CH_3); 24.74 (CH_2 (h)); 29.84 (CH_2 (f)); 30.64 (CH_2 (g)); 39.57 (CH_2 (e)); 41.91 (CH_2 (d)); 48.45 (CH_2 (b)); 48.55 (CH_2 (a)); 54.51 (CH_2 (c)); 112.75 (C); 123.77 (CH); 124.52 (CH); 125.34 (CH); 125.50 (C); 126.02 (C); 126.08 (C); 126.35 (C); 126.64 (CH); 127.59 (C); 127.88 (C); 128.12 (C); 128.92 (CH); 129.43 (CH); 131.73 (CH); 133.57 (CH); 134.03 (CH); 142.34 (C3/C5-pz); 152.13 (C3/C5-pz); 171.52 (C=O); 194.82 (CO).

HPLC: t_R (column **A**; method **A**) = 24.12 min

ESI/MS (m/z) ($C_{31}H_{35}N_5O_4Re$) = **[M^+]** calculated 728.22, found 728.5 (100%).

5.5 Synthesis and characterization of the ^{99m}Tc complexes

5.5.1 Precursor *fac*-[$^{99m}Tc(H_2O)_3(CO)_3]^+$

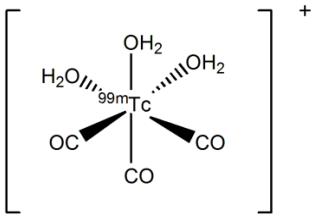

Sodium pertechnetate (Na[$^{99m}TcO_4$]), typically with activity of ca. 400 mCi, was obtained in sealed vials under vacuum after elution of a ^{99}Mo/^{99m}Tc generator (ELUMATIC III®) with a solution of NaCl 0.9% (5 mL). *fac*-[$^{99m}Tc(H_2O)_3(CO)_3]^+$ was prepared by adding the Na[$^{99m}TcO_4$] eluate (3mL) to a lyophilized Isolink® kit (*Covidien*, Petten) under N_2 atmosphere. The mixture was heated to 100 ºC for 30 min in dry bath and then neutralized with a solution of HCl 1M (145 µL) at room temperature. The organometallic precursor was obtained with an activity of c.a. 200 mCi. The radiochemical purity was evaluated by HPLC.

5.5.2 *fac*-[^{99m}Tc(CO)$_3$(Ant-CH$_2$-pzNN)]$^+$ (Tc1)

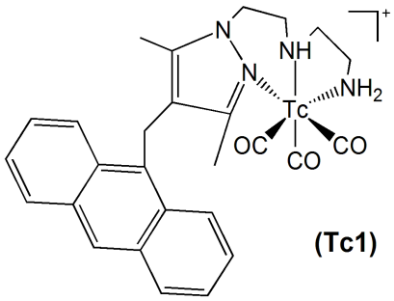

(Tc1)

A solution of Ant-CH$_2$-pzNN **(L1)** in EtOH (750 µL, 1x10^{-3} M) was added to an empty sealed vial under N$_2$ atmosphere. A solution of the precursor *fac*-[^{99m}Tc(H$_2$O)$_3$(CO)$_3$] (750 µL) was added to the vial, leading to a final ligand concentration of 5x10^{-4} M. The mixture was heated to 80 ºC for 30 min in a dry bath. Typically the complex was synthesized with activities of ca. 20 mCi. The analytical control and purification were performed by HPLC. The purified complex was usually recovered with activities of ca. 10 mCi.

HPLC: t_R (column **B**; method **B**) = 24.29 min

5.5.3 *fac*-[^{99m}Tc(CO)$_3$(Ant-(CH$_2$)$_3$-pzNN)]$^+$ (Tc2)

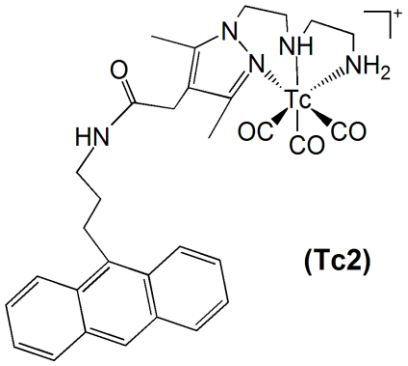

(Tc2)

A solution of Ant-(CH$_2$)$_3$-pzNN **(L2)** in EtOH (50 µL, 1x10^{-2} M) was added to an empty sealed vial under N$_2$ atmosphere. A solution of the precursor *fac*-[^{99m}Tc(H$_2$O)$_3$(CO)$_3$] (950 µL) was added to the vial, leading to a final ligand concentration of 5x10^{-4} M. The mixture was heated to 100 ºC for 30 min in dry bath. Typically the complex was synthesized with activities of ca. 20 mCi. The analytical control and purification were performed by HPLC. The purified complex was usually recovered with activities of ca. 10 mCi.

HPLC: t_R (column **B**; method **B**) = 23.53 min

Log ($P_{o/w}$) = 2.62 ± 0.19

5.6 Spectroscopic studies of the interaction of the ligands and Re complexes with the DNA molecule

These studies were performed at IST, Lisbon, with the collaboration of Dr. Sofia Gama (CR Group, C^2TN).

The DNA sodium salt from calf thymus (CT) DNA (1mg, Sigma) was dissolved in PBS (10 mM, pH = 7.2) (1 mL) overnight then quantified per nucleotide, after adequate dilution with the buffer, by absorption spectroscopy at 260 nm (ε_{260nm} = 6600 $M^{-1}cm^{-1}$).[67] The solutions of the ligand and Re complex were prepared with DMSO and its concentrations were kept constant while the concentration of the CT-DNA was varied at each measurement during the titrations. All the measurements were carried out in PBS (10 mM, pH = 7.2). To obtain the intrinsic binding constant (K) all calculations were done by considering the DNA concentration in base pairs, and the data were corrected for volume changes.

UV-visible spectroscopy

The UV-Vis spectra were recorded on a Perkin Elmer Lambda 35 UV-vis spectrometer, using quartz cuvettes (1cm). Equivalent amounts of the CT-DNA solution were added to the sample and reference (PBS) to eliminate possible interferences of DNA absorbance in the region of absorbance of the chromophores, and the mixtures were allowed to equilibrate after each addition. The UV-Vis spectra were recorded until no further changes in the absorbance were observed.

Fluorescence spectroscopy

The fluorescence spectra were recorded on a Perkin Elmer LS 55 fluorescence spectrometer, using quartz cuvette (1cm). After each addition of CT-DNA suspension, the mixture was allowed to equilibrate and the absorption at the excitation wavelength was recorded. The ligand and corresponding Re complex were excited at 320 nm and the emission spectra were recorded from λ = 350 - 550 nm, with a scan speed of 300 nm min^{-1}. Emission and excitation slits were chosen in order to maximize the fluorescence intensity. The fluorescence spectra were recorded until there were no further changes in the fluorescence intensity.

5.7 *In vitro* studies of the ^{99m}Tc-Ant-$(CH_2)_3$-pzNN (Tc2)

5.7.1 Lipophilicity

The lipophilicity of the ^{99m}Tc complex **Tc2** was evaluated by determining its partition-coefficient (logP) in a biphasic system n-octanol/PBS 0.1M (pH=7.4):

To three polyethylene vials were added n-octanol (1 mL) and PBS 0.1M (pH=7.4) (1 mL) and the mixtures were vortexed for 1 min. Then, a solution of purified complex **Tc2** (25 µL) was added to each vial and vortexed again, followed by centrifugation at 3000 rpm for 5 min. With the aqueous and organic phases well separated, small aliquots (100 µL x three replicates) of each phase were removed to new vials and the activities were measured in a Gamma counter. The log $P_{o/w}$ was calculated by applying the following expression:

$$\log (P_{o/w}) = \log \frac{\text{Activity in the organic phase (cpm)}}{\text{Activity in the aqueous phase (cpm)}} \times 100$$

5.7.2 *In vitro* stability

5.7.2.1 Stability in the presence of histidine

A solution of complex **Tc2** (100 µL) was added to a solution of histidine (900 µL, $1x10^{-3}$M) in PBS 0.1 M (pH=7). The mixture was incubated at 37 ºC in water bath and analyzed by HPLC after 1 and 2 h.

5.7.2.2 Stability in Human serum and determination of protein binding

A solution of complex **Tc2** (100 µL) was added to a polyethylene vial containing human serum (500 µL) and the mixture was incubated at 37 ºC in water bath. A small aliquot (100 µL) of the mixture was collect to an eppendorf after 1, 2, 3 and 6 h incubating. The aliquot was treated with EtOH (200 µL) and centrifuged at 3000 rpm for 15 min. The supernatant was separated and analyzed by HPLC. The pellet was washed with EtOH and centrifuged again, then separated and its activity was measured in an ionization chamber. The activity present in the pellet estimates the proportion of the complex associated to proteins by the following expression:

$$\text{Protein-binding (\%)} = \frac{\text{Activity in the pellet}}{\text{Activity in the supernatant}} \times 100$$

5.8 Cell studies

These studies were performed with the collaboration of Dr. Paula Raposinho (CR group, C^2TN).

5.8.1 Cell lines and cultures

B16-F1 murine melanoma cells (*European Collection of Cell Cultures,* UK*)* were grown in Dulbecco's Modified Eagle Medium (DMEM) containing Glutamax-I (Gibco, Invitrogen).

PC-3 human prostate cancer cells (*American Type Culture Collection,* USA) were grown in Roswell Park Memorial Institute medium (RPMI 1640) containing L-glutamine (Gibco, Introgen).

Both mediums were supplemented with 10% of heat inactivated fetal bovine serum (FBS) and 1% of antibiotic solution (penicillin:streptomycin) (all from Gibco, Invitrogen) and were changed every two days. The cell lines were incubated in a humidified atmosphere of 95% air and 5% CO_2 at 37°C. When confluent in a monolayer, the adherent cells would be detached after treatment with trypsin-EDTA (Gibco, Invitrogen) and seeded in new cell culture flasks.

5.8.2 Cell internalization of the ^{99m}Tc complexes

The cells of each cell lines were seeded into 24-well tissue culture plates ($2x10^5$ cells/500 µL of culture medium *per* well) and allowed to attach overnight at 37°C.

The solution of the purified ^{99m}Tc complex in PBS 0.1 M (pH=7) was diluted to the intended final activity value, in the assay medium MEM containing 0.2% BSA (Bovine Serum Albumin) and HEPES 25 mM (N-(2-hydroxyethyl)piperazine-N'-ethanesulfonic acid).

After removing the culture medium of each well, small aliquots (500 µL) of the radioactive solution were added to the attached cells. The cells were incubated in a humidified atmosphere of 95% air and 5% CO_2 at 37°C and the studies proceeded for an incubation period of 5 min to 4 hours. For each time point, the unbound radioactive compound of four wells (4 replicates) were

removed; the cells were washed with cold assay medium and then, twice, with glicine/HCl buffer pH 2.8 (500 µL) for 4 min at room temperature to remove the possible cell-surface bound radiocompounds. The buffer washes were separated and its activities measured. The pH of the cells was then neutralized with cold PBS containing 0.2% BSA, followed by lysis with NaOH 1M (500 µL) at 37°C for 10 min. The lysates were separated and its activity measured to determine the total of internalized radiocompounds.

$$\% \text{ Cell internalization} = \frac{\text{Lysates activity (cpm)}}{\text{Total added activity (cpm)}} \times 100$$

$$\% \text{ Surface bound} = \frac{\text{Glicine/HCl buffer whashes activity (cpm)}}{\text{Total added activity (cpm)}} \times 100$$

$$\% \text{ Total cell uptake} = \text{Internalization (\%)} + \text{Surface bound (\%)}$$

5.8.3 Cellular and nuclear uptake of the ^{99m}Tc complexes

The 24-well tissue culture plates were prepared, treated with the radioactive solution and incubated as described in the previous section. At each giving time, the cells of each four replica wells were washed with PBS (250 µL) containing 2% BSA and detached with trypsin (100 µL) at 37°C for a few minutes. DMEM medium (250 µL) was added to inactivate trypsin and the suspension was transferred to an eppendorf to be centrifuged at 800 rpm for 2 min. The supernatant was removed and the pellet was washed and centrifuged, twice, with PBS (250 µL) containing 2% BSA at 4°C. The pellet was resuspended in lysis buffer (10 mM Tris, 1.5 mM $MgCl_2$, 140 mM NaCl) (500 µL) with Nonidet (P-40 0.02%, pH 8.0-8.3) (1 µL) to disrupt the cell membrane. After 15 min incubation on ice the suspension was centrifuged at 1300 *g* for 1 min at 4°C. The activities of the supernatant (extra-nuclear) and pellet (nuclear) were measured separately.

$$\% \text{ Nuclear uptake} = \frac{\text{Pellet activity (cpm)}}{\text{Total added activity (cmp)}} \times 100$$

$$\% \text{ Cell uptake} = \frac{\text{Supernatant activity (cpm)} + \text{Pellet activity (cpm)}}{\text{Total added activity (cpm)}} \times 100$$

5.8.4 **Mitochondrial and nuclear uptake of the ^{99m}Tc complexes**

PC3 and B16F1 adherent cells (T75 culture flask) were incubated with the purified ^{99m}Tc-complexes (about 300 µCi/2 mL of culture medium) for 2h at 37ºC. The harvested cell suspension was centrifuged at 850 *g* for 2 min and cells washed with PBS to remove the unbound radioactive compound. The activity of the pellet was measured to allow the determination of cellular uptake.

The mitochondria (and nucleus) were isolated from PC3 and B16-F1 cells using the commercial kit *Mitochondria Isolation Kit for Cultured Cells* (Thermo Scientific) as instructed on the manufacturer's protocol, by Reagent-based method. Briefly, the pellet (about 2 x 10^7 cells) was treated with Mitochondria Isolation Reagent A supplemented with a protease inhibitors cocktail (800 µL), vortexed at medium speed for 5 seconds and incubated on ice for 2 min. Mitochondria Isolation Reagent B (10 µL) was added and the mixture was vortexed at maximum speed for 5 seconds, incubated on ice and vortexed every minute for 5 min. Mitochondria Isolation Reagent C supplemented with a protease inhibitors cocktail (800 µL) was then added and the suspension was centrifuged for 10 min at 700 *g* at 4°C. The activity of the pellet (nuclear fraction) was measured. The supernatant was centrifuged for 15 min at 3000 *g* at 4°C to remove the lysosomal and peroxisomal contaminants. The pellet, containing the isolated mitochondria, was again treated with Mitochondria Isolation Reagent C (500 µL) and centrifuged for 5 min at 12,000 *g*. The supernatant was discarded and the activity of the mitochondria pellet was count.

$$\%\text{Nuclear uptake} = \frac{\text{Nuclear Pellet activity (cpm)}}{\text{Total added activity (cmp)}} \text{ x } 100$$

$$\%\text{ Mitochondrial uptake} = \frac{\text{Mitochondrial Pellet activity (cpm)}}{\text{Total added activity (cmp)}} \text{ x } 100$$

5.8.5 **Radio-Cytotoxicity of the ^{99m}Tc complexes**

PC3 and B16-F1 cells were seeded into 96-well tissue culture plates (9x10^3 cells/200 µL of culture medium *per* well) and allowed to attach overnight at 37°C.

Several solutions of the purified ^{99m}Tc-complex (in PBS 0.1 M, pH=7) with different activities were prepared by successive dilution in DMEM complete medium.

The radioactive solutions (200 µL) were added to the cells in order to get eight replicas for each activity. Cells exposed to only DMEM complete medium and $[^{99m}TcO_4]^-$ in DMEM complete

medium were used as control. The cells were incubated in a humidified atmosphere of 95% air and 5% CO_2 at 37°C for 36-40 hours.

At the end of the incubation period, the compounds were removed and cells were washed with PBS (200 µL). Cell viability was then determined by incubating cells with 200 µL of MTT solution (0.5 mg/mL in PBS). After 3 h at 37°C/5% CO_2, the solution was removed and the purple formazan crystals formed inside the cells were dissolved in DMSO (200 µL) by thorough shaking. The absorbance at 570 nm was measured using a microplate spectrophotometer (PowerWave Xs, Bio-Tek Instruments, Winooski, VT, USA).

5.8.6 **Cytotoxicity of the ligands and Re complexes**

PC3 and B16-F1 cells were seeded into 96-well tissue culture plates ($9x10^3$ cells/200 µL of culture medium per well) and allowed to attach overnight at 37°C.

A high concentrated (20 mM) solution of inactive ligands and Re-complexes was prepared in DMSO (stock solution). From the stock solution, solutions with concentrations ranging from 200 µM to 0.1 µM were prepared by successive dilution in culture medium with 0.1% DMSO. The solutions (200 µL) were added to the cells (eight replicates for each concentration). The cells were incubated with the compounds in a humidified atmosphere of 95% air and 5% CO_2 at 37°C for 36-40 hours. The effect of the vehicle solvent (DMSO) on the growth of these cell lines was evaluated in all experiments by exposing untreated control cells to both concentrations of DMSO used (0.2% and 0.1%).

The cellular viability was determined by performing the MTT assay as described in the previous section.

For each test compound and for each cell line, a dose−response curve was obtained. The cytotoxic effects of ligands and Re-complexes were quantified by calculating the compound concentration inhibiting tumor cell growth by 50% (IC_{50}), based on non-linear regression analysis of dose–response data (GraphPad Prisma 5 software).

6 References

1. Saha GB. *Fundamentals of Nuclear Pharmacy, Fifth Edition*. 5th ed. Springer-Verlag New York, LLC; 2003.

2. Bartholomä MD. Recent developments in the design of bifunctional chelators for metal-based radiopharmaceuticals used in Positron Emission Tomography. *Inorganica Chim Acta*. 2012;389:36-51. doi:10.1016/j.ica.2012.01.061.

3. Hamoudeh M, Kamleh MA, Diab R, Fessi H. Radionuclides delivery systems for nuclear imaging and radiotherapy of cancer. *Adv Drug Deliv Rev*. 2008;60(12):1329-46. doi:10.1016/j.addr.2008.04.013.

4. Wadsak W, Mitterhauser M. Basics and principles of radiopharmaceuticals for PET / CT. *Eur J Radiol*. 2010;73(3):461-469. doi:10.1016/j.ejrad.2009.12.022.

5. Liu S. Bifunctional coupling agents for radiolabeling of biomolecules and target-specific delivery of metallic radionuclides. *Adv Drug Deliv Rev*. 2008;60(12):1347-70. doi:10.1016/j.addr.2008.04.006.

6. Pimlott SL, Sutherland A. Molecular tracers for the PET and SPECT imaging of disease. *Chem Soc Rev*. 2011;40(1):149-62. doi:10.1039/b922628c.

7. *Radiation Biology: A Handbook for Teachers and Students*. Vienna: IAEA; 2010. Available at: http://www.osti.gov/scitech/biblio/4810865. Accessed August 22, 2014.

8. Wang W, Yu Z, Su W. Ion irradiation and biomolecular radiation damage II. Indirect effect. *arXiv Prepr arXiv10044394*. 2010;(1). Available at: http://arxiv.org/abs/1004.4394. Accessed August 22, 2014.

9. Chaffer CL, Weinberg RA. A perspective on cancer cell metastasis. *Science*. 2011;331:1559-1564. doi:10.1126/science.1203543.

10. Buchegger F, Perillo-Adamer F, Dupertuis YM, Delaloye AB. Auger radiation targeted into DNA: a therapy perspective. *Eur J Nucl Med Mol Imaging*. 2006;33(11):1352-63. doi:10.1007/s00259-006-0187-2.

11. Bhattacharyya S, Dixit M. Metallic radionuclides in the development of diagnostic and therapeutic radiopharmaceuticals. *Dalt Trans*. 2011;40(23):6112-6128. doi:10.1039/c1dt10379b.Metallic.

12. Häfliger P, Agorastos N, Spingler B, Georgiev O, Viola G, Alberto R. Induction of DNA-double-strand breaks by auger electrons from 99mTc complexes with DNA-binding ligands. *Chembiochem*. 2005;6(2):414-21. doi:10.1002/cbic.200400210.

13. Tavares AAS, Tavares JMRS. 99m Tc Auger Electrons for Targeted Tumor Therapy : A Review 99m Tc Auger Electrons for Targeted Tumor Therapy : A Review. *Int J Radiat Biol*. 2010;86(4):261-270.

14. Carlson T a., White RM. Formation of Fragment Ions from CH3Te125 and C2H5Te125 Following the Nuclear Decays of CH3I125 and C2H5I125. *J Chem Phys*. 1963;38(12):2930. doi:10.1063/1.1733622.

15. Kassis AI. Cancer therapy with Auger electrons: are we almost there? *J Nucl Med*. 2003;44(9):1479-81. Available at: http://www.ncbi.nlm.nih.gov/pubmed/12960195.

16. Bousis C, Emfietzoglou D, Hadjidoukas P, Nikjoo H. Monte Carlo single-cell dosimetry of Auger-electron emitting radionuclides. *Phys Med Biol*. 2010;55(9):2555-72. doi:10.1088/0031-9155/55/9/009.

17. Ginj M, Hinni K, Tschumi S, Schulz S, Maecke HR. Trifunctional somatostatin-based derivatives designed for targeted radiotherapy using auger electron emitters. *J Nucl Med*. 2005;46(12):2097-103. Available at: http://www.ncbi.nlm.nih.gov/pubmed/16330576.

18. Griffiths GL, Govindan S V, Sgouros G, Ong GL, Goldenberg DM, Mattes MJ. Cytotoxicity with Auger electron-emitting radionuclides delivered by antibodies. *Int J Cancer*. 1999;81(6):985-92. Available at: http://www.ncbi.nlm.nih.gov/pubmed/10362149.

19. Panyutin IG, Neumann RD. Radioprobing of DNA: distribution of DNA breaks produced by decay of 125I incorporated into a triplex-forming oligonucleotide correlates with geometry of the triplex. *Nucleic Acids Res*. 1997;25(4):883-7. Available at: http://www.pubmedcentral.nih.gov/articlerender.fcgi?artid=146516&tool=pmcentrez&rendertype=abstract.

20. Balagurumoorthy P, Xu X. Effect of distance between decaying 125I and DNA on Auger-electron induced double-strand break yield. *Int J Radiat Biol*. 2012;88(12):998-1008. doi:10.3109/09553002.2012.706360.Effect.

21. Mjos KD, Orvig C. Metallodrugs in medicinal inorganic chemistry. *Chem Rev*. 2014;114(8):4540-63. doi:10.1021/cr400460s.

22. Liu S. The role of coordination chemistry in the development of target-specific radiopharmaceuticals. *Chem Soc Rev*. 2004;33(7):445-61. doi:10.1039/b309961j.

23. Wadsak W, Mitterhauser M. Basics and principles of radiopharmaceuticals for PET/CT. *Eur J Radiol*. 2010;73(3):461-9. doi:10.1016/j.ejrad.2009.12.022.

24. Jonge FAA De, Pauwels EKJ. Review article Technetium , the missing element. 1996;23(3).

25. Mahmood A, Jones A. Handbook of Radiopharmaceuticals: Radiochemistry and Applications. In: Welch MJ, Redvanly CS, eds. *Handbook of Radiopharmaceuticals: Radiochemistry and Applications*. Wiley; 2002:323-362.

26. Nystrom a., Thoennessen M. Discovery of yttrium, zirconium, niobium, technetium, and ruthenium isotopes. *At Data Nucl Data Tables*. 2012;98(2):95-119. doi:10.1016/j.adt.2011.12.002.

27. Ogasawara K, Mizoi K, Fujiwara S, Yoshimoto T. Case Report and 99m Tc-HMPAO SPECT Imaging in Early Spontaneous Reperfusion of Cerebral Embolism 99m Tc-Bicisate. 1999;(April):626-628.

28. Remote Sensing. Available at: http://wtlab.iis.u-tokyo.ac.jp/~wataru/lecture/rst/Intro/Part2_26d.html. Accessed September 15, 2014.

29. Bandoli G, Dolmella A, Porchia M. Structural overview of technetium compounds (1993–1999). *Coord Chem …*. 2001;214:43-90. Available at:

http://www.sciencedirect.com/science/article/pii/S0010854500003842. Accessed August 23, 2014.

30. Abram U, Alberto R. Technetium and rhenium: coordination chemistry and nuclear medical applications. *J Braz Chem Soc*. 2006;17(8):1486-1500. Available at: http://www.scielo.br/scielo.php?pid=S0103-50532006000800004&script=sci_arttext. Accessed August 23, 2014.

31. Dilworth J, Parrott S. The biomedical chemistry of technetium and rhenium. *Chem Soc Rev*. 1998;27. Available at: http://pubs.rsc.org/en/content/articlehtml/1998/cs/a827043z. Accessed August 23, 2014.

32. Arano Y. Recent advances in 99mTc radiopharmaceuticals. *Ann Nucl Med*. 2002;16(2):79-93. Available at: http://www.ncbi.nlm.nih.gov/pubmed/12043913.

33. Bandoli G, Tisato F, Dolmella A, Agostini S. Structural overview of technetium compounds (2000–2004). *Coord Chem Rev*. 2006;250(3-4):561-573. doi:10.1016/j.ccr.2005.09.012.

34. Alberto R, Schibli R, Schubiger AP, et al. A Novel Organometallic Aqua Complex of Technetium for the Labeling of Biomolecules : Aqueous Solution and Its Reaction with a Bifunctional Ligand. 1998;3(13):7987-7988.

35. Alberto R, Ortner K, Wheatley N. Synthesis and properties of boranocarbonate: a convenient in situ CO source for the aqueous preparation of +. *J …*. 2001;3(12):3135-3136. Available at: http://pubs.acs.org/doi/pdf/10.1021/ja003932b. Accessed August 23, 2014.

36. Morais M, Paulo A, Gano L, Santos I, Correia JDG. Target-specific Tc(CO)3-complexes for in vivo imaging. *J Organomet Chem*. 2013;744:125-139. doi:10.1016/j.jorganchem.2013.05.050.

37. Jürgens S, Herrmann W a., Kühn FE. Rhenium and technetium based radiopharmaceuticals: Development and recent advances. *J Organomet Chem*. 2014;751:83-89. doi:10.1016/j.jorganchem.2013.07.042.

38. Silva CR, Valsa JO, Caniné MS, Caldeira-de-Araújo a, Bernardo-Filho M. Evaluation of technetium-99m decay on Escherichia coli inactivation: effects of physical or chemical agents. *Yale J Biol Med*. 1998;71(1):7-14. Available at: http://www.pubmedcentral.nih.gov/articlerender.fcgi?artid=2578916&tool=pmcentrez&rendertype=abstract.

39. Pedraza-López M, Ferro-Flores G, Mendiola-Cruz MT, Morales-Ramírez P. Assessment of radiation-induced DNA damage caused by the incorporation of 99mTc-radiopharmaceuticals in murine lymphocytes using single cell gel electrophoresis. *Mutat Res*. 2000;465(1-2):139-44. Available at: http://www.ncbi.nlm.nih.gov/pubmed/10708979.

40. Schipper ML, Riese CGU, Seitz S, et al. Efficacy of 99mTc pertechnetate and 131I radioisotope therapy in sodium/iodide symporter (NIS)-expressing neuroendocrine tumors in vivo. *Eur J Nucl Med Mol Imaging*. 2007;34(5):638-50. doi:10.1007/s00259-006-0254-8.

41. Jiménez-Mancilla N, Ferro-Flores G, Santos-Cuevas C, et al. Multifunctional targeted therapy system based on 99m Tc/ 177 Lu-labeled gold nanoparticles-Tat(49-57)-Lys 3 -bombesin internalized in nuclei of prostate cancer cells. *J Label Compd Radiopharm*. 2013;56(13):663-671. doi:10.1002/jlcr.3087.

42. Haefliger P, Agorastos N, Renard A, Giambonini-Brugnoli G, Marty C, Alberto R. Cell uptake and radiotoxicity studies of an nuclear localization signal peptide-intercalator conjugate labeled with [99mTc(CO)3]+. *Bioconjug Chem*. 2005;16(3):582-7. doi:10.1021/bc0500084.

43. Agorastos N, Borsig L, Renard A, et al. Cell-specific and nuclear targeting with [M(CO)(3)](+) (M=(99m)Tc, Re)-based complexes conjugated to acridine orange and bombesin. *Chemistry*. 2007;13(14):3842-52. doi:10.1002/chem.200700031.

44. Zelenka K, Borsig L, Alberto R. Trifunctional 99mTc based radiopharmaceuticals: metal-mediated conjugation of a peptide with a nucleus targeting intercalator. *Org Biomol Chem*. 2011;9(4):1071-8. doi:10.1039/c0ob00504e.

45. Vitor RF, Correia I, Videira M, et al. Pyrazolyl-diamine ligands that bear anthracenyl moieties and their rhenium(I) tricarbonyl complexes: synthesis, characterisation and DNA-binding properties. *Chembiochem*. 2008;9(1):131-42. doi:10.1002/cbic.200700433.

46. Esteves T, Xavier C, Gama S, et al. Tricarbonyl M(I) (M = Re, (99m)Tc) complexes bearing acridine fluorophores: synthesis, characterization, DNA interaction studies and nuclear targeting. *Org Biomol Chem*. 2010;8(18):4104-16. doi:10.1039/c0ob00073f.

47. Esteves T, Marques F, Paulo A, et al. Nuclear targeting with cell-specific multifunctional tricarbonyl M(I) (M is Re, (99m)Tc) complexes: synthesis, characterization, and cell studies. *J Biol Inorg Chem*. 2011;16(8):1141-53. doi:10.1007/s00775-011-0803-x.

48. Vitor RF, Esteves T, Marques F, et al. (99m)Tc-tricarbonyl complexes functionalized with anthracenyl fragments: synthesis, characterization, and evaluation of their radiotoxic effects in murine melanoma cells. *Cancer Biother Radiopharm*. 2009;24(5):551-63. doi:10.1089/cbr.2009.0647.

49. Alves S, Paulo A, Correia JDG, Domingos Â, Santos I. Coordination capabilities of pyrazolyl containing ligands towards the fac-[Re(CO)3]+ moiety. *J Chem Soc Dalt Trans*. 2002;(24):4714. doi:10.1039/b207164a.

50. Vitor RF, Alves S, Correia JDG, Paulo A, Santos I. Rhenium(I)- and technetium(I) tricarbonyl complexes anchored by bifunctional pyrazole-diamine and pyrazole-dithioether chelators. *J Organomet Chem*. 2004;689(25):4764-4774. doi:10.1016/j.jorganchem.2004.09.033.

51. Moura C, Fernandes C, Gano L, et al. Influence of the ligand donor atoms on the in vitro stability of rhenium(I) and technetium (I)-99m complexes with pyrazole-containing chelators: Experimental and DFT studies. *J Organomet Chem*. 2009;694(6):950-958. doi:10.1016/j.jorganchem.2008.11.027.

52. Alves S, Paulo A, Correia JDG, et al. Pyrazolyl derivatives as bifunctional chelators for labeling tumor-seeking peptides with the fac-[M(CO)3]+ moiety (M = 99mTc, Re): synthesis, characterization, and biological behavior. *Bioconjug Chem*. 2005;16(2):438-49. doi:10.1021/bc0497968.

53. Keter FK, Darkwa J. Perspective: the potential of pyrazole-based compounds in medicine. *Biometals*. 2012;25(1):9-21. doi:10.1007/s10534-011-9496-4.

54. Alves S, Correia JDG, Santos I, et al. Pyrazolyl conjugates of bombesin: a new tridentate ligand framework for the stabilization of fac-[M(CO)3]+ moiety. *Nucl Med Biol*. 2006;33(5):625-34. doi:10.1016/j.nucmedbio.2006.03.007.

55. Morais M, Raposinho PD, Oliveira MC, Correia JDG, Santos I. Evaluation of novel 99mTc(I)-labeled homobivalent α-melanocyte-stimulating hormone analogs for melanocortin-1 receptor targeting. *J Biol Inorg Chem*. 2012;17:491-505. doi:10.1007/s00775-011-0871-y.

56. Haq I. Thermodynamics of drug-DNA interactions. *Arch Biochem Biophys*. 2002;403(1):1-15. doi:10.1016/S0003-9861(02)00202-3.

57. Palchaudhuri R, Hergenrother PJ. DNA as a target for anticancer compounds: methods to determine the mode of binding and the mechanism of action. *Curr Opin Biotechnol*. 2007;18:497-503. doi:10.1016/j.copbio.2007.09.006.

58. Rohs R, Bloch I, Sklenar H, Shakked Z. Molecular flexibility in ab initio drug docking to DNA: Binding-site and binding-mode transitions in all-atom Monte Carlo simulations. *Nucleic Acids Res*. 2005;33:7048-7057. doi:10.1093/nar/gki1008.

59. Sinha R, Islam MM, Bhadra K, Kumar GS, Banerjee A, Maiti M. The binding of DNA intercalating and non-intercalating compounds to A-form and protonated form of poly(rC).poly(rG): spectroscopic and viscometric study. *Bioorg Med Chem*. 2006;14(3):800-14. doi:10.1016/j.bmc.2005.09.007.

60. Double-helix disruption. *Nat Chem*. 2012;4(8):587. doi:10.1038/nchem.1423.

61. Sirajuddin M, Ali S, Badshah A. Drug-DNA interactions and their study by UV-Visible, fluorescence spectroscopies and cyclic voltametry. *J Photochem Photobiol B*. 2013;124:1-19. doi:10.1016/j.jphotobiol.2013.03.013.

62. LERMAN LS. Structural considerations in the interaction of DNA and acridines. *J Mol Biol*. 1961;3:18-30. doi:10.1016/S0022-2836(61)80004-1.

63. Cholewiński G, Dzierzbicka K, Kołodziejczyk AM. Natural and synthetic acridines/acridones as antitumor agents: their biological activities and methods of synthesis. *Pharmacol Rep*. 2011;63(2):305-36. Available at: http://www.ncbi.nlm.nih.gov/pubmed/21602588.

64. Kumar R, Kaur M, Kumari M. REVIEW ACRIDINE : A VERSATILE HETEROCYCLIC NUCLEUS. 2012;69(1):3-9.

65. Biver T, Eltugral N, Pucci A, et al. Synthesis, characterization, DNA interaction and potential applications of gold nanoparticles functionalized with Acridine Orange fluorophores. *Dalton Trans*. 2011;40(16):4190-9. doi:10.1039/c0dt01371d.

66. Yoshizawa M, Klosterman JK. Molecular architectures of multi-anthracene assemblies. *Chem Soc Rev*. 2014;43(6):1885-98. doi:10.1039/c3cs60315f.

67. Kumar C V., Asuncion EH. DNA binding studies and site selective fluorescence sensitization of an anthryl probe. *J Am Chem Soc*. 1993;115(19):8547-8553. doi:10.1021/ja00072a004.

68. Sakamoto S, Hatakeyama M, Ito T, Handa H. Tools and methodologies capable of isolating and identifying a target molecule for a bioactive compound. *Bioorg Med Chem*. 2012;20(6):1990-2001. doi:10.1016/j.bmc.2011.12.022.

69. Boonen K, Creemers JW, Schoofs L. Bioactive peptides, networks and systems biology. *Bioessays*. 2009;31(3):300-14. doi:10.1002/bies.200800055.

70. Gugger M, Reubi JC. Gastrin-releasing peptide receptors in non-neoplastic and neoplastic human breast. *Am J Pathol*. 1999;155(6):2067-76. doi:10.1016/S0002-9440(10)65525-3.

71. Beer M, Montani M, Gerhardt J, et al. Profiling gastrin-releasing peptide receptor in prostate tissues: clinical implications and molecular correlates. *Prostate*. 2012;72(3):318-25. doi:10.1002/pros.21434.

72. Smith CJ, Volkert W a, Hoffman TJ. Radiolabeled peptide conjugates for targeting of the bombesin receptor superfamily subtypes. *Nucl Med Biol*. 2005;32(7):733-40. doi:10.1016/j.nucmedbio.2005.05.005.

73. Markwalder R, Reubi JC. Gastrin-releasing Peptide Receptors in the Human Prostate : Relation to Neoplastic Transformation Gastrin-releasing Peptide Receptors in the Human Prostate : Relation to Neoplastic Transformation. 1999:1152-1159.

74. Liu Y, Hu X, Liu H, et al. A comparative study of radiolabeled bombesin analogs for the PET imaging of prostate cancer. *J Nucl Med*. 2013;54(12):2132-8. doi:10.2967/jnumed.113.121533.

75. Schroeder RPJ, van Weerden WM, Bangma C, Krenning EP, de Jong M. Peptide receptor imaging of prostate cancer with radiolabelled bombesin analogues. *Methods*. 2009;48(2):200-4. doi:10.1016/j.ymeth.2009.04.002.

76. Maina T, Nock B, Mather S. Targeting prostate cancer with radiolabelled bombesins. *Cancer Imaging*. 2006;6:153-7. doi:10.1102/1470-7330.2006.0025.

77. Smith CJ, Volkert W a., Hoffman TJ. Gastrin releasing peptide (GRP) receptor targeted radiopharmaceuticals: A concise update. *Nucl Med Biol*. 2003;30(8):861-868. doi:10.1016/S0969-8051(03)00116-1.

78. Schlenstedt G. Protein import into the nucleus. *FEBS Lett*. 1996;389(1):75-9. Available at: http://www.pubmedcentral.nih.gov/articlerender.fcgi?artid=1326308&tool=pmcentrez&rendertype=abstract.

79. Görlich D. Nuclear protein import. *Curr Opin Cell Biol*. 1997;9(3):412-9. Available at: http://www.ncbi.nlm.nih.gov/pubmed/9159081.

80. Escriou V, Carrière M, Scherman D, Wils P. NLS bioconjugates for targeting therapeutic genes to the nucleus. *Adv Drug Deliv Rev*. 2003;55(2):295-306. Available at: http://www.ncbi.nlm.nih.gov/pubmed/12564982.

81. Pouton CW, Wagstaff KM, Roth DM, Moseley GW, Jans D a. Targeted delivery to the nucleus. *Adv Drug Deliv Rev*. 2007;59(8):698-717. doi:10.1016/j.addr.2007.06.010.

82. Wu J, Corbett AH, Berland KM. The intracellular mobility of nuclear import receptors and NLS cargoes. *Biophys J*. 2009;96(9):3840-9. doi:10.1016/j.bpj.2009.01.050.

83. Gama S, Mendes F, Esteves T, et al. Synthesis and Biological Studies of Pyrazolyl-Diamine PtII Complexes Containing Polyaromatic DNA-Binding Groups. *ChemBioChem*. 2012;13:2352-2362. doi:10.1002/cbic.201200472.

84. Moura C, Esteves T, Gano L, Raposinho PD, Paulo A, Santos I. Synthesis, characterization and biological evaluation of tricarbonyl M(i) (M = Re, 99mTc) complexes

functionalized with melanin-binding pharmacophores. *New J Chem*. 2010;34(11):2564. doi:10.1039/c0nj00256a.

85. Fernandes C, Maria L, Gano L, Santos IC, Santos I, Paulo A. Re(I) and 99mTc(I) tricarbonyl complexes with ether-containing pyrazolyl-based chelators: Chemistry, biodistribution and metabolism. *J Organomet Chem*. 2014;760:138-148. doi:10.1016/j.jorganchem.2013.11.013.

86. Lazarova N, James S, Babich J, Zubieta J. A convenient synthesis, chemicalcharacterization and reactivity of [Re(CO)3(H2O)]Br: the crystal and molecular structure of [Re(CO)3(CH3CN)2Br]. *Inorg Chem Commun*. 2004;7(9):1023-1026.

87. Vitor RF. Complexos de Rénio e Tecnécio com ligandos N-Heterocíclicos Dirigidos ao Núcleo de Células Tumorais: Da Imagiologia Molecular à Terapia com 99mTc. 2007.

88. Forcha D, Brown KJ, Assefa Z. Luminescence, absorption, and Stern-Volmer studies of cerium chloride and nitrate compounds in acidic and neutral aqueous, and non-aqueous solutions. *Spectrochim Acta - Part A Mol Biomol Spectrosc*. 2013;103:90-95. doi:10.1016/j.saa.2012.11.015.

89. Czyrski A, Kupczyk B. The Determination of Partition Coefficient of 6-Mercaptopurine Derivatives by Thin Layer Chromatography. *J Chem*. 2013;2013:1-4. doi:10.1155/2013/419194.

90. Liu X, Testa B, Fahr A. Lipophilicity and its relationship with passive drug permeation. *Pharm Res*. 2011;28(5):962-77. doi:10.1007/s11095-010-0303-7.

91. James S, Maresca KP, Babich JW, Valliant JF, Doering L, Zubieta J. Isostructural Re and 99mTc complexes of biotin derivatives for fluorescence and radioimaging studies. *Bioconjug Chem*. 2006;17(3):590-6. doi:10.1021/bc050298o.

92. Singh BN. A quantitative approach to probe the dependence and correlation of food-effect with aqueous solubility, dose/solubility ratio, and partition coefficient (LogP) for orally active drugs administered as immediate-release formulations. *Drug Dev Res*. 2005;65(2):55-75. doi:10.1002/ddr.20008.

93. Modica-Napolitano JS, Singh KK. Mitochondria as targets for detection and treatment of cancer. *Expert Rev Mol Med*. 2002;4(9):1-19. doi:doi:10.1017/S1462399402004453.

94. Van Meerloo J, Kaspers GJL, Cloos J. Cell sensitivity assays: The MTT assay. *Methods Mol Biol*. 2011;731:237-245. doi:10.1007/978-1-61779-080-5-20.

95. Perrin D, Armarego W. *Purification of Laboratory Chemicals*. 3rd ed. Oxford: Pergamon Press; 1988.